2006

Thermal response analysis from in-cylinder combustion to exhaust aftertreatment.

Usman Asad
University of Windsor

THERMAL RESPONSE ANALYSIS FROM IN-CYLINDER COMBUSTION TO EXHAUST AFTERTREATMENT

By

Usman Asad

A Thesis
Submitted to the Faculty of Graduate Studies and Research
through Mechanical, Automotive & Materials Engineering
in Partial Fulfilment of the Requirements for
the Degree of Master of Applied Science at the
University of Windsor

Windsor, Ontario, Canada

2006

Copyright © 2006 Usman Asad

Library and
Archives Canada

Bibliothèque et
Archives Canada

Published Heritage
Branch

Direction du
Patrimoine de l'édition

395 Wellington Street
Ottawa ON K1A 0N4
Canada

395, rue Wellington
Ottawa ON K1A 0N4
Canada

NOTICE:

The author has granted a non-exclusive license allowing Library and Archives Canada to reproduce, publish, archive, preserve, conserve, communicate to the public by telecommunication or on the Internet, loan, distribute and sell theses worldwide, for commercial or non-commercial purposes, in microform, paper, electronic and/or any other formats.

The author retains copyright ownership and moral rights in this thesis. Neither the thesis nor substantial extracts from it may be printed or otherwise reproduced without the author's permission.

AVIS:

L'auteur a accordé une licence non exclusive permettant à la Bibliothèque et Archives Canada de reproduire, publier, archiver, sauvegarder, conserver, transmettre au public par télécommunication ou par l'Internet, prêter, distribuer et vendre des thèses partout dans le monde, à des fins commerciales ou autres, sur support microforme, papier, électronique et/ou autres formats.

L'auteur conserve la propriété du droit d'auteur et des droits moraux qui protège cette thèse. Ni la thèse ni des extraits substantiels de celle-ci ne doivent être imprimés ou autrement reproduits sans son autorisation.

In compliance with the Canadian Privacy Act some supporting forms may have been removed from this thesis.

While these forms may be included in the document page count, their removal does not represent any loss of content from the thesis.

Conformément à la loi canadienne sur la protection de la vie privée, quelques formulaires secondaires ont été enlevés de cette thèse.

Bien que ces formulaires aient inclus dans la pagination, il n'y aura aucun contenu manquant.

Canada

ABSTRACT

The thermal response from in-cylinder combustion to exhaust aftertreatment was investigated for a 4-stroke single cylinder Yanmar diesel engine. The thermal characteristics of late post-injection inside the cylinder for enabling aftertreatment operations were simulated and experimentally verified. The cylinder head of the Yanmar engine was modified for measurement of in-cylinder pressure and temperature. A real-time heat release model was developed for analyzing the diesel combustion based upon the acquired cylinder pressure. However, the in-cylinder measurements could not be realized due to limitations of the thermocouple signal conditioning system.

A complicated practical exhaust system for the Yanmar diesel engine was prepared for determining the thermal characteristics of the single-wall exhaust pipe. Experiments were performed to cover a wide range of engine operation conditions. The response of the exhaust system for both steady–state and transient engine operations has been reported. A 1-D transient heat transfer model for the Yanmar exhaust system was developed. A similar model was also setup using WAVE Software. The calibration and validation of the models were performed with the experimental results. The thermal energy loss from the exhaust system was estimated by simulating the heat transfer from different exhaust pipe structures under steady-state and transient engine operating conditions. It was found that the predictions of the in-house model are in agreement with the experimental results. The heat transfer characteristics of a double-wall exhaust pipe with air-gap were simulated and the potential benefits highlighted through an energy efficiency analysis.

The thermal response from in-cylinder combustion to exhaust aftertreatment for the Yanmar diesel engine was characterized in terms of a heat loss coefficient and a time constant. Moreover, the effect of mass flowrate on both these factors was also evaluated. The procedure for quantifying the overall thermal response has been reported in detail.

DEDICATION

This work is dedicated to my wife Marrium and my daughter Sharmeen who have selflessly put up with the long hours I work and are always there to give me support and love. It is also dedicated to my parents, who have unconditionally supported me throughout all of my endeavours.

ACKNOWLEDGEMENTS

LIST OF PUBLICATIONS

The following publications resulted from the research conducted during the course of this work.

1. **Usman Asad**, Ming Zheng, David S-K. Ting, Raj Kumar, Siddhartha Banerjee, Graham T. Reader, Jimi Tjong, 2006, *"Real-time Heat Release Analysis towards On-fly Combustion Control for Diesel Engines"*, Combustion Institute/Canadian Section 2006 Spring Technical Meeting, University of Waterloo, Canada.

2. M.C. Mulenga, M. Zheng, G.T. Reader, D.S-K. Ting, Y. Tan, **U. Asad** and M. Wang, 2006, *"Investigating EGR on Low-temperature Combustion NOx and PM in Diesel Engines"*, Combustion Institute/Canadian Section 2006 Spring Technical Meeting, University of Waterloo, Canada.

3. Ming Zheng, Graham T Reader, Dong Wang, Jun Zuo, Raj Kumar, Mwila C Mulenga, **Usman Asad**, David S-K Ting, and Meiping Wang, 2005, *"A Thermal Response Analysis on the Transient Performance of Active Diesel Aftertreatment"*, Society of Automotive Engineers (SAE) 2005 Transactions Journal of Fuels and Lubricants, Paper 2005-01-3885, **114-4**, 1804-1815..

4. **Usman Asad**, Ming Zheng, David S-K Ting, Graham Reader, 2005, *"Effect of Internal Exhaust Gas Recycling on n-Heptane HCCI Combustion"*, ICEF 2005-1245, American Society of Mechanical Engineers (ASME) 2005 Fall Technical Conference, Ottawa, Canada

TABLE OF CONTENTS

LIST OF TABLES

x

LIST OF FIGURES

xi

xiii

LIST OF APPENDICES

NOMENCLATURE

ABDC	After bottom dead centre
ATDC	After top dead centre
BBDC	Before bottom dead centre
BTDC	Before top dead centre
CARS	Coherent Anti-Stokes Raman Spectroscopy
CI	Compression ignition
CO	Carbon monoxide
CO_2	Carbon dioxide
c_p	Specific heat at constant pressure (J/kg K)
c_v	Specific heat at constant volume (J/kg K)
d	Diameter (m)
DOC	Diesel oxidation catalyst
DPF	Diesel particulate filter
EGR	Exhaust gas recirculation
EPA	Environmental Protection Agency
f	Friction factor
F_s	Radiation shape factor
g	Acceleration due to gravity (m^2/s)
H	Enthalpy (J)
h	Heat transfer coefficient (W/m^2 K)
HC	Hydrocarbon
IMEP	Indicated mean effective pressure (bar)
ISO	Internal Standards Organization
k	Thermal conductivity (W/m K)
LNT	Lean NOx trap
m	Spacing step
$\dot{m}$	Mass flow rate (kg/s)
n	Time step of marching
NMHC	Non-methane hydrocarbons

NO_2	Nitrogen dioxide
NOx	Oxides of Nitrogen
Nu	Nusselt number
p	Pressure (Pa)
PM	Particulate matter
ppm	Parts per million
Pr	Prandtl number
Q_{Lexh}	Heat loss coefficient
R	Specific gas constant (J/kg K)
Ra	Rayleigh number
Re	Reynolds number
rpm	Revolution per minute
s	Thickness (m)
SCR	Selective Catalytic Reduction
SI	Spark ignition
T	Temperature (K)
t	Time (sec)
TDC	Top dead centre
TWC	Three-way catalytic converter
u	Velocity (m/s)
V	Volume (m^3)
x	Axial distance (m)

Greek Letters

α	Thermal diffusivity
ρ	Density
ε_R	Emissivity
ε	Absolute surface roughness
γ	Ratio of specific heats
η	Efficiency
β	Coefficient of thermal expansion

τ	Time constant
δ	Thickness

Subscripts

cv	Convection
env	Environment
exh	Exhaust
g	Exhaust gas
i	Inner
o	Outer
p	Pipe
rad	Radiation
tc	Thermocouple

xvii

1. INTRODUCTION

Diesel's nearly universal use in a wide range of applications reflects its acceptance as one of the most efficient internal combustion engine. This can be attributed to the intrinsic performance advantages of the continuously improving diesel technology – power, low fuel consumption, safety, durability, and robustness. In addition to the inherent high efficiency leading to low carbon dioxide emission, diesel exhaust also contains low levels of carbon monoxide and hydrocarbon emissions. However, the perception of the diesel engine as "dirty" is based on the comparatively higher emission levels of particulate matter (PM) and oxides of nitrogen (NOx) as compared to gasoline engines [1].

Within the last decade, there has been a significant improvement in the emission performance of the diesel engine. The level of engine-out PM emission of new on-highway diesel engines has been reduced by nearly 80% since 1988 while the NOx emissions have been reduced by about 60% over the same time period [2]. This has been accomplished largely through improvements in the diesel combustion process, together with the use of exhaust gas recirculation (EGR) and advanced turbocharging systems. Electronic fuel injection/combustion control systems have enabled the engine manufacturers to control fuel injection independently of engine speed, permitting injection strategies favourable to low pollutant production. The use of higher injection pressures and flexible injection timings has resulted in higher combustion efficiency and the flexibility to meet emission goals under different operating conditions.

Although substantial developments as outlined above have been made in the diesel engine technology to reduce the engine-out NOx and PM emissions, the improvement in diesel combustion alone will not be enough to conform to the requirements of the impending stringent emission standards. For meeting these standards, diesel engines would require the use of aftertreatment devices such as the Diesel Particulate Filter (DPF) and the Lean NOx Trap (LNT). However, the task of reducing the exhaust pollutants from lean-burn engines like diesel using aftertreatment devices is complicated by two facts. First, there is an abundance of

oxygen in the diesel exhaust and secondly, the exhaust gas temperature is relatively low due to the high compression ratios and the temperature also varies widely with load. Both these factors result in a lower efficiency of the diesel aftertreatment systems. This also implies that aftertreatment systems like the three-way catalytic converter cannot be effectively used with diesel engines [3].

In order to enable aftertreatment operations, diesel engines commonly use an amount of supplemental energy to raise the otherwise relatively low exhaust temperature internally in the engine. However, this commonly results in lowering the engine thermal efficiency that is obviously characterized with the very rise in exhaust temperature [3]. Also, the transient thermal response of the aftertreatment devices is inevitably affected by the configurations of the exhaust pipes that include the pipe structure, the wall thickness, and the exterior thermal management. The exhaust gas temperature at the inlet of the aftertreatment responds at a much slower rate due to the exhaust pipe plenums that can effectively dump and delay the exhaust temperature spikes generated inside the engine [4]. Additionally, the amount of thermal energy loss to the environment along the exhaust pipe is commonly substantial, resulting in a considerably lower exhaust temperature at the inlet of the aftertreatment devices compared to the temperature of the engine-out exhaust [5].

A possible means of improving the performance of the aftertreatment devices is to address the engine and the exhaust aftertreatment technology together as one system. This includes managing the thermal characteristics of the exhaust gas from in-cylinder combustion, together with reducing the heat energy loss from the exhaust piping to shift the exhaust gas condition to favourable windows for aftertreatment operation.

The research work presented here attempts to quantify the thermal response of the in-cylinder combustion measures and the exhaust pipe plenums, and their effects on the exhaust gas temperature at the inlet of the aftertreatment devices. The measurement and modelling of the dynamic thermal response in this research intend to improve the performance of diesel aftertreatment devices.

1.1. OVERALL PICTURE OF RESEARCH

The overall picture of this research consisting of theoretical and experimental investigations of the thermal response analysis is shown in Figure 1.1.
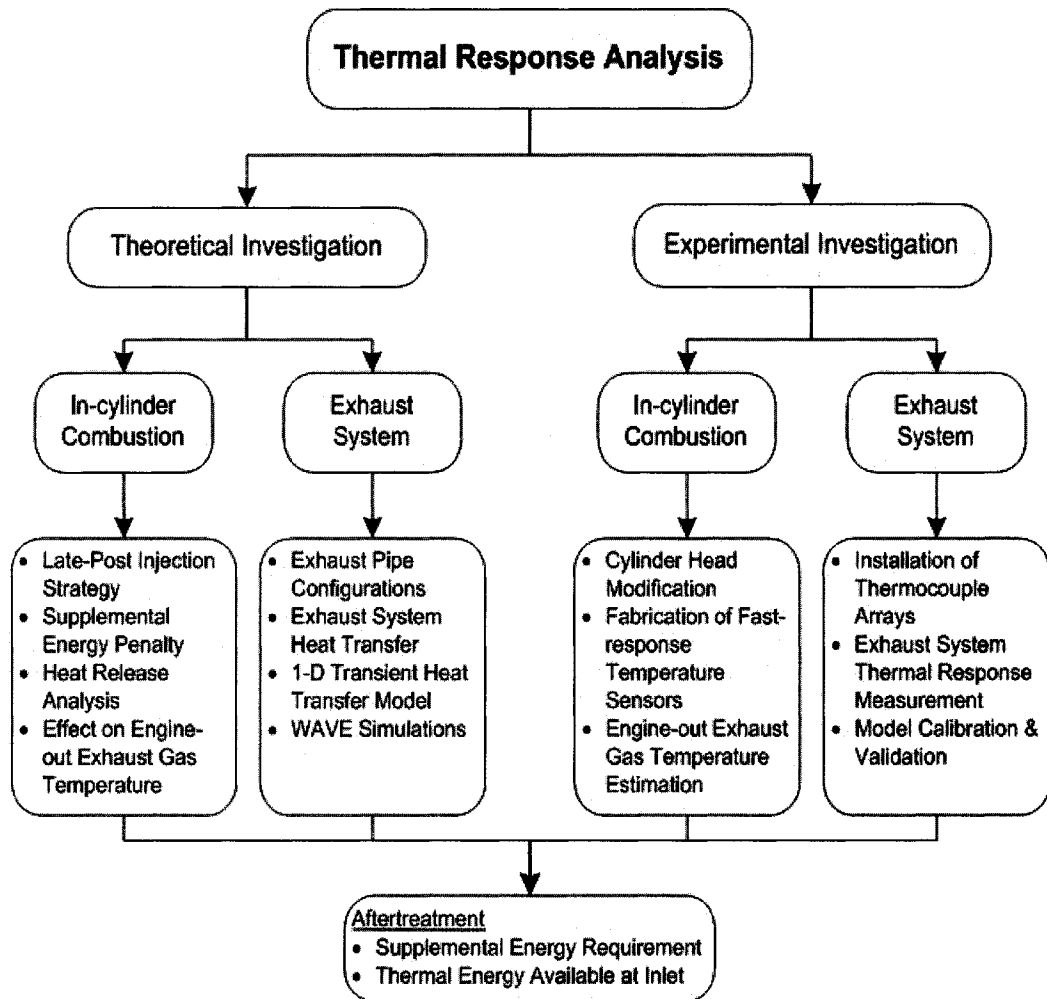
Figure 1.1: Overall Picture of Research

1.2. THERMAL RESPONSE ANALYSIS

If one considers a control volume around a diesel engine, it is apparent that roughly 33 percent of the energy of the fuel into the engine is available in the exhaust gas [1]. Utilization of this otherwise wasted exhaust gas energy is crucial for the satisfactory performance of diesel aftertreatment devices. Moreover, since supplemental energy may be added inside the engine for the aftertreatment, the

3

thermal management of the exhaust gas even before it leaves the combustion chamber is deemed necessary. This means maintaining the high efficiency of the diesel combustion along with reducing the thermal energy loss from the exhaust system.

The in-cylinder thermal response is principally difficult to quantify and previous research has focused mainly on improving the thermal response of the exhaust system. However, to maximize the efficiency of the aftertreatment with minimum energy penalty, the transient thermal response analysis from in-cylinder combustion to the exhaust aftertreatment is required. This can provide a reasonable estimate of the total energy that is available at the exhaust valve and the energy that can be made available at the inlet of the aftertreatment devices. It can also aid in significantly reducing the energy penalty associated with aftertreatment operation. Figure 1.2 provides an overview of the thermal response analysis.

In-cylinder	**Exhaust Plenum**	**Aftertreatment**
• Energy penalty with supplemental energy for aftertreatment • Reduced engine thermal efficiency	• Thermal energy loss through heat transfer to the environment • Dumps and delays the energy spikes from the engine	• Low efficiency • Low exhaust gas temperature at inlet • High supplemental energy requirement

Thermal Response Analysis

• Minimize the energy penalty • Manage the engine-out exhaust temperature	• Reduce heat loss from the exhaust • Improve the thermal response to engine transients	• Higher temperature at inlet • Reduce supplemental energy requirement • Improve performance

Figure 1.2: Overview of the Thermal Response Analysis

4

1.3. OBJECTIVES

The principal objective of the work described in this thesis was to perform a thermal response analysis from in-cylinder combustion to the exhaust aftertreatment devices for improving the performance/efficiency of the engine and aftertreatment devices.

The main steps of the research were to:

(1)   Modify a laboratory engine cylinder head to enable in-cylinder measurements.

(2)   Measure the in-cylinder pressure and temperature to analyze the combustion process and to estimate the engine-out exhaust gas temperature.

(3)   Simulate the effect of supplemental fuel injection timing on the engine-out exhaust gas temperature and to assess the energy penalty associated with supplemental fuel injection.

(4)   Develop a one-dimensional transient heat transfer model for automotive exhaust systems.

(5)   Simulate and study the thermal response of the exhaust system for various configurations.

(6)   Conduct the verification experiments for calibrating and validating the exhaust system thermal response simulation results.

(7)   Implement a combustion heat-release model and temperature prediction model for carrying out real-time analysis.

(8)   Characterize the thermal response of the overall system.

5

2. LITERATURE REVIEW

2.1. DIESEL COMBUSTION PROCESS

In compression ignition (CI) engines, the intake air drawn into the cylinders, is compressed to very high compression ratios while its temperature typically increases to 600~900°C [2]. Combustion is initiated by auto-ignition of the diesel fuel injected shortly before the end of the compression stroke, as the piston approaches the top-dead-centre (TDC). The resulting combustion process is highly heterogeneous and is dominated by diffusion controlled processes [6].

The overall diesel combustion process, from the commencement of the fuel injection can be divided into the several stages which are shown graphically on the typical rate of heat release diagram for a diesel engine in Figure 2.1.
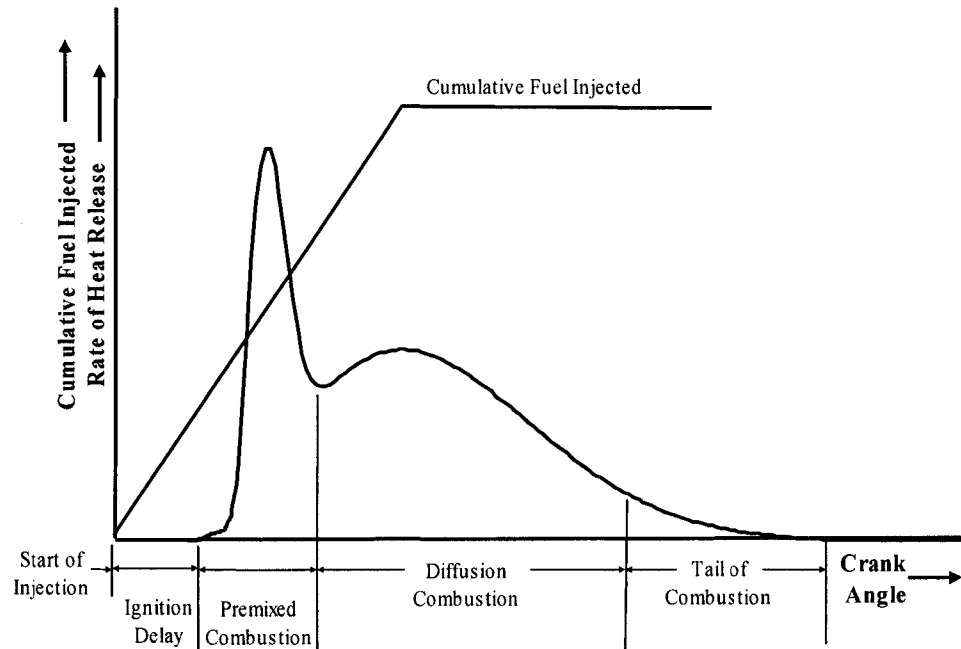
Figure 2.1: Typical Rate of Heat Release Diagram [7]

The ignition delay is the time between the start of fuel injection and the start of combustion. The duration of this delay is related to the time needed for evaporation and mixing of the fuel and air to within flammability limits (physical delay) and the chemical delay time, which depends on the pressure and temperature fields within the combustion chamber. The actual combustion can be divided into

6

three phases: the premixed phase, the mixing-controlled phase and the late combustion phase. During the premixed phase that lasts for a few crank angle degrees, there is a rapid burning of the fuel-air mixture in regions that are close to stoichiometric, resulting in a rapid rise in cylinder pressure. Once the near-stoichiometric fuel-air mixture prepared during the ignition delay period has been consumed, the rate of combustion or heat release is controlled by the preparation rate of the fuel vapour-air mixture. During this mixing-controlled combustion phase, the ignition delay is much shorter, due to the higher cylinder pressure and gas temperature. The major controlling factor is the ability of the fuel to find oxygen. The late combustion phase, also referred to as the tail of combustion, occurs well into the expansion stroke. The rate of combustion is typically low as most of the fuel and oxygen have already been consumed, and depends on the mixing of combustible residuals with excess oxygen. The energy present in soot and fuel-rich combustion products may also be released during this phase [1, 7]

2.2.   DIESEL EXHAUST EMISSIONS

Internal combustion engines emit the same basic types of emissions regardless of the type of fuel or combustion cycle used. Only the relative quantities of each emission type vary with the type of engine. The regulated emissions of diesel engines are carbon monoxide (CO), unburnt hydrocarbons (HC), NOx and PM. HC and CO emissions of a Diesel are typically very low, but PM and NOx may be produced in significant quantities [2].

2.2.1.   CO & HC Emissions

CO and HC are the result of incomplete combustion of the injected fuel, that is, the fuel carbon has not been completely oxidized to carbon dioxide (CO_2) producing CO as the intermediate product, while HC originates from unburned or partially burned fuel. CO and HC emissions represent the unused fraction of the fuel's chemical energy and are a measure of the combustion inefficiency [1]. If one does a control volume around the engine, with the reactants

(fuel and air) flowing into the control volume and the products (exhaust gases) flowing out, the combustion efficiency can be given by:

$$\eta_c = \frac{H_R(T_A) - H_P(T_A)}{m_f Q_{LHV}}$$

(1)

where

H_R	=	Enthalpy of reactants (J)
H_P	=	Enthalpy of products (J)
T_A	=	Ambient Temperature (K)
m_f	=	Mass of fuel injected (kg)
Q_{LHV}	=	Lower heating value of fuel (J/kg)

In Equation (1), the inefficiency is given by the enthalpy H_p of the products of combustion, and is based on the HC, CO and PM concentrations. Diesel engines which generally operate with an overall lean air-fuel ratio, produce very small amounts of CO and HC. Therefore, the combustion efficiency for diesel engines is normally very high (about 98 %).

2.2.2. PM & NOx Emissions

While the performance of diesel engines is quite good with respect to the emissions just described, diesel combustion inherently tends to produce significant quantities of PM and NOx. Diesel's compression combustion process results in very high in-cylinder temperatures which tend to generate more NOx than the less efficient, spark-ignition engines. The heterogeneous nature of diesel's air-fuel mixture causes low levels of oxygen around individual fuel droplets in the combustion zone. This prevents complete burning of the diesel fuel which results in emission of soot (unburned carbon particles from the fuel) also known as PM [2].

> *"The reduction of both PM and NOx simultaneously presents a unique emission control challenge: some techniques used to control one of these pollutants increase the production of the other. For example, a major technique to reduce PM is to cause more complete combustion of the fuel. This reduces PM but also produces more heat, conflicting with the goal of lowering combustion temperatures to reduce NOx. The technical challenge of emission reduction is to reduce both PM and NOx at the same time, without degrading the overall performance of the system" [2].*

8

2.2.3. CO_2 Emissions

Although CO_2 is not a pollutant regulated by the United States Environmental Protection Agency (EPA), CO_2 is a greenhouse gas and is believed to be a key factor in the global warming process. CO_2 emission is closely related to the overall fuel consumption. Modern diesel engines with a high fuel efficiency (overall lean of stoichiometric operation) are low in emissions of CO_2 [2].

2.3.   EMISSION REGULATION

In the year 2000, the EPA established a comprehensive emission regulation for heavy-duty diesel vehicles to be implemented in 2007 [8]. It includes two components: emission standards, and diesel fuel regulation [9]. The first component of the regulation introduces new, very stringent emission standards as summarized in Table 2.1.

Table 2.1: Emission Standards for Heavy-Duty Diesel Engines Model Year 2007 and Beyond (Adapted from [9])

		Standard (g/bhp-hr)	Phase-In By Model Year			
			2007	2008	2009	2010
Diesel	NO_x	1.20	100 %	100 %	100%	–
		0.20	–	–	–	100 %
	NMHC	0.14	50 %	50 %	50 %	100 %
	PM	0.01	100 %	100 %	100 %	100 %

The PM emission standard will take full effect in the 2007 heavy-duty engine model year. The non-methane hydrocarbon (NMHC) standard will be phased in for diesel engines between 2007 and 2010. The phase-in would be on a percent-of-sales basis: 50% from 2007 to 2009 and 100% in 2010. These standards are based on the use of high-efficiency catalytic exhaust emission control devices or comparably effective technologies. The crankcase emission control exemption, allowed earlier for turbocharged heavy-duty diesel engines has also been eliminated. Crankcase emissions from these engines are now added to other

9

exhaust emissions and must be controlled by either routing them back to the engine intake or to the exhaust stream, upstream of the exhaust emission control devices [9].

The diesel fuel regulation requires the sulphur content of on-highway diesel fuel to be capped at 15 parts per million (ppm) by weight, down from the previous 500 ppm. Highway diesel fuel sold as low sulphur fuel must meet the 15 ppm sulphur standard after July 15, 2006 [9,10].

> *"Ultra low sulphur diesel fuel has been introduced as a "technology enabler" to enable the use of advanced, sulphur-intolerant exhaust emission control technologies, such as catalytic diesel particulate filters and oxides of nitrogen (NOx) catalysts, which will be necessary to meet the 2007 emission standards." [9]*

A survey of the literature with regards to current diesel in-cylinder emission control strategies such as EGR, variable valve timing, suggests that these technologies alone may not be able to reduce emissions below the required 2007 levels. Therefore, diesel engines will need to utilize aftertreatment devices to meet the new emission standards.

2.4. AFTERTREATMENT DEVICES

The three-way catalytic converter (TWC) has been widely used with spark-ignition engines for the past 2 decades. It can simultaneously remove NOx, CO and HC from the exhaust stream with high conversion efficiencies. This is achieved by operating the engine in a narrow range of air-fuel ratios near stoichiometric. However, outside the narrow air-fuel ratio window of operation, the conversion efficiency reduces considerably on both rich- and lean-side of stoichiometry. This implies that devices such as the TWC cannot be effectively used with diesel engines that operate lean of stoichiometric composition.

As a result, a number of different devices are being researched for use with diesel engines. For PM control, DPFs are being targeted. The DPF consists of a wall-flow filter which physically traps the soot particles as the exhaust gases flow through the flow channels blocked at alternate ends. Collected particulates have to be removed from the filter, continuously or periodically, through thermal

10

regeneration, that is, by burning or oxidizing the particulate in the filter at sufficiently high temperatures [10, 11].

A number of devices are being investigated for NOx reduction. These include the Selective Catalytic Reduction (SCR), Lean NOx Catalyst, and LNT (also known as NOx Adsorber). The SCR works by injecting a reducing agent (typically ammonia) into the exhaust gas stream before the catalyst. As the exhaust gases, along with the reducing agent, pass over a catalyst coated substrate, NOx is reduced to nitrogen. Frequently, urea is used as the source of ammonia and such systems are called Urea SCR systems. The lean NOx Catalyst requires a diesel post-injection in the exhaust stream to add HC which act as a reducing agent. The LNT temporarily adsorbs or stores the exhaust NOx in the system during lean exhaust environment. A fuel-rich exhaust is then produced either by adjusting the engine operation or by a diesel post-injection to catalytically reduce the stored NOx. The efficiency of all these devices ranges from low at low temperatures to above 90% at high temperatures.

Several other devices such as the Diesel Oxidation Catalyst (DOC), sulphur traps may be used in conjunction with the above mentioned devices. A typical example is the continuous-acting catalytic DPF which utilizes a DOC in front of the filter to generate nitrogen dioxide. The nitrogen dioxide is then used for oxidation of the accumulated soot.

2.5. CHALLENGES FOR DIESEL AFTERTREATMENT

There are a number of challenges for use of the aftertreatment devices in diesel engines. Unlike the spark-ignition (SI) engines where the exhaust temperature is relatively high and within the temperature window for catalyst reactions, the exhaust from diesel engines is generally low and outside the optimum temperature range. This can especially be a problem during cold starts, where the requirement of rapid heating up of the catalyst may not be satisfied by the low temperature exhaust, causing problems with catalytic light-off. This is compounded by the fact that the EPA emission test cycles include transient cold test starts.

Suitable chemical composition in the exhaust is also required for these aftertreatment devices to perform efficiently. The Urea SCR and LNT systems, for example, provide better conversion efficiency when nitrogen dioxide (NO_2) is present in the exhaust instead of nitric oxide (NO). However, the quantity of NO_2 in the diesel exhaust is small, accounting for only 10-30% of the total oxides of nitrogen emitted by the engine [1].

A major difficulty with the satisfactory use of these devices with diesel engines is the abundance of oxygen in the exhaust. The LNT requires a periodic oxygen-deficient environment for conversion of the stored NOx to nitrogen and oxygen, and recovery of the NOx storage sites. Diesel exhaust normally contains 4~20% of oxygen. The minimum exhaust oxygen for naturally aspirated engines can be 4~5% and for turbocharged engines around 6~8%. This implies that an oxygen-deficient environment has to be artificially produced for enabling reduction of NOx. This can be achieved either through a late injection of fuel inside the cylinder during the blowdown phase or using a secondary fuel injector in the exhaust pipe for direct fuel injection near the entrance of the LNT device. Both these options require complex control strategies and accurate calibration to minimize the loss in fuel economy from the use of extra fuel.

The aftertreatment devices also require periodic high exhaust temperatures for the desulphation process. The sulphur present in the diesel fuel can contaminate the catalysts and deactivate them. For example, sulphur oxides are adsorbed in the LNT, thereby reducing the number of available sites for NOx storage. In a DOC, the formation of sulphur dioxide increases at temperatures above 400°C, resulting in lower conversion efficiency [12]. To recover the efficiency of these devices, the substrate temperature has to be increased until the sulphur is released from the catalyst surface. This occurs at high temperatures, greater than 600°C for an LNT (13), and may lead to deactivation of the catalyst itself.

To regulate the TWC operation, lambda sensors are typically placed before and after the converter to sense any unburnt oxygen in the exhaust. These provide the necessary feedback to the engine controller for managing the air-fuel ratio slightly lean or rich of stoichiometric. However, aftertreatment devices for diesels

require an accurate knowledge of the air-fuel ratio to enable control of the exhaust oxygen which cannot be provided by current lambda sensors. Moreover, exhaust NOx sensors are also needed to estimate the LNT storage capacity and subsequently, the requirements of the regeneration phase. Currently, oxygen sensors known as lean-lambda sensors, are being produced that can provide feedback on the actual air-fuel ratio. NOx sensors are also being developed for diesel aftertreatment. However, issues of durability, aging, stability etc. need to be resolved before such sensors can be effectively used.

2.6. THERMAL RESPONSE

2.6.1. In-cylinder

Measured cylinder pressure traces can provide an insight into the combustion process in a diesel engine. The thermodynamic analysis of this pressure data over the compression and expansion strokes can be effectively used to quantify the combustion parameters that include the indicated mean effective pressure (IMEP), the rate of heat-release, maximum rate of pressure rise etc. For diesel engine combustion studies, one common approach is the calculation of the rate of heat release with the units of joules/degree. The rate of heat release is a very important parameter since this may have a very significant influence on combustion noise, pressure rise rate and NOx emissions [1,14].

When complicated commercial indicating equipment for combustion is not available, heat release analysis is usually performed offline from the cylinder pressure data recorded during experiments. However, this might prove to be inadequate in circumstances where in-cylinder post-injection strategy is employed for enabling diesel aftertreatment. A means of performing the heat-release analysis in real-time is necessary to provide feedback on the effectiveness of the post-injection.

The measurement of the engine-out exhaust gas temperature can directly show the temperature raise-ability of the in-cylinder post-injection. In SI engines, the end-gas temperature measurements inside the cylinder have been

13

widely carried out with infrared and laser diagnostic techniques like Coherent Anti-Stokes Raman Spectroscopy (CARS) [15]. This requires small optical windows in the combustion chamber and a host of complicated equipment for managing the high-intensity laser beams. This technique however, is difficult to apply to diesel engines because of the dissimilar nature of the diesel combustion process. The diffusion-controlled diesel combustion process produces a significant quantity of soot which can quickly block the optical access and induce large errors into the measurements.

Thin-wire resistance thermometers and fine-wire thermocouples have been used for measuring the rapidly fluctuating exhaust gas temperatures in the exhaust pipe [16, 17]. However, their use for in-cylinder temperature measurements is extremely difficult due to a number of reasons. First is the difficulty in gaining direct access to the combustion chamber of a diesel engine. The valves and the diesel fuel injector generally leave little space for probes to be installed through the cylinder head. Secondly, the probe assembly must be able to withstand the high combustion temperatures and also effectively seal the combustion chamber and the water jackets in the cylinder head. Moreover, the life span of the thermocouple probes under such conditions can be very short (up to a few seconds) and hence requires frequent replacement as well as special manufacturing techniques. Thermocouples have been generally used in rapid compression machines which have a lower compression ratio and provide direct access to the combustion chamber. When put in actual engines, their use is generally limited to heat flux measurements under motored engine conditions. As such, there is no simple solution reported in the text for carrying-out the in-cylinder gas temperature measurements.

2.6.2. Exhaust System & Aftertreatment

The heat transfer in automotive exhaust systems has frequently been modelled using empirical correlations for fully developed flow in straight pipes. Konstantinidis and co-workers [18] developed a transient heat transfer model for different configurations of the exhaust pipes (single wall, double wall with air gap

or insulation) and illustrated its application in the comparative assessment of different exhaust configurations for gasoline engines. They used the exhaust gas temperature, measured at the inlet of a straight section of the exhaust pipe as the input to the model and predicted the gas temperature at the inlet of the TWC, 500 mm downstream. Chan et al. [20] also employed a similar approach to model the thermal response of the exhaust gas during the engine cold-start phase. Moreover, they included the chemical reactions inside the TWC to predict the emissions downstream of the converter. The input to the model was again the gas temperature measured at the exhaust port.

The use of measured gas temperature at any point along the exhaust system as input to the heat transfer model has certain disadvantages, the first and foremost being the inability of such models to accurately predict the actual gas temperature at any location. Thermocouples due to their thermal inertia take five of their time-constants to approach 100% of the step change value. Therefore, this methodology may not be able to accurately estimate the delay caused by the exhaust system thermal response to temperature spikes generated during engine transients. Secondly, when in-cylinder combustion measures like the effect of post-injection on the exhaust temperature have to be analyzed, it may be necessary to estimate the engine-out exhaust gas temperature either numerically or empirically and use that as the input. This will ensure that the thermal response analysis characterizes the actual engine processes.

For diesel aftertreatment modelling, the thermal characteristics of aftertreatment devices have commonly been investigated by ignoring the thermal response of the exhaust system. The common approach is to use the temperature measured at the inlet of the device as the input [22]. This approach is suitable as long as the aftertreatment device is analyzed in isolation. However, when diesel aftertreatment operations are enabled with in-cylinder combustion and post injection measures, the exhaust plenum may significantly affect the performance of the aftertreatment systems. Hence, any analysis of the aftertreatment should invariably include the thermal response of the exhaust system.

3.   IN-CYLINDER COMBUSTION

Since diesel combustion is generally lean and essentially quality controlled, that is, the fuelling rate determines the load, the exhaust temperature is generally low and varies widely. This implies that aftertreatment operations like thermal regeneration of a DPF may not be possible under all engine conditions. To raise the exhaust temperature, a temperature spike can be generated in the engine by increasing the fuelling rate. Conversely, the in-cylinder post injection is an effective way to raise the exhaust temperature and/or to supply the combustible substances to the aftertreatment substrates as shown in Figure 3.1. The exhaust gas temperature management at low exhaust gas temperatures is important to achieve higher efficiency of the diesel aftertreatment systems.
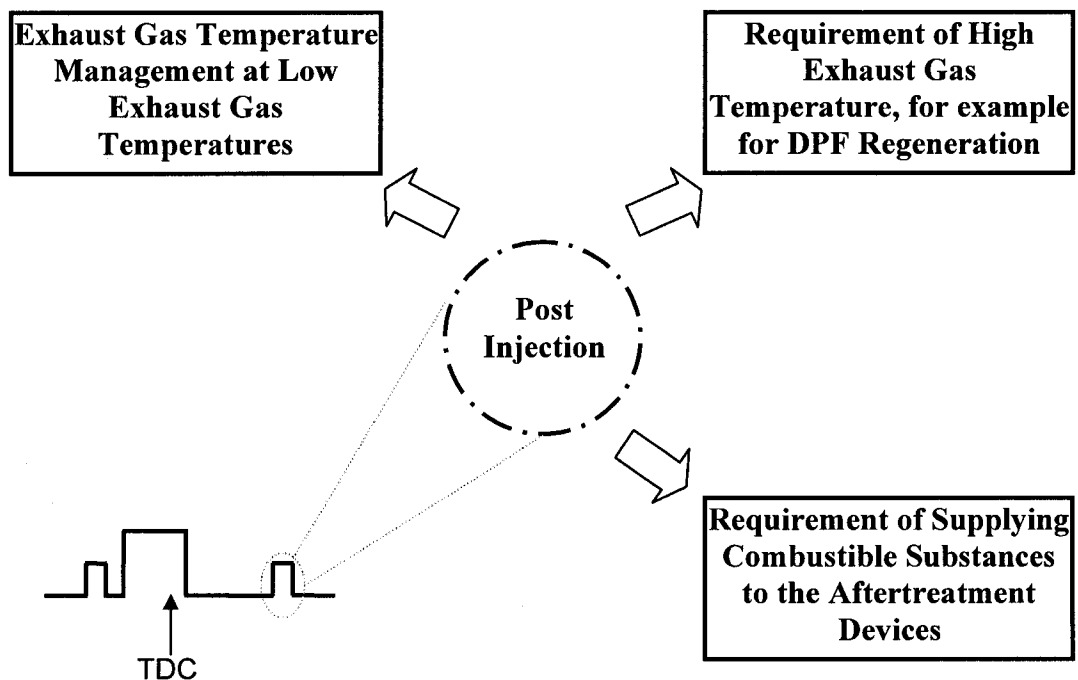
Figure 3.1: Purpose of Late Post Injection (Adapted from [21])

16

3.1. STUDY OF POST-INJECTION STRATEGY

To investigate the thermal characteristics of the post injection strategy for aftertreatment operation, theoretical investigations were carried out using Ricardo's WAVE software (Ricardo, UK). The engine model of WAVE is a time-dependent simulation of in-cylinder processes, solved using equations for mass and energy. The mass balance equation accounts for changes in the in-cylinder mass due to intake and exhaust flows and also due to fuel injection. The energy equation is based on the first law of thermodynamics and balances the change in internal energy of in-cylinder gases to the sum of enthalpy fluxes in and out of the cylinder, heat transfer and work done by the piston.

3.1.1. Effect of Injection Timing on Exhaust Gas Temperature

The supplemental fuel injection timing can have a significant impact on the exhaust gas temperature and the energy penalty associated with it. A simulation was setup for a single cylinder diesel engine to study the effects of injection timing on the exhaust gas temperature and the energy utilization ability of the post-injection. The engine specifications used in the simulation were similar to the actual engine used for experimental investigation and are given in Table 3.1:

Table 3.1: Simulated Engine Specifications

Type	Single Cylinder, 4 Stroke, Diesel
Bore	102 mm
Stroke	105 mm
Displacement	0.857 Litres
Compression Ratio	17.8:1
Connecting Rod Length	178 mm
No of Valves	2
Main Injection Timing	5 ° BTDC
Post Injection Timing	10 ~ 150 ° ATDC
Engine Speed	1200 ~ 1500 rpm

17

The simulations were first configured for constant engine power output. The main injection timing was fixed at $5°$BTDC and the post-injection timing was shifted from $10°$ATDC to $150°$ATDC. The power was kept constant by increasing the fuel quantity of the main injection pulse to compensate the power loss caused by the delay of the fixed post fuel quantity. If the logarithm of the cylinder pressure is plotted against the logarithm of the cylinder volume, the effect of the late post-injection on the exhaust temperature for the same power output can be clearly identified as shown in Figure 3.2.
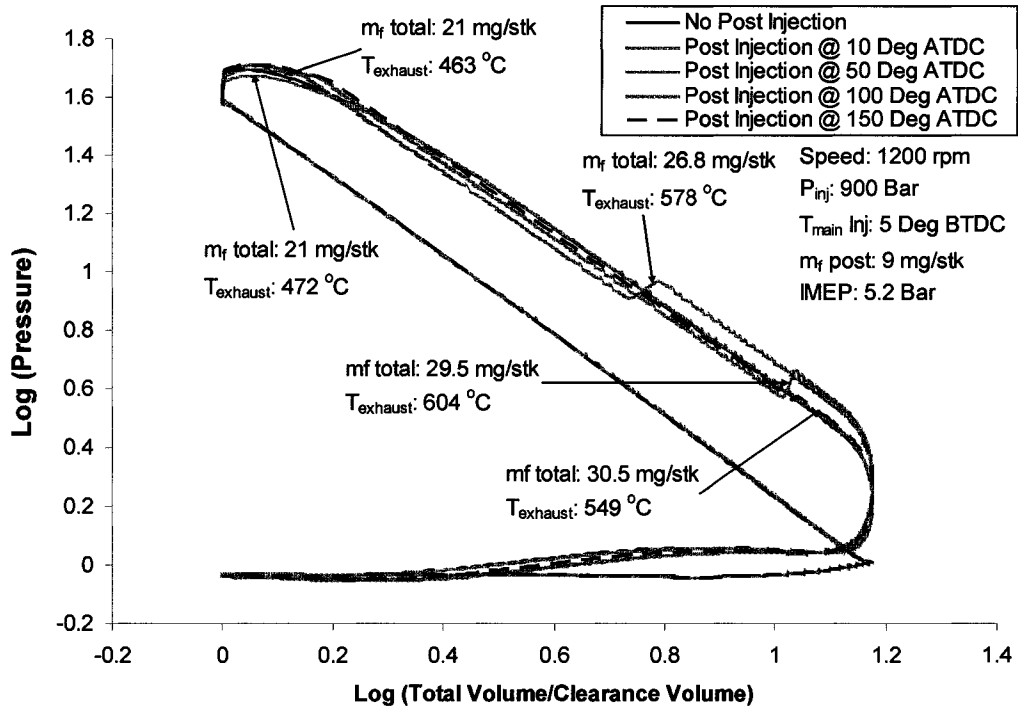
Figure 3.2: Effect of Post Injection Timing on Exhaust Gas Temperature (Constant Power)

The modelling results indicate that as the post fuel injection is progressively delayed, there is a trade off between the energy recovery and the exhaust temperature rise. When post injections commence near the end of the expansion stroke, the exhaust valve has already started to open and due to the high compression ratio of diesels, the average cylinder temperature is quite low; hence the effectiveness of the post-injection to raise the exhaust temperature may decrease significantly.

18

In this research, the position or timing of the in-cylinder post injection pulses has been classified into the following three categories:

Table 3.2: Proposed Classification of Post Injection Timing

Post Fuel Injection Timing	Capability	
	Produce Power	Raise T_{exh}
early	high	low
mid	medium	high
late	low	medium

Simulations were also carried out on the same energy and same engine-out exhaust temperature basis to analyze the fundamental effects of post-injection on diesel combustion. For the same energy simulations, the aim was to estimate the maximum temperature raising potential of the post-injection. The total fuel injection quantity was kept constant while the post-injection timing was retarded from TDC. The main- and the post-injection quantities were equal and user-defined burn profiles were input to ensure complete combustion of the post-injection. As the post-injection was delayed, the temperature raise-ability increased with a corresponding decline in power as shown in Figure 3.3.
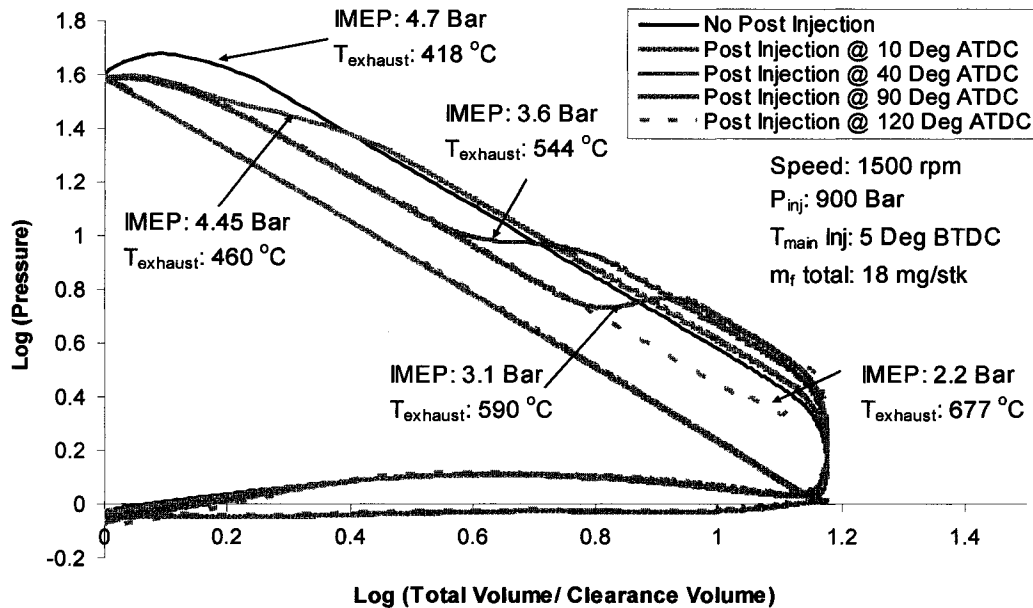
Figure 3.3: Same Energy Results for Different Post-injection Timing

19

For the same engine-out exhaust temperature simulations, the target temperature was set at 430°C, equivalent to a typical mid-load diesel exhaust temperature. The injection quantities for both the injections were adjusted as the post injection was retarded to achieve the target temperature. The results are shown in Figure 3.4. It can be seen that that the injected fuel quantity slightly decreased as the post-injection timing was retarded. The power output also decreased significantly, indicating the low energy utilization ability of the late-post injection.
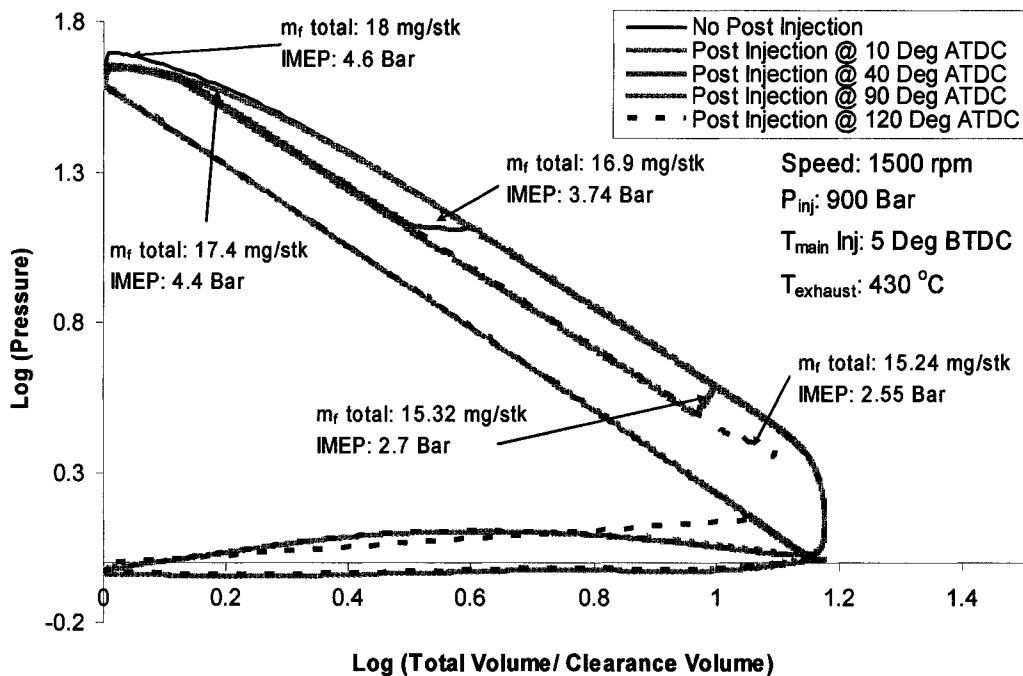
Figure 3.4: Same Energy Results for Different Post-injection Timing

The early post injection is very effective to produce power owing to the almost unaffected cylinder effective expansion ratio after the post fuel pulse catches fire. However, the temperature raise-ability is minimal. The mid post injection, especially the late-mid post, has the strongest effect to raise the engine exhaust temperature, while its power production capability is compromised by the reduced effective cylinder expansion ratio of the post flame. The late-post injection has little power production capability because of the minimum effective expansion ratio. The ΔT_{exh} effect can be significant under high load engine operations that

20

have a high cylinder charge temperature at the time of the post injection. Under low load operations, however, the late post may not get ignited thus the fuel supplied in-cylinder will be passed to the aftertreatment devices downstream [24].

The energy utilization ability reduces as the post pulse is postponed, which can be explained by the effective expansion ratio of the post injection flame. Conversely, the T raise ability peaks at a mid post injection timing as shown in Figure 3.5.
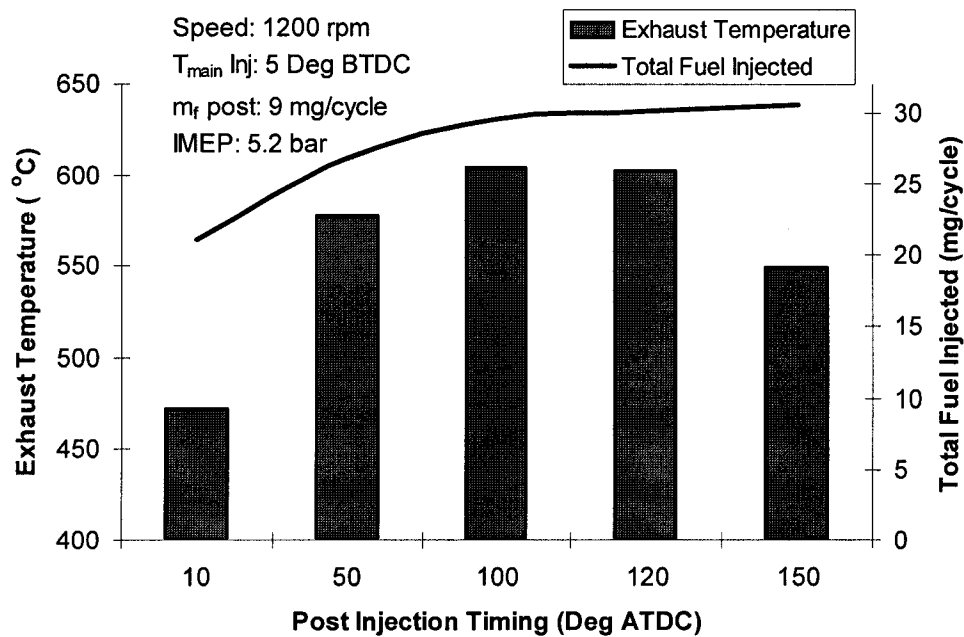
Figure 3.5: Summary of the Post Injection Simulations (Constant Power)

3.2. POST-INJECTION EXPERIMENTS

To verfiy the post injection simulation results, physical experiments were performed on a single cylinder diesel engine with specifications similar to those shown in Table 3.1. Based on the classification of the post-injection timing (Table 3.2), the effect of early, mid and late post injection timings on the exhaust gas temperature were analyzed. The test was configured in such a way that the pilot and main fuel injection quantities and timings were fixed when the post pulse was turned on. The fuel quantity of the post injection was moderated to maintain the same IMEP as the post timing was shifted. A summary of the results is shown in Figure 3.6 on the next page.

21
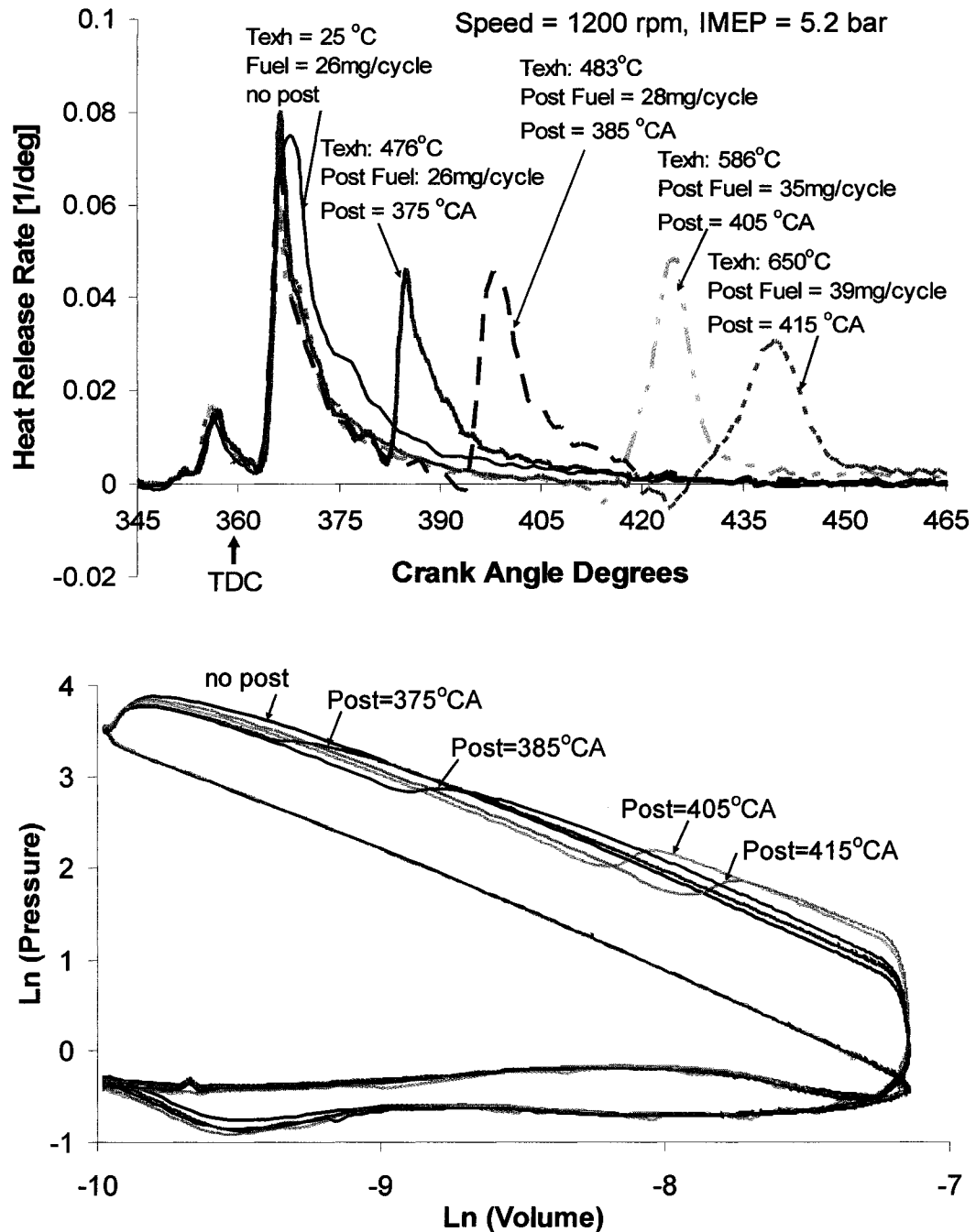
Figure 3.6: The Effect of Post-injection Timing in Raising the Engine Exhaust
Temperature. Upper: Heat Release Rate; Lower: Ln (p) versus Ln (V).

The empirical results also indicated that as the post fuel injection was delayed, there was a trade off between the energy recovery and the exhaust temperature rise [24].

22

3.3. EXPERIMENTAL SETUP FOR IN-CYLINDER MEASUREMENTS

The experimental part of the in-cylinder research focused mainly on designing and setting up the measurement of in-cylinder temperature and pressure. The measurement of in-cylinder pressure and temperature are essential for assessing the quality of combustion. Analysis of cylinder pressure history over the closed part of the engine cycle provides a classical diagnostic for studies of heat release rates and overall combustion efficiency [1]. Exhaust gas temperature measurements can give a better understanding of various engine processes and can help in performance improvement of the catalytic converter [25]. With supplemental fuel being supplied for aftertreatment in the cylinder, it is critical to be able to estimate the engine-out exhaust temperature. Moreover, the in-cylinder measurements can give a fairly good estimate of the energy penalty and the resulting decrease in the combustion efficiency.

Foregoing in view, the cylinder head of a single cylinder diesel engine, manufactured by Yanmar Corporation, was modified so that the direct measurement of the cylinder pressure and temperature could be carried out. The detailed specifications of the engine are given in Table 3.3.

Table 3.3: Engine Specifications for Yanmar NFD 170E

Type	Single Cylinder, 4 Stroke, Diesel
Bore x Stroke (mm)	102 mm x 105 mm
Displacement	0.857 Litres
Compression Ratio	17.8:1
Connecting Rod Length	178 mm
Injection Timing	17 ° BTDC
Intake Valve Opens	7 °BTDC
Intake Valves Closes	45 °ABDC
Exhaust Valve Opens	45 °BBDC
Exhaust Valve Closes	15 °ATDC
Combustion System	Direct Injection
Cooling System	Water Cooled

23

This engine was also used in carrying out the thermal analysis of the exhaust system which is discussed in Chapter 4. The secction of the cylinder head showing modifications is shown in Figure 3.7. The modifications included making holes in the cylinder head, manufacturing of mounting sleeves and dummy sensors. These are explained in detail in the following sections.
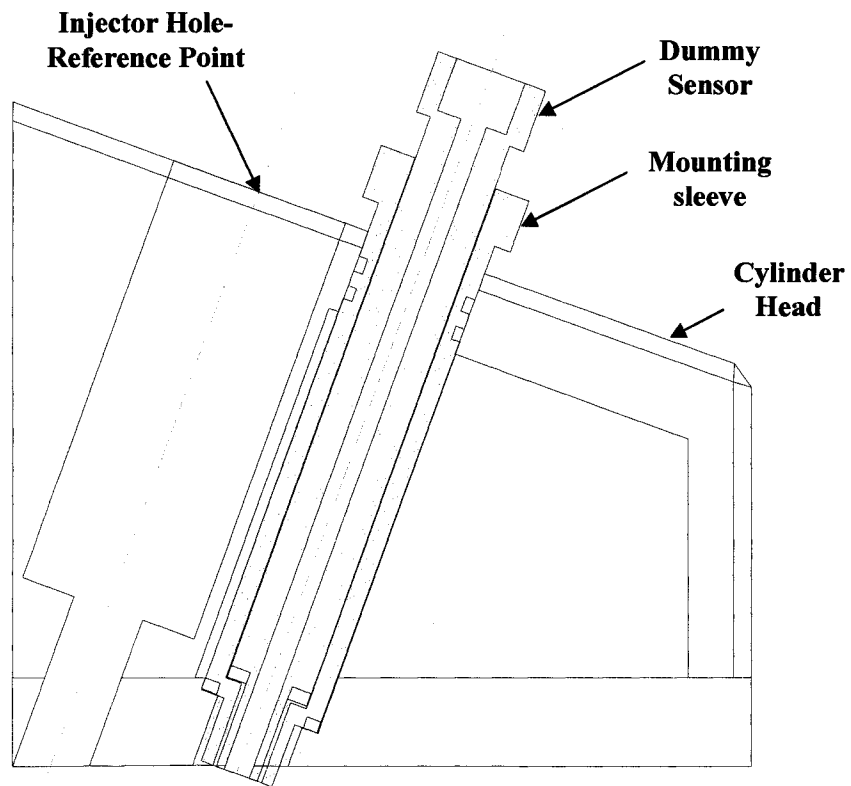
Figure 3.7: Section of the Cylinder Head showing Modifications

3.3.1. Cylinder Head Modification

The cylinder head was modified to allow placement of both the pressure sensor and the thermocouples. For this purpose, two suitable locations were identified on the cylinder head. Besides the availability of space which was dictated by the physical dimensions of the cylinder head, important considerations for selection of the locations included mounting the sensors as close as possible to the combustion chamber and utilizing the cooling jackets for cooling the mounting

24

sleeves/sensors. Two holes were machined for placement of the mounting sleeve as

shown in Figure 3.8.

Figure 3.8: Details of the Cylinder Head Modification

The correct finish of the machined surfaces (indicated in Figure 3.8) is essential for adequately sealing the combustion chamber and the cylinder head water jackets. The surface finish is commonly defined in terms of its roughness values. Roughness consists of surface irregularities resulting from various machining processes and is defined by the International Standards Organization (ISO) standard "DIN ISO 1320:1992" in terms of "N numbers". These numbers or roughness grades correspond to the average roughness values in micrometers or microinches. The N numbers and their equivalent roughness values are given in Table 3.4.

Table 3.4: Surface Roughness Grades

Roughness Values		Roughness Grade	Finish
Micrometers	**Microinches**	**N Numbers**	
50	2000	N12	Rough Machined
25	1000	N11	
12.5	500	N10	
6.4	250	N9	Medium Turned
3.2	125	N8	
1.6	63	N7	Smooth Turned
0.8	32	N6	
0.4	16	N5	Ground Finishes
0.2	8	N4	
0.1	4	N3	
0.05	2	N2	
0.025	1	N1	

When o-rings are used for sealing, a smooth surface finish with a roughness grade of N5 or less is desirable. Therefore, the two holes were finished

26

with jig grinding to achieve the required surface finish. The machined cylinder head is shown in Figure 3.9.
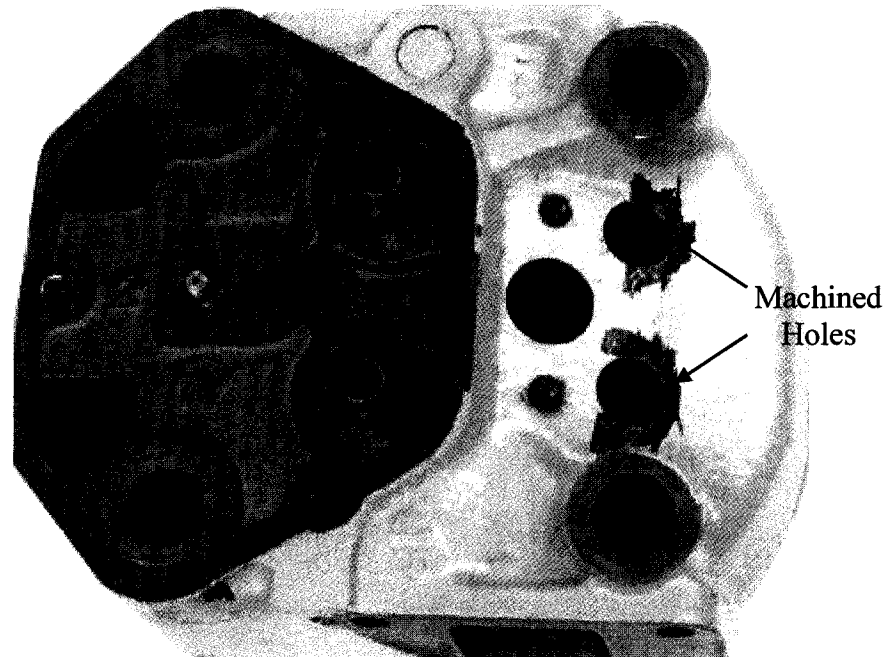
Figure 3.9: Machined Cylinder Head

3.3.2. Mounting Sleeve

Two mounting options exist for the pressure transducer: it can be mounted directly in the cylinder head or a sleeve can be used to mount the transducer. Since it was not possible to avoid passing through the cylinder head water jacket for the hole location, it was decided to install a sleeve for mounting the pressure transducer. This has the advantage that both the sleeve and the sensor are cooled by the coolant flow of the engine. Since such a sleeve was not available from the transducer manufacturer, a mounting sleeve was designed and fabricated. The design of the sleeve was generous so that it could also accommodate adapters for mounting thermocouples or other probes.

The sealing at the combustion chamber end was provided by a bronze seal while o-rings were installed at the other end to seal the water jacket. For ensuring proper sealing with o-rings, the o-ring dimensions and the groove design must fulfil the following requirements. First, the o-ring must be compressed

by a predetermined amount, and this compression determines the o-ring cross-section diameter. Moreover, the groove width must be larger than the o-ring cross-section diameter, to accommodate the radial expansion of the o-ring when it is axially compressed. The correct use of an o-ring is illustrated in Figure 3.10 and the mounting sleeve design along with the manufactured sleeve is shown in Figure 3.11. All dimensions are in millimetres (mm).

O-ring ID = 0.98 x Gd
O-ring CS = (Bd - Gd) / 2
GW ≅ 1.5 x O-ring CS

where
Gd = Groove Diameter
CS = Cross Section Diameter
Bd = Bore Diameter
GW = Groove Width

Groove Width
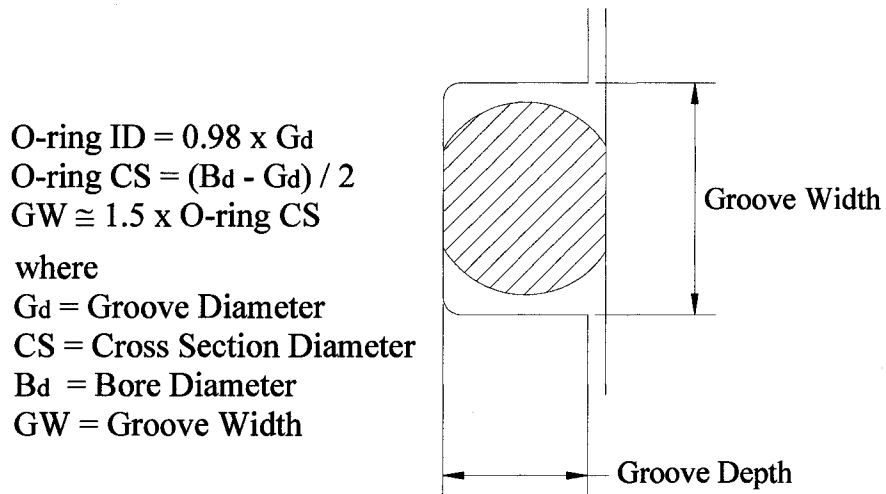
Groove Depth

Figure 3.10: O-ring and Groove Design
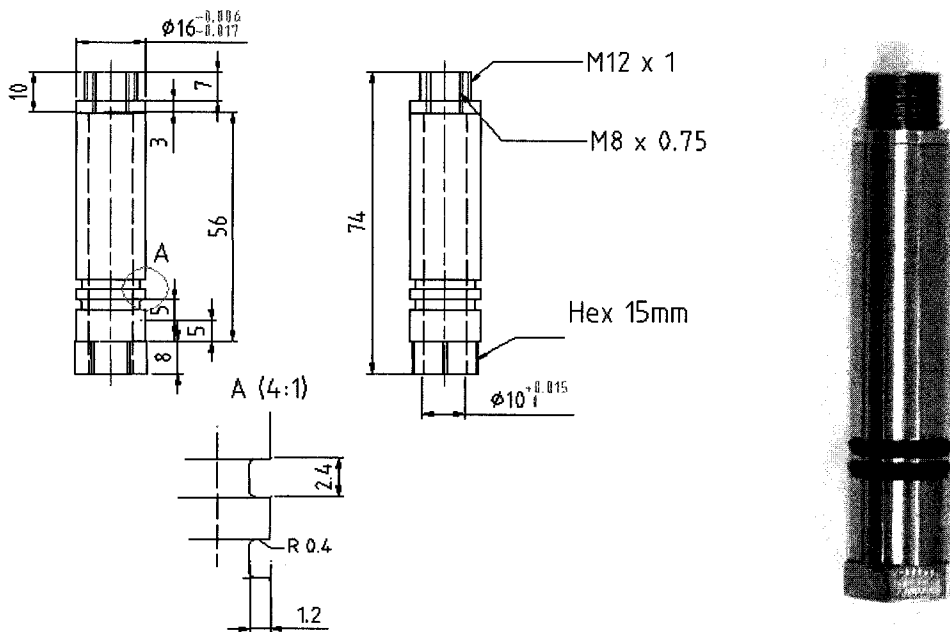
Figure 3.11: Mounting Sleeve

28

3.3.3. Dummy Sensor

To mount the thermocouples, a dummy sensor was designed and fabricated similar to the pressure transducer as shown in Figure 3.12. A 9/64" hole drilled through the dummy sensor, allowed thermocouple probes up to 1/8" thickness to be inserted into the combustion chamber. Standard compression fittings were installed at the top end of the dummy sensor to hold the thermocouple probes in place and provide adequate sealing. Moreover, a dummy sensor (plug) without the centre hole was also fabricated to seal the combustion chamber if and when required. All dimensions are in millimetres (mm).
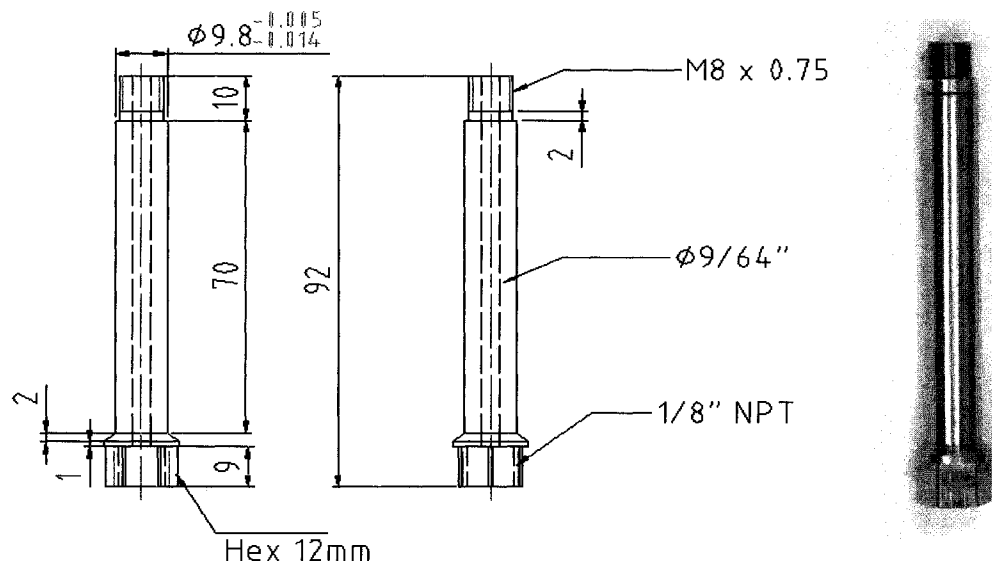
Figure 3.12: Dummy Sensor for Thermocouple Placement

3.3.4. Thermocouple Probes

Bare-wire fine-gauge K-type thermocouples of two different sizes (25 and 127 μm wire diameter) were selected for making the thermocouple probes. To electrically insulate the thermocouple wires and expose only the thermocouple junction to the combustion gases, ceramic insulators with maximum service temperature of 1950°C were used. These insulators, available in two-hole and four-hole configurations were used to construct single- and two-thermocouple probes. The insulator along with the thermocouple wires was housed in 1/8" diameter stainless steel protection tubing and the assembled probe was secured in the

dummy sensor using stainless steel compression fittings. A finished thermocouple probe is shown in Figure 3.13.
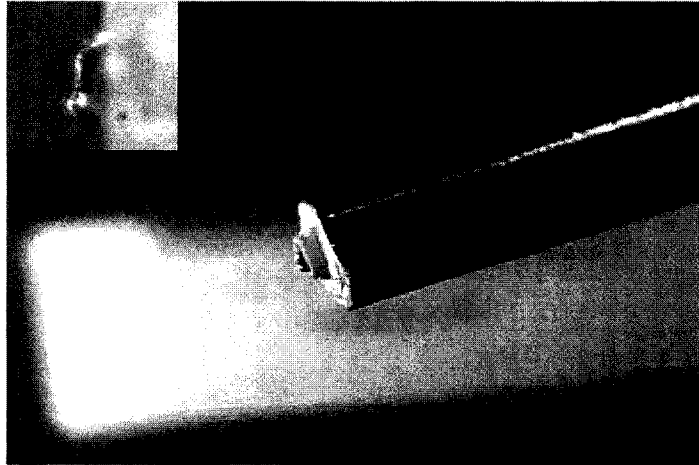
Figure 3.13: Thermocouple Probe (The insert shows the Thermocouple Junction at 100x Magnification)

3.3.5. Assembled Cylinder Head

The existing cylinder head of the Yanmar engine was replaced with the modified head. A piezo-electric pressure transducer was installed in one sleeve while a dummy plug was placed in the other. The new setup was tested for operational stability before the temperature measurements were attempted. The modified cylinder head installed on the engine is shown in Figure 3.14.
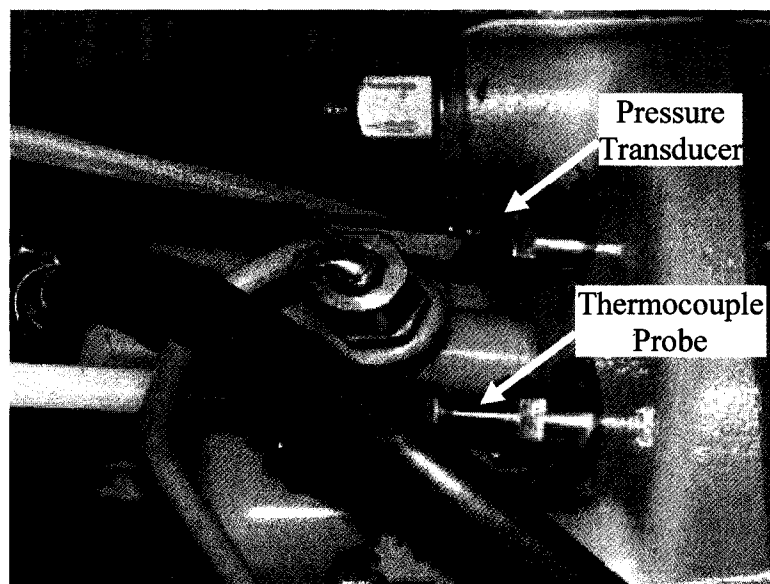
Figure 3.14: Installed Cylinder Head

30

3.4. TEMPERATURE AND PRESSURE MEASUREMENT

Ideally, the instantaneous in-cylinder temperature is needed, so that the transient phenomenon can be observed. However, the accurate measurement of in-cylinder temperature is complicated because of two reasons: first, the temperature varies from about room temperature to around 2000°C every combustion cycle and the frequency of this temperature variation is typically in the order of several kHz. If temperature is to be recorded at a crank angle resolution of 1 degree, the required sampling rate is 6 kHz at 1000 rpm and 10 kHz at 2000 rpm. Second, thermocouples are normally used for measuring time-averaged temperatures and they cannot measure the instantaneous temperature because of their limited dynamic response (typically 0.1 Hz to 10 Hz). Hence, to improve the response of the thermocouples, a two thermocouple temperature reconstruction technique was adapted.

3.4.1. Temperature Reconstruction Technique [25 – 28]

Assuming that the temperature distribution of any cross-section of the thermocouple wire is uniform at any instant, from energy balance, we get

$$T_g - T_{tc} = \underbrace{\frac{\rho_{tc} c_{tc} d_{tc}}{4h} \frac{\partial T_{tc}}{\partial t}}_{\substack{\text{Dynamic} \\ \text{Effect}}} - \underbrace{\frac{k_{tc} d_{tc}}{4h} \frac{\partial^2 T_{tc}}{\partial x^2}}_{\substack{\text{Conduction} \\ \text{Term}}} + \underbrace{\frac{\varepsilon_R \sigma}{h}(T_{tc}^4 - T_{surr}^4)}_{\substack{\text{Radiation} \\ \text{Term}}} \qquad (2)$$

where

T_g	=	gas temperature (K)
T_{tc}	=	thermocouple wire temperature (K)
ρ_{tc}	=	density of the thermocouple wire (kg/m^3)
c_{tc}	=	specific heat capacity of thermocouple wire (J/kg K)
k_{tc}	=	thermal conductivity of thermocouple wire (W/m K)
d_{tc}	=	diameter of the thermocouple wire (m)
h	=	local heat transfer coefficient (W/m^2 K)
ε_R	=	emissivity
σ	=	Stefan-Boltzmann constant (5.67 x 10^{-8} W/m^2 K^4)
T_{surr}	=	Surrounding Temperature (K)

Equation (2) states that the difference between the gas temperature and the thermocouple wire temperature is due to three terms on the right-hand side. The first term is the dynamic effect. Because the thermocouple wire has a finite mass, its temperature cannot follow the changes in gas temperature instantaneously. The second part is the conduction term: the probe support will generally respond to the change in gas temperature more slowly than the wire, so a temperature gradient will exist between the wire and the support, and heat will conduct from or to the wire. The last part of the equation is the radiation term. The surroundings are normally colder than the thermocouple, so heat will radiate from the thermocouple to the surrounding [25]. For thermocouples with high length to diameter ratio, conduction can be assumed negligible. Moreover, since the temperature difference between the exhaust gas and the pipe-wall is mostly less than $400^{\circ}C$, the radiative heat transfer from the thermocouple can also be neglected and Equation (2) can be reduced to

$$T_g - T_{tc} = \tau \frac{dT_{tc}}{dt}$$ (3)

Equation (3) is not strictly true but has been shown to be a good approximation [29,30]. Equation 3 is a first-order differential equation, completely characterized by τ where τ is the time constant defined as

$$\tau = \frac{\rho_{tc} c_{tc} d_{tc}}{4h} = \frac{\rho_{tc} c_{tc} d_{tc}^2}{4 Nu\, k}$$ (4)

In Equation 4, the local heat transfer coefficient h plays an essential role in estimating the time constant and is normally given by a non-dimensional expression for its Nusselt number, Nu.

The temperature reconstruction technique using two fine-wire thermocouples for simultaneous estimation of the thermocouple time constants and the fluctuating temperatures (proposed by Tagawa and Ohta [27]) can be adapted to transient temperature measurements in the internal combustion engine for both in-cylinder gas or the engine exhaust-gas temperature measurement.

This technique involves placing two thermocouples of different thermal inertia as close as possible inside the combustion chamber or the exhaust system in either a parallel or a radial configuration, as shown in Figure 3.15. If T_1 and T_2 are the temperatures of thermocouples 1 and 2, while τ_1 and τ_2 denote time constants of thermocouples 1 and 2, then Equation (3) can be written as

$$\left.\begin{aligned} T_{g1} &= T_1 + \tau_1 \frac{dT_1}{dt} \\[2ex] T_{g2} &= T_2 + \tau_2 \frac{dT_2}{dt} \end{aligned}\right\} \quad (5)$$
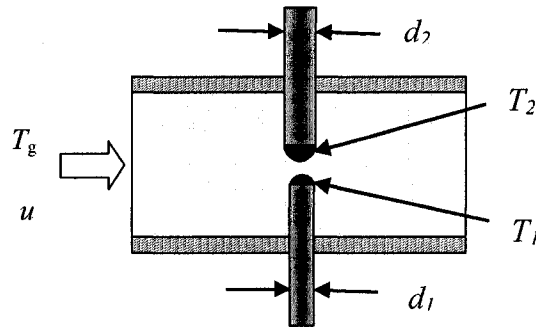
Figure 3.15: Two-Thermocouples in Radial Configuration (Adapted from [28])

Tagawa and Ohta showed that by minimizing the time-averaged difference between the compensated temperatures T_{g1} and T_{g2} using the method of least squares, the time constants $\overline{\tau_1}$ and $\overline{\tau_2}$ become

$$\left.\begin{aligned} \overline{\tau}_1 &= \frac{(\sum G_2^2)(\sum G_1 \Delta T_{21}) - (\sum G_1 G_2)(\sum G_2 \Delta T_{21})}{(\sum G_1^2)(\sum G_2^2) - (\sum G_1 G_2)^2} \\[2ex] \overline{\tau}_2 &= \frac{(\sum G_1 G_2)(\sum G_1 \Delta T_{21}) - (\sum G_1^2)(\sum G_2 \Delta T_{21})}{(\sum G_1^2)(\sum G_2^2) - (\sum G_1 G_2)^2} \end{aligned}\right\} \quad (6)$$

where

$$\sum = (1/N) \sum\nolimits_{i=1}^{N} \qquad \Delta T_{21} = T_2 - T_1$$

$$G_1 = dT_1 / dt \qquad G_2 = dT_2 / dt$$

N is the number of samples per thermocouple in the time interval Δt and superscript i is the sample at the time $i\Delta t$.

33

Having determined the time constants from Equation (6), the temperatures T_{g1} and T_{g2} can be found from Equation (5). The reconstructed temperature may be taken as an average or the reconstruction from the thermocouple with the smaller time constant. This model was programmed in LabVIEW for both in-cylinder and exhaust gas temperature prediction. The temperature and time constant data were concurrently saved to a file. The model was also programmed in 'C' language for offline analysis. The application of the technique to reconstruct the exhaust gas temperature is given in APPENDIX A.

3.4.2. Combustion Heat Release Analysis

Cylinder pressure versus crank angle data can be processed to obtain quantitative information on the progress and quality of combustion. One useful technique is the heat release analysis, which yields the rate of release of the fuel's chemical energy [1]. This can help in determining the combustion efficiency as well as the indicating the effectiveness of the post-injection in raising the exhaust gas temperature for aftertreatment.

The phenomenological "engine heat release" model is based on the First Law of Thermodynamics and encompasses the following assumptions [14, 31]:

(1) Uniform thermodynamic properties and gas composition throughout the combustion chamber; Heterogeneity of the charge is neglected (fuel vapour and products are treated as a mixture of ideal gases)

(2) The apparent heat release process is based on the average properties in a single zone, and thus does not distinguish between burned and unburned zones.

(3) Equilibrium thermo-chemistry is assumed (chemical dissociation is ignored).

(4) The sensible enthalpy from fuel injection is neglected.

34

Based upon these assumptions, the first law for the in-cylinder charge during the period from intake valve closure (IVC) to exhaust valve closure (EVC) for the crank angle interval $d\theta$, can be written as:

$$\frac{dQ_n}{d\theta} = \frac{dQ_{gr}}{d\theta} - \frac{dQ_{ht}}{d\theta} = \frac{dU}{d\theta} - p\frac{dV}{d\theta} \tag{7}$$

where

dU	=	change in sensible internal energy (J)
dQ_{gr}	=	gross heat release due to combustion (J)
dQ_n	=	net heat release (J)
dQ_{ht}	=	heat transfer to cylinder wall (J)
dV	=	change in cylinder volume, and (m^3)
p	=	cylinder pressure (Pa)

Assuming the working fluid as an ideal gas, further equations can be written as follows:

$$\frac{dU}{d\theta} = mc_v \frac{dT}{d\theta} \tag{8}$$

$$p\frac{dV}{d\theta} + V\frac{dp}{d\theta} = mR\frac{dT}{d\theta} \tag{9}$$

$$c_v = \frac{R}{\gamma - 1} \tag{10}$$

where

m	=	trapped mass (kg)
R	=	specific gas constant (287 J/kg K)
c_v	=	specific heat at constant volume (J/ kg K)
γ	=	ratio of specific heats, and
T	=	temperature (K)

Substituting Equations (8) to (10) in Equation (7) gives the apparent heat release rate equation:

$$\frac{dQ_n}{dt} = \frac{1}{\gamma - 1}\left[\gamma\, p\frac{dV}{dt} + V\frac{dp}{dt}\right] \qquad (11)$$

Equation (11) omits the effect of crevice volumes and assumes the charge to be at the same temperature. The cylinder pressure is assumed to be uniform throughout the combustion chamber which is valid for the direct injection diesel engines. Previous research [32 –34] has shown that, with the exception of cylinder charge-to-wall heat transfer, these additional effects are usually small and can be neglected with minimal loss of accuracy. The charge-to-wall heat transfer is also often omitted for simplicity and the heat release thus determined is referred to as the "net" heat release. When heat transfer effects are included, the heat release energy calculated is described as the "gross" heat release. Net heat release values are typically 15% lower than those obtained on a gross heat release basis [1]. Net heat release values are very often used in preference to gross heat release values because this reduces the amount of computation and avoids the need for heat transfer parameters to be specified.

The heat release rate from Equation (11) can either be obtained with constant gas properties or with crank angle-resolved gas properties. Investigation of the effect of temperature-dependent versus constant γ on the heat release rate showed that the general shape of the heat release curve remains the same while the magnitudes of the burn rates would be inaccurate. A comparison with a comprehensive heat release model which accounts for charge-to-wall heat transfer, crevice volume effects etc was also carried out. It was observed that the heat release rate computed from Equation (11) was comparable in terms of the combustion phasing and varied in magnitude to some extent. The results were put into a conference paper which is reproduced in APPENDIX B.

The heat release model described above was programmed in LabVIEW for performing online analysis to study the effect of variation of different combustion parameters on the quality of combustion. Moreover,

36

combustion parameters like peak pressure and position of peak pressure, maximum rate of pressure rise and its position, IMEP & start of combustion were also determined as shown in Figure 3.16.
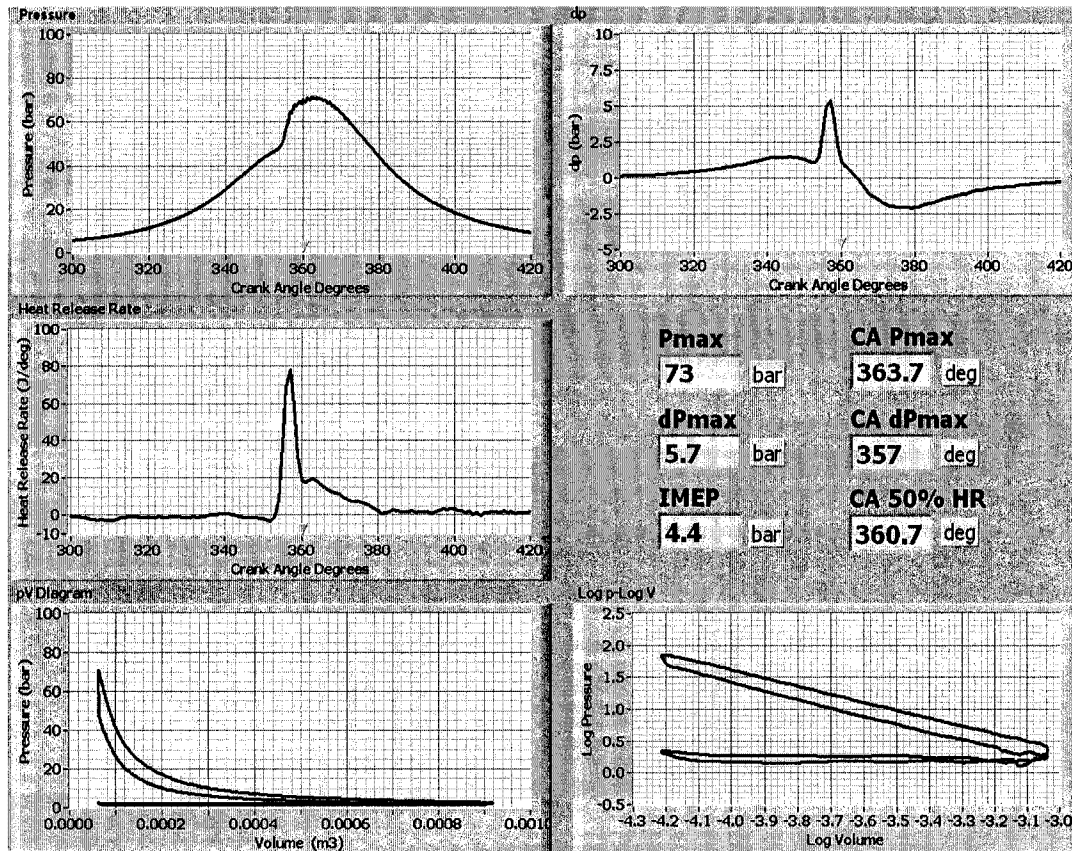
Figure 3.16: Heat Release Program

3.5. EXPERIMENTAL RESULTS

The measurement of in-cylinder temperature was attempted according to the test matrix given in Table 3.5 on the next page. The fine-wire thermocouples had a short life-span when exposed to the diesel combustion environment as indicated by the time duration of the test.

Table 3.5: Test Matrix for In-Cylinder Measurements

Thermocouple Probe #	1	2	3	4
Number of Thermocouples	One	Two	One	Two
Wire Size	127 μm	127 μm 127 μm	127 μm	127 μm 127 μm
Engine Speed (rpm)	1200	1400~1500	1300~1500	1300~1500
Torque (Nm)	20~50	20~50	10~45	10~45
Time Duration (sec)	~70	~180	~150	>240

The thermocouple temperature was amplified and conditioned using a National Instruments' (NI) SCXI-1102 thermocouple signal conditioning module. The sampling rate was set at 7.2 ~ 9 kHz to correspond to the engine speed and provide temperature data at each crank angle. The initial results for one combustion cycle are shown in Figure 3.17.
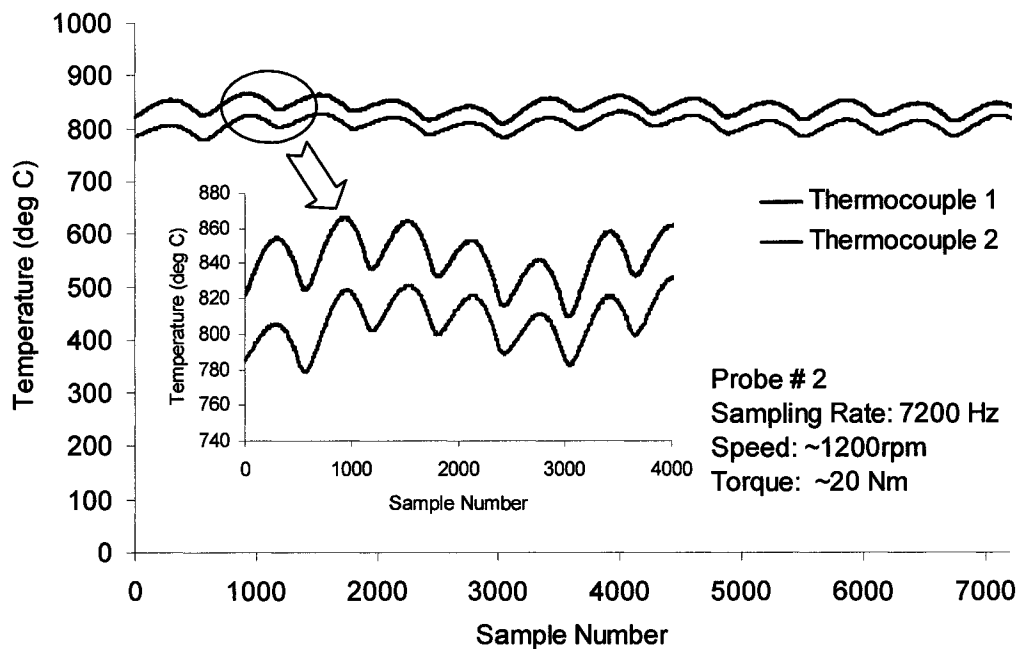
Figure 3.17: Measured Temperature using NI SCXI-1102

The initial results were far-off from the expected in-cylinder temperature profile that should have shown the four processes (intake, compression, expansion or exhaust) of the diesel combustion cycle. The temperature data from probes 1,3 and 4 also failed to capture the transient in-cylinder temperature response. This could be attributed to the slow response of either the thermocouples or the data-acquisition system. Thermocouples with wire diameter of 125 µm have been shown to provide adequate response for instantaneous exhaust temperature measurement [30]. Therefore, the inability to capture the transient phenomenon indicated that the problem possibly existed in the data-acquisition system.

A closer look at the signal conditioning unit, SXCI-1102 revealed that it had a built-in low pass filter with a cut-off frequency of 2 Hz. This meant that the unit essentially blocked frequencies in the range required for in-cylinder measurements (5~9 KHz). To confirm the limitation of the signal conditioning unit, the raw output of the thermocouple was observed with an oscilloscope along with the raw output of the piezo-electric pressure transducer. The results are displayed in Figure 3.18.
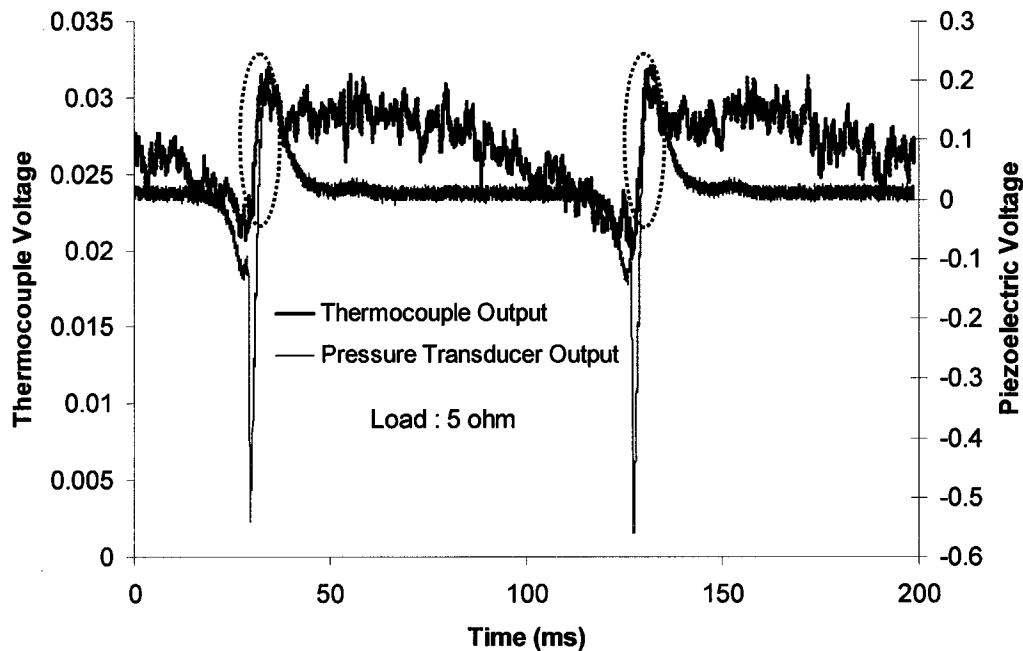
Figure 3.18: Analysis of the Thermocouple Raw Signal

The piezo-electric voltage drops as it is compressed during the compression storke. The sharp drop in the piezo-electric transducer signal specified the start of combustion near the end of the compression stroke and a corresponding sharp rise

in the thermocouple output voltage was also observed as marked in the figure. This indicated that the thermocouple was generally able to capture the effect of the combustion event but the same could not be concluded for the complete diesel cycle due to the low signal-to-noise ratio of the thermocouple output. As the pressure starts to decrease, the piezo-electric sensor starts to expand which results in reversal of the raw voltage as shown in the figure.

The response of an '80TK' thermocouple module, manufactured by Fluke was also checked by generating a millivolt source which could simulate the output of a Type K thermocouple. The frequency of the signal was varied and the response of the temperature module observed on the oscilloscope is shown in Figure 3.19.
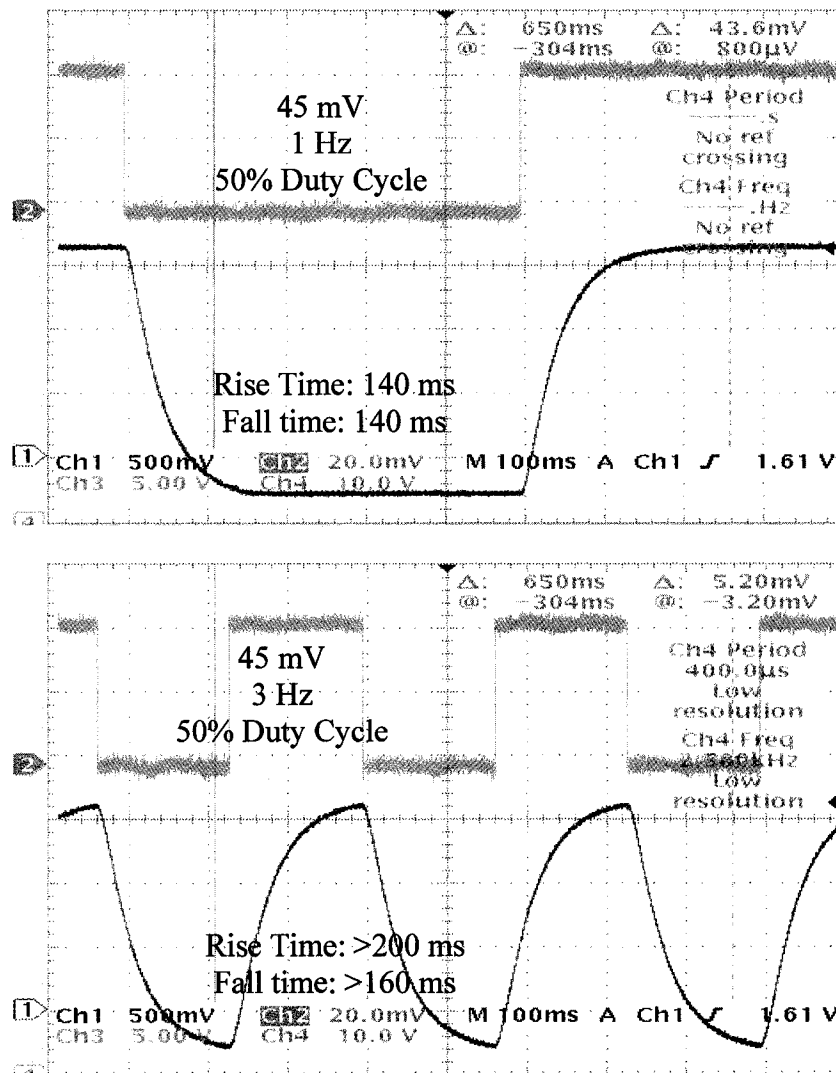
Figure 3.19: Response Time of Fluke® 80TK Thermocouple Module

40

The response time of the module was observed to be more than 100 ms at a frequency of 1 Hz due to the builtin low-pass filter. On the other hand, for an engine running at 1200 rpm, the compression and the expansion strokes (one engine revolution) occur within approximately 50 ms. Hence, this module could not be used for in-cylinder temperature measurement.

3.6. CONCLUDING REMARKS OF CHAPTER 3

The effect of post-injection on the exhaust gas temperature was simulated using WAVE. The results indicated that as the post fuel injection is progressively delayed, there is a trade off between the energy recovery and the exhaust temperature rise. The same was verified through experimental investigations. To analyze the diesel combustion, an online heat release analysis program was written in LabVIEW. Moreover, a temperature reconstruction technique for estimating the instantaneous temperature using two thermocouples was also implemented. To realize in-cylinder temperature and pressure measurements, the cylinder head of the Yanmar single cylinder diesel engine was modified. The component design and modifications were proved successful as the modified cylinder head passed the operational stability and leakage tests. The measurement of in-cylinder temperature could not be accomplished because of the limitation of the data acquisition system. A few attempts with direct measurement using oscilloscope and other thermocouple conditioning modules did not prove successful.

41

4. EXHAUST SYSTEM THERMAL RESPONSE

The design of the exhaust manifold and takedown piping significantly affects the exhaust gas inlet temperature into the aftertreatment converter and, consequently, the temperature levels attainable inside the converter substrate. Varying the exhaust system design particularly the exhaust pipe structure, wall thickness etc can be a viable option for reducing the heat transfer. As part of this research, two different exhaust pipe structures were analyzed as shown in Figure 4.1. The single-layer exhaust pipe is the conventional design employed in most vehicles. An alternate option can be a double-layer exhaust pipe with an air gap between the outer wall and the inner wall. Since air is a good insulator (k value ranges from $0.025 \sim 0.06$ W/ m K from $25°C$ to $600°C$), this air gap can be effective in reducing the thermal energy loss from the exhaust pipe.
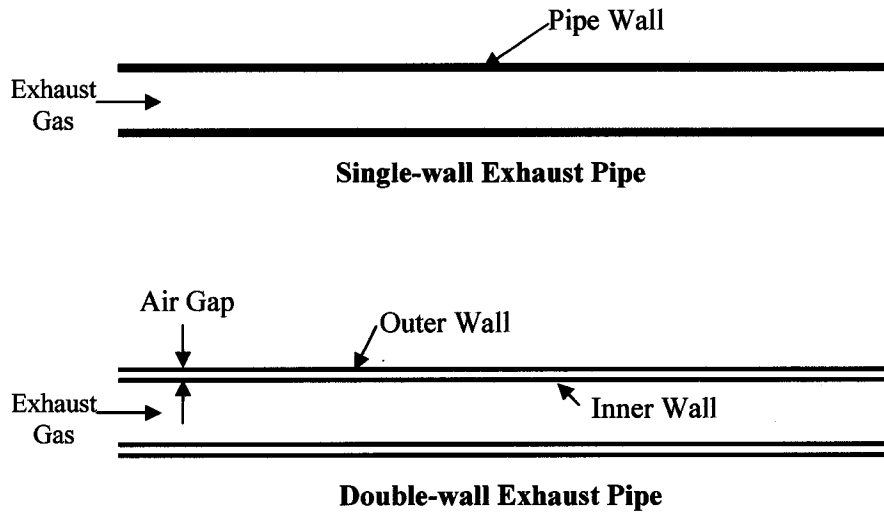
Figure 4.1: Exhaust Pipe Structures

4.1. HEAT TRANSFER IN THE EXHAUST PIPE

Heat transfer in the exhaust pipe is mainly due to conduction along the exhaust pipe, convection and radiation between the exhaust gas and the exhaust pipe, and between the exhaust pipe and the environment [35]. In the usual case of a moving vehicle, forced convection and radiation to the underhood airflow become significant and must be taken into account [19].

The different modes of heat transfer for the two configurations of the exhaust pipe are represented in Figure 4.2.
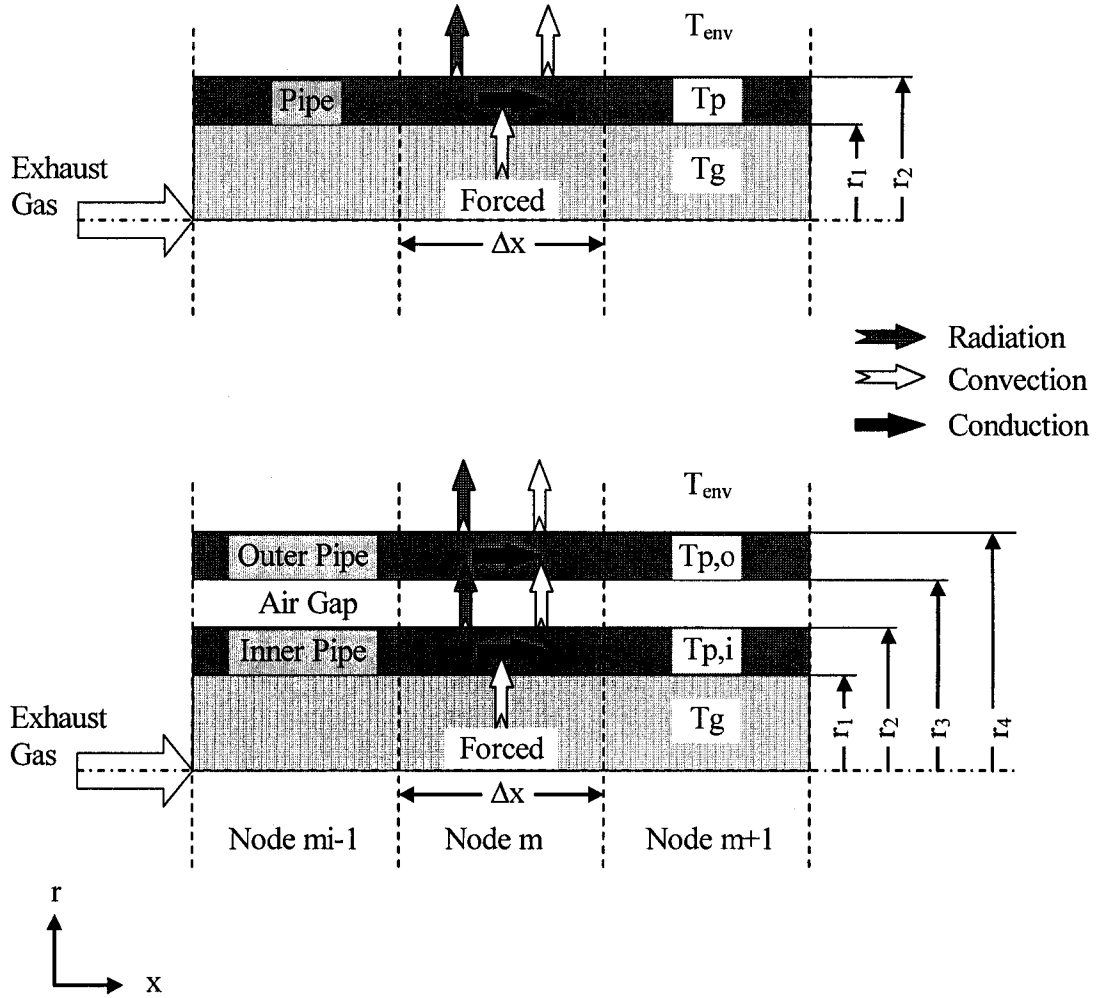
Figure 4.2: Heat Transfer in different Exhaust Pipe Configurations (Adapted from [18])

In the single-wall structure, heat transfer occurs due to forced convection between the exhaust gas and the pipe walls, heat conduction along the pipe and either natural or forced convection from the pipe wall to the environment. Moreover, at temperatures about 400°C, convection and radiation heat transfer from the pipe wall to the environment increases significantly. [18].

For the double-wall pipe, in addition to the modes for a single wall pipe, heat transfer is characterised by natural convection through the air gap and radiative heat transfer between the outer surface of the inner pipe and the inner surface of the outer pipes.

43

4.1.1. Governing Equations

The flow inside the exhaust pipe can be described by three variables: pressure, density and velocity which are governed by the equations of energy, mass and momentum. The pressure range of the flow in automotive exhaust systems is generally quite narrow since the pressure variations in automotive exhaust systems are of the order of a few millibars. Hence, the pressure can be assumed constant. This also allows the computation of the exhaust gas density as a function of temperature only. Assuming quasi-steady, incompressible exhaust flow, the energy balance equation for the exhaust gas can be written as

$$\frac{\partial T_g}{\partial t} + u \frac{\partial T_g}{\partial x} = -\frac{\dot{q}_{cv,i}}{\rho_g c_{pg} V_1} \tag{12}$$

where

u	=	exhaust gas velocity (m/s)
T_g	=	exhaust gas temperature (K)
t	=	time (s)
x	=	axial coordinate of the exhaust pipe (m)
$q_{cv,i}$	=	convective heat transfer rate inside the pipe (W)
ρ_g	=	exhaust gas density (kg/m^3)
c_{pg}	=	specific heat of gas at constant pressure (J/kg K)
V_1	=	control volume of exhaust gas in the pipe (m^3)

For the single-wall exhaust pipe, the radial temperature gradients can be neglected due to the thin wall structure and the high thermal diffusivity of the metal. Considering the heat transfer between the exhaust gas and the pipe through convection and the heat transfer to the environment through convection and radiation, the energy balance equation for the pipe wall can be written as

$$\frac{\partial T_p}{\partial t} = \alpha_p \frac{\partial^2 T_p}{\partial x^2} + \frac{\dot{q}_{cv,i} - \dot{q}_{cv,o} - \dot{q}_{rad}}{\rho_p c_{pp}(\Delta V_p)} \tag{13}$$

where

T_p	=	pipe wall temperature (K)
α_p	=	thermal diffusivity (m^2/s)

44

$q_{cv,o}$	=	convective heat transfer rate to environment (W)
q_{rad}	=	radiative heat transfer rate to environment (W)
ρ_p	=	density of the pipe material (kg/m^3)
c_{pp}	=	specific heat of the pipe material (J/kg K)
ΔV_p	=	segment volume of pipe wall (m^3)

In case of the double-wall pipe, the air gap between the inner and the outer layers of the double-walled pipe utilizes the insulating properties of air. The inner layer is usually kept very thin to reduce the thermal inertia and the outer layer is made thicker to provide strength and rigidity to the pipe structure. Neglecting the radial temperature gradients in both the pipes, and taking into account the heat transfer between the two pipes through natural convection and radiation, the energy balance equation for the inner pipe is

$$\frac{\partial T_{p,i}}{\partial t} = \alpha_{p,i} \frac{\partial^2 T_{p,i}}{\partial x^2} + \frac{\dot{q}_{cv,i} - \dot{q}_{cv,gap} - \dot{q}_{rad,gap}}{\rho_{p,i} c_{p_{p,i}} (\Delta V_{p,i})} \tag{14}$$

and for the outer pipe is

$$\frac{\partial T_{p,o}}{\partial t} = \alpha_{p,o} \frac{\partial^2 T_{p,o}}{\partial x^2} + \frac{\dot{q}_{cv,gap} + \dot{q}_{rad,gap} - \dot{q}_{cv,o} - \dot{q}_{rad,o}}{\rho_{p,o} c_{p_{p,o}} (\Delta V_{p,o})} \tag{15}$$

where

$T_{p,i}$	=	inner pipe wall temperature (K)
$T_{p,o}$	=	outer pipe wall temperature (K)
$\alpha_{p,i}$	=	thermal diffusivity of inner pipe (m^2/s)
$\alpha_{p,o}$	=	thermal diffusivity of outer pipe (m^2/s)
$q_{cv,gap}$	=	convective heat transfer rate inside air gap (W)
$q_{rad,gap}$	=	radiative heat transfer rate inside air gap (W)
$\rho_{p,i}$	=	density of the inner pipe material (kg/m^3)
$\rho_{p,o}$	=	density of the outer pipe material (kg/m^3)
$c_{pp,i}$	=	specific heat of the inner pipe material (J/kg K)
$c_{pp,o}$	=	specific heat of the outer pipe material (J/kg K)

45

$$\Delta V_{p,i} = \text{segment volume of the inner pipe wall (m}^3)$$

$$\Delta V_{p,o} = \text{segment volume of the outer pipe wall (m}^3)$$

4.1.2. Heat Transfer from Exhaust Gas to Pipe

The convective heat transfer rate from the exhaust gas to the pipe wall for each node is given by the following equation:

$$\dot{q}_{cv,i} = h_{cv,i}\pi d_1 \Delta x (T_g - T_p) \tag{16}$$

where

$h_{cv,i}$ = inside convective heat transfer coefficient (W/m^2 K)

$\qquad = \dfrac{Nu\, k_i}{d_1}$

d_1 = pipe inside diameter (m)

Nu = Nusselt number

k_i = thermal conductivity of exhaust gas (W/m K)

To estimate the convective heat transfer coefficient inside the pipe, a number of empirical Nusselt number correlations for fully developed flow in a straight pipe are available in the literature [18, 36]. These are usually applied based on the average flowrate of the exhaust gas. The following correlation proposed by Petukhov and Gnielinski is generally used for estimating the heat transfer in automotive exhaust systems and was adopted [18, 37, 38]:

$$Nu = \frac{(f/8)(Re-1000)Pr}{1.07+12.7(f/8)^{1/2}(Pr^{2/3}-1)}$$
$$\text{for } 10^4 < Re < 5 \times 10^6 \tag{17}$$

$$Nu = \frac{(f/8)(Re)Pr}{1.07+12.7(f/8)^{1/2}(Pr^{2/3}-1)}$$
$$\text{for } Re < 10^4 \tag{18}$$

where

f = friction factor

Re = Reynolds number

Pr = Prandtl number

The friction factor f accounts for the effect of surface roughness and can be determined by the following equation:

$$\frac{1}{\sqrt{f}} + 2\log\left(\frac{\varepsilon/d_1}{3.7} + \frac{2.51}{Re\sqrt{f}}\right) = 0 \qquad (19)$$

where

ε =   absolute surface roughness (m)

Typical values for surface roughness are 2.59×10^{-4} m for cast iron pipe and 1.52×10^{-6} m for steel pipe [20].

The heat transfer between the exhaust gas and the pipe wall is enhanced in the vicinity of 90° pipe bends as the turbulence of the flow increases. This effect is accounted for by using the following correlation [18]:

$$\frac{Nu_{bend}}{Nu_{straight}} = 1 + \frac{21d_1}{Re^{0.14}d_{bend}} \qquad (20)$$

Since the actual flow in the exhaust system is pulsating, the observed heat transfer rates are higher than those predicted by correlations for straight pipes with fully developed flow. Therefore, a gas pulsation factor or convective augmentation factor (CAF) with values between 1.5 and 3 is used to account for fluctuations in the exhaust flow [18, 20]. The thermal properties of the exhaust gas are evaluated at T_g.

4.1.3. Heat Transfer from Pipe to Environment

The convective heat transfer from the pipe outer surface to the environment is given by:

$$\dot{q}_{cv,o} = h_{cv,o}\pi d_o \Delta x (T_p - T_{env}) \qquad (21)$$

where

$h_{cv,o}$ =   outside convective heat transfer coefficient (W/m^2 K)

T_{env} =   environment temperature (K)

$$d_o \quad = \quad \text{outer diameter of the pipe for single-wall structure}$$

and outer diameter of the outer pipe in case of double-wall structure (m)

The outside convective heat transfer can either be due to free convection (in case of a stationary vehicle) or forced convection (in case of a moving vehicle). If heat transfer due to free convection is assumed, the Nusselt number is expressed by [18, 37]:

$$Nu = \left(0.75 + \frac{0.387 Ra^{1/6}}{\left[1 + (0.599 / Pr)^{9/16} \right]^{8/27}} \right)^2 \qquad (22)$$

where

$$Ra = \frac{d_o^3 g \beta \left(T_p - T_{env} \right)}{\alpha_{env} \nu_{env}} \qquad (23)$$

$Ra \quad = \quad$ Rayleigh number

$g \quad = \quad$ gravitational acceleration (9.81 m/s^2)

$\beta \quad = \quad$ volumetric thermal expansion coefficient (K^{-1})

$$\quad = \quad \frac{1}{T_{env}}$$

For forced convection, the correlation proposed by Gnielinski is used for estimating the Nusselt number:

$$Nu = 0.3 + \sqrt{\left(Nu_{la\,min\,ar}^2 + Nu_{turbulent}^2 \right)}$$
$$\text{for } 10 < Re < 10^7 \qquad (24)$$

where

$$Nu_{la\,min\,ar} = 0.664 \sqrt{Re} \sqrt[3]{Pr} \qquad (25)$$

$$Nu_{turbulent} = \frac{0.037 Re^{0.8} Pr}{1 + 2.443 Re^{-0.1} \left(Pr^{2/3} - 1 \right)} \qquad (26)$$

All properties are evaluated at the average temperature $(T_p + T_{env})/2$.

48

Chapter 4: Exhaust System Thermal Response

The radiation heat transfer rate from the pipe outer surface to the environment is given by:

$$\dot{q}_{rad,o} = \varepsilon_R \sigma \pi d_o \Delta x (T_p^4 - T_{env}^4)$$ (27)

where

ε_R = emissivity

4.1.4. Heat Transfer between Inner and Outer Pipes (Air Gap)

For a double-wall pipe, the inner pipe has typically a much higher temperature than the outer pipe which is cooled by either natural or forced convection to the environment. The primary modes of heat transfer between the two pipe layers are natural convection and radiation. For estimating the heat transfer due to natural convection, Stamatelos et al [18] used the following empirical correlations for two long horizontal concentric cylinders.

$$h_{gap} = \frac{Nu_{gap} k_{gap}}{s_{gap}}$$ (28)

$$Nu_{gap} = 0.2 Ra_{gap}^{0.25} \left(\frac{d_3}{d_2}\right)^{0.5}$$ (29)

$$Ra_{gap} = \frac{s_{gap}^3 \beta_{gap} (T_{p,i} - T_{p,o})}{\alpha_{gap} \nu_{gap}}$$ (30)

$$s_{gap} = \frac{\sqrt{d_2 d_3}}{2} \ln\left(\frac{d_3}{d_2}\right)$$ (31)

where

s_{gap} = air gap thickness (m)

The convection heat transfer in the air gap is then given by:

$$\dot{q}_{cv,gap} = h_{gap} \pi d_2 \Delta x (T_{p,i} - T_{p,o})$$ (32)

The relationships in Equations (28) to (31) are valid for $Ra_{gap} > 7.1 \times 10^3$.

49

Reproduced with permission of the copyright owner. Further reproduction prohibited without permission.

A frequently used method to estimate the free convection heat transfer in the annular space between long, horizontal concentric cylinders was proposed by Raithby and Hollands [41]. Using this method, the heat transfer due to free convection in the air gap is expressed as:

$$\dot{q}_{cv,gap} = \frac{2\pi k_{eff}\Delta x\left(T_{p,i} - T_{p,o}\right)}{\ln\left(\frac{d_3}{d_2}\right)} \tag{33}$$

where k_{eff} is the effective thermal conductivity and is defined as the thermal conductivity that a stationary fluid should have to transfer the same amount of heat as the moving fluid. The suggested correlation for k_{eff} is

$$\frac{k_{eff}}{k_{gap}} = 0.386\left(\frac{Pr}{0.861 + Pr}\right)^{1/4} F_{gap}^{1/4}$$

$$\text{for } 10^2 < F_{gap} < 10^7 \tag{34}$$

where

$$F_{gap} = \frac{\left[\ln\left(\frac{d_3}{d_2}\right)\right]^4}{\delta^3\left(d_2^{-3/5} + d_3^{-3/5}\right)^5}Ra_{gap} \tag{35}$$

$$\delta = \frac{\left(d_3 - d_2\right)}{2} \tag{36}$$

For $F_{gap} < 100$, $k_{eff}/k_{gap} \cong 1$ and the mode of heat transfer is mainly conduction through the air gap.

The heat transfer due to radiation between the outer surface of the inner pipe and the inner surface of the outer pipe is given by:

$$\dot{q}_{rad,gap} = F_s\sigma\pi d_2\Delta x(T_{p,i}^4 - T_{p,o}^4) \tag{37}$$

where

F_s = overall radiation shape factor

The shape factor between two surfaces A_i and A_o is defined as

$$F_{i\rightarrow o} = \frac{\textit{radiation energy leaving } A_i \textit{ directly towards and intercepted by } A_o}{\textit{total radiation energy leaving } A_i} \tag{38}$$

50

In the case of double-wall exhaust pipe, all the radiation from the outer surface of the inner pipe reaches the inner surface of the outer pipe. Hence, the radiation shape factors can be written as

$$F_{i \to o} = 1 \qquad\qquad F_{i \to i} = 0$$

$$F_{o \to i} = 1 - F_{o \to o}$$

$$F_{o \to o} = 1 - \frac{1}{R} - \frac{\sqrt{H^2 + 4R^2} - H}{4R} + \frac{1}{\pi}\left(\frac{2}{R}\tan^{-1} \frac{2\sqrt{R^2 - 1}}{H} \right.$$

$$\left. - \frac{H}{2R}\left\{ \frac{\sqrt{4R^2 + h^2}}{H}\sin^{-1} \frac{H^2 + 4(R^2 - 1) - 2H^2/R^2}{H^2 + 4(R^2 - 1)} - \sin^{-1} \frac{R^2 - 2}{R^2} \right\} \right) \qquad (39)$$

where

$$R = \frac{d_3}{d_2} \qquad \& \qquad H = \frac{2\Delta x}{d_2}$$

The value of F_s can then be computed by the following equation:

$$F_s = \frac{1}{\dfrac{1}{\varepsilon_{R,i}} + F_{o \to i}\left(\dfrac{1}{\varepsilon_{R,o}} - 1 \right)} \qquad (40)$$

where

$\varepsilon_{R,i}$ =   emissivity of the outer surface of inner pipe

$\varepsilon_{R,o}$ =   emissivity of the inner surface of outer pipe

4.1.5. Numerical Scheme

The finite difference method was implemented with a defined grid space Δx and time interval of marching Δt for the complete exhaust system. The inputs for the model are the gas temperature and flowrate at the exhaust port. Both the gas and wall temperatures are predicted along the exhaust pipe by the heat transfer model.

To solve for exhaust gas temperature, Equations (12) and (13) are solved simultaneously for the single-wall pipe and Equations (12), (14) and (15) for the double-wall pipe, using the number of transfer units (NTU) method. Assuming quasi-steady exhaust gas flow, the wall temperatures can be assumed constant

51

within the time step of marching and the time derivative in Equation (12) can also be neglected. Therefore, the gas temperature along the pipe was computed using the following equation:

$$T^n_{g,m+1} = T^n_{p,m} + \left(T^n_{g,m} - T^n_{p,m}\right)e^{-NTU} \tag{41}$$

where

$$NTU = \frac{h_{cv,i}\pi d_1 \Delta x}{\dot{m}_g c_{P_g}} \tag{42}$$

m	=	spacing step
n	=	time step of marching
$\dot{m}_g$	=	exhaust mass flow rate

The pipe wall temperatures are calculated by using a forward-time, centre-space finite difference approximation. The discretized form of Equation (13) is:

$$T^{n+1}_{p,m} = T^n_{p,m} + \alpha_p \frac{\Delta t}{(\Delta x)^2}\left(T^n_{p,m+1} - 2T^n_{p,m} + T^n_{p,m-1}\right) + \left(\frac{\dot{q}_{cv,i} - \dot{q}_{cv,o} - \dot{q}_{rad}}{\rho_p c_{P_p}(\Delta V_p)}\right)\Delta t \tag{43}$$

Similar equations are written for Equations (14) and (15) to calculate the inner and outer wall temperatures for the double-wall pipe.

For the explicit solution just described for the energy balance equations, the following stability criteria must be satisfied for the solution to converge [37]:

$$\alpha_p \frac{\Delta t}{(\Delta x)^2} \leq 0.5 \tag{44}$$

The procedure generally is to select a grid space size and then choose a time step that fulfils the above criteria. For the exhaust heat transfer model, the grid space size was fixed at 0.01m with a time step of 0.5 s to match the sampling frequency of the data acquisition during experiments.

52

4.1.6. Single Thermocouple Model

The gas temperature calculated from Equation (41) at any location along the exhaust pipe is used as the starting point for predicting the thermocouple temperature in the heat transfer model. The estimated of the thermocouple time constant τ requires the estimation of the local heat transfer coefficient at each time-step. The following expression, commonly used for the heat transfer to a wire in cross flow is used for this purpose [26]:

$$Nu = 0.42Pr^{0.2} + 0.57Pr^{0.33}Re^{0.5}$$
$$\text{for } 0.01 < Re < 10000 \qquad (45)$$

The time constant of the thermocouple is calculated using Equation (4). Equation (3) is then solved using finite difference method to get the thermocouple temperature as follows:

$$T_{tc}^{n+1} = T_{tc}^{n} + (T_{g}^{n} - T_{tc}^{n})(1 - e^{-dt/\tau}) \qquad (46)$$

4.2. EXPERIMENTAL SETUP

The estimation of the thermal energy lost from the exhaust system requires the measurement of the exhaust gas temperature profiles along the exhaust system. This constituted an essential part for the experimental verification of the thermal response analysis. The existing single-wall exhaust pipe of the Yanmar engine was adapted for measuring both the gas and pipe-wall temperatures at several locations along the exhaust pipe. The physical properties of the system are given in Table 4.1.

Table 4.1: Exhaust System Data

Type	Single –wall Pipe
Length (till inlet of aftertreatment)	~1.55 m
Total Mass	~ 6 kg
Pipe Material	Stainless Steel
Pipe Outer Diameter	50.8 mm (2 inch)
Pipe Wall Thickness	1.78 mm (0.07 inch)

To record the gas and wall temperatures, thermocouple arrays were embedded in the exhaust system. A total of 12 thermocouples were installed at 6 different locations along the exhaust pipe to measure the temperature distribution in the exhaust system. A complex flow field for external forced convection from the exhaust pipe was setup. Besides the main ventilation system of the laboratory which included the HVAC system as well as an external exhaust fan, two fans were also installed to provide forced flow over the exhaust system and to assist the engine cooling system. The layout of the system is shown in Figure 4.3.
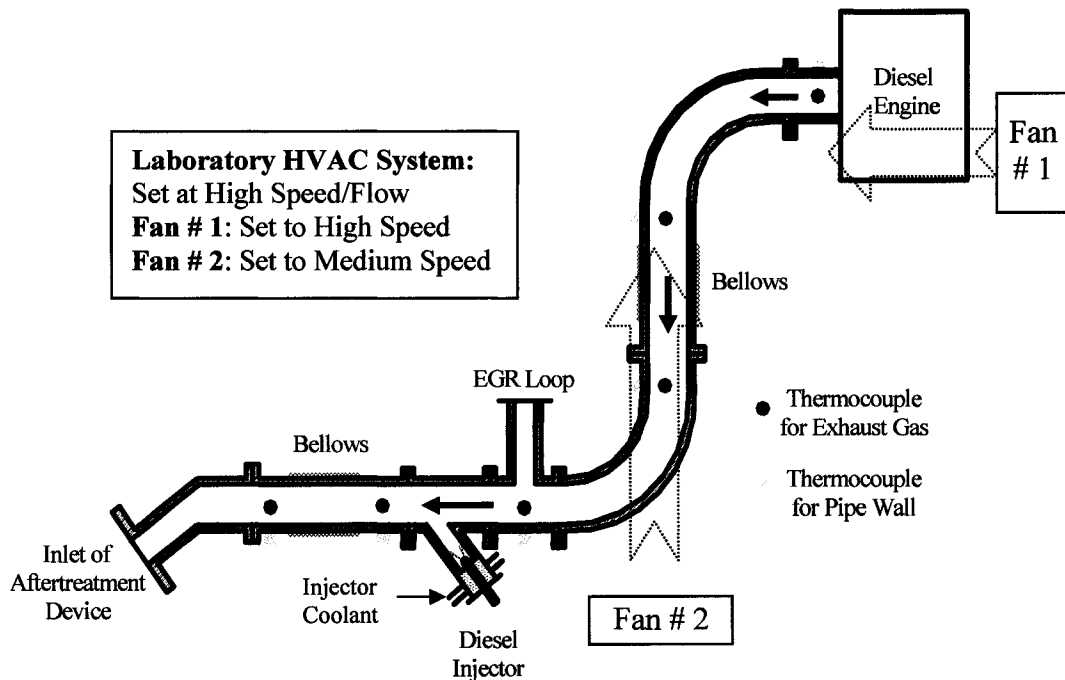
Figure 4.3: Exhaust System Layout

During the experiments, the two fans and the ventilation system were always operated at a fixed setting to minimize the variations in the flow field around the exhaust system and to maintain a consistent flow field across the experiments

4.2.1. LabVIEW Exhaust System Program

For online analysis of the thermal response of the exhaust system, a program was written in LabVIEW which acquires the temperature data from the

engine, exhaust pipe and the aftertreatment device. The temperature is acquired at a fixed sampling frequency of 2 Hz. The program displays the instantaneous temperature profiles for both the exhaust gas and the pipe wall along the length of the exhaust pipe. Moreover, the temperature history for all the locations is also displayed graphically and recorded in a tab-delimited text file. The front panel of the program is shown in Figure 4.4.
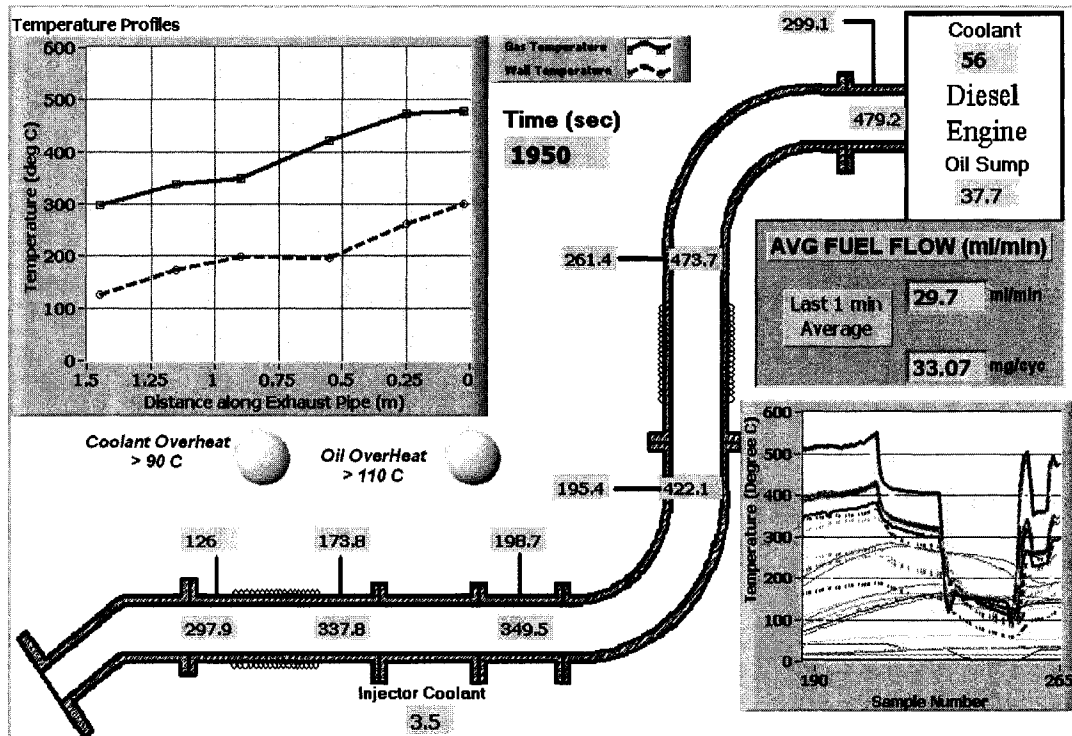
Figure 4.4: Online Exhaust System Thermal Response Program

4.2.2. Continuous Pressure Recording

The input to the heat transfer model is the engine-out exhaust gas temperature. To estimate this temperature, a code was written in LabVIEW to continuously record the cylinder pressure data with a crank angle resolution of 1 degree. The pressure data for 2000 consecutive cycles was saved in binary format. The engine speed from the dynamometer was also saved at a frequency of 2 Hz. This data was then processed using a 'C' code to calculate the average cylinder temperature at exhaust valve opening and to convert it from the cycle-resolved domain to the time-resolved domain. The 'C' code and the details of the LabVIEW program are given in APPENDIX C.

55

4.3. MODEL SETUP

The 1-D transient heat transfer model was programmed in 'C' language. The execution of the code occurs in the following sequence:

(1)   The model takes the engine-out exhaust temperature generated from the pressure data as the input. The engine speed data recorded during the experiments is also used as an input for calculating the mass flow rate of the exhaust at each time step.

(2)   The initial temperature of the pipe-wall is user selectable, the default value being equal to the external environment temperature, which is the case in case of a cold-starting engine.

(3)   The user can select either a single-wall pipe structure or a double-wall pipe structure with air gap and also input the physical and thermal properties for the system.

Additional mass (like flanges, V-clamps, injector assembly etc) can be added to the model as thermal inertia at the end of the ducts.

(4)   The locations along the exhaust pipe for which the temperature histories are required to be generated can be specified.

At each time step, the energy balance equations are solved along the discretized exhaust pipe system to calculate the exhaust gas and pipe-wall temperatures.

(5)   The thermal properties of the exhaust gas are calculated at each node based on the gas temperature T_g. The thermal properties of the external flow field are calculated at the average temperature $(T_p + T_{env})/2$.

(6)   At each time step, the code checks if the stability criteria has been met. Otherwise, an error is reported.

(7)   The simulation runs for the time duration specified by the user.

(8)   The gas and pipe-wall temperatures and the thermocouple temperatures at the desired locations are written to tab-delimited text files before the program exits.

The Yanmar exhaust system was divided into 9 pipe sections in the model as shown in Figure 4.5. Since the temperature calculated from the pressure

56

data is not the actual temperature at the inlet of the exhaust pipe (due to the complex thermal characteristics of the exhaust manifold), an additional section at the inlet of the exhaust pipe was added to represent the effect of the exhaust manifold. The thermal inertia due to flanges and clamps etc was specified at the ends of the pipe sections during the model setup. The external flow field for the actual engine setup is quite complex as described earlier. A few of the pipe section lie across the flow field while others are parallel to the flow field. The effect of all these factors was taken into account during the calibration process.
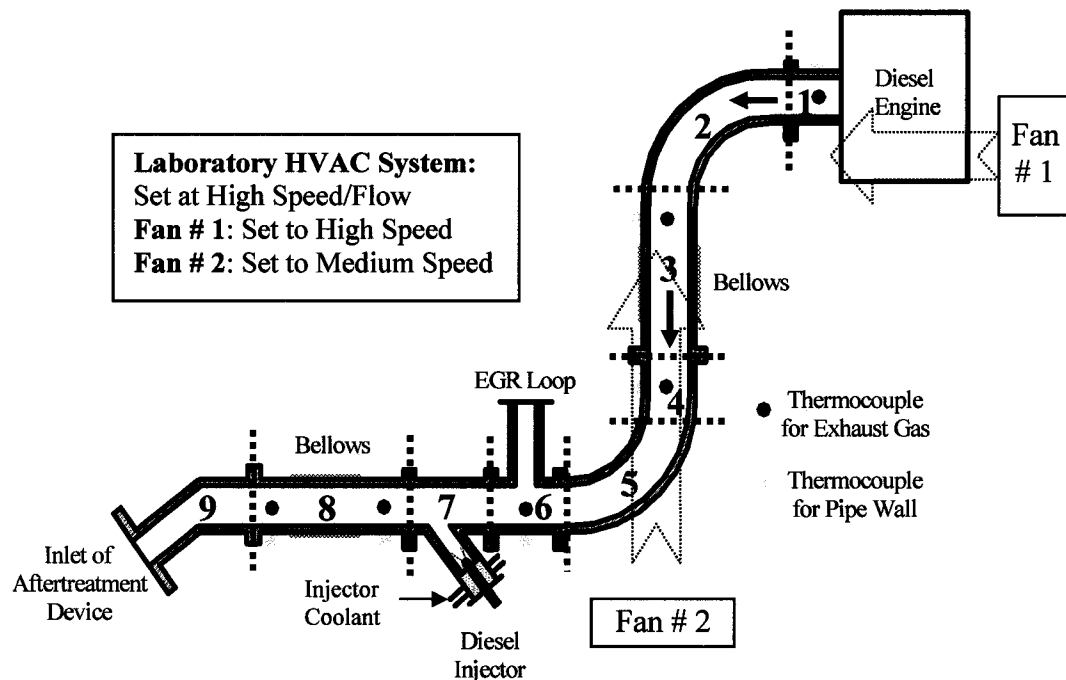
Figure 4.5: Exhaust System Layout in Heat Transfer Model

4.4. WAVE MODEL FOR EXHAUST HEAT TRANSFER

The thermal response of the exhaust system was also investigated using Ricardo's engine cycle simulation software, WAVE®, which integrates the simulation capabilities of 1-dimensional flow modelling in the intake and exhaust systems, together with component models that include transient heat transfer in the exhaust system [23]. This was done to highlight the limitations of the in-house code as well as to provide useful information for improving it. Moreover, the coupling of the in-cylinder post injection with the exhaust system thermal response was also carried out in WAVE.

57

The exhaust piping was modelled using the structural heat conduction/duct warm-up model in WAVE. This model calculates either the steady-state temperature distributions and/or the temperature histories of ducts and junctions. It is a 2-D (axial and radial) conduction model which makes use of the internal boundary conditions of temperature and heat transfer coefficients generated by the WAVE flow model. The external boundary conditions of the warm-up model can be user specified to simulate adiabatic or convective and radiative heat transfer from the pipe surface to the ambient surroundings. The model allows calculation of temperature distributions in radially inhomogeneous duct networks comprised of up to two layers of materials (e.g. air gap, insulations, etc.). Additionally, contact resistances and thermal inertia due to connecting flanges can be also be specified. The thermocouple model accounts for radiation, convection, and conduction to a physical geometry and mass described by user inputs, and the duct wall temperature and changing gas temperatures are used as boundary conditions [23].

The WAVE model was setup similar to the in-house model and is shown in Figure 4.6. WAVE allows either the external heat transfer to be modelled as free convection in which case it uses a built-in model. For forced convection, a fixed external heat transfer coefficient has to be specified for each pipe section.
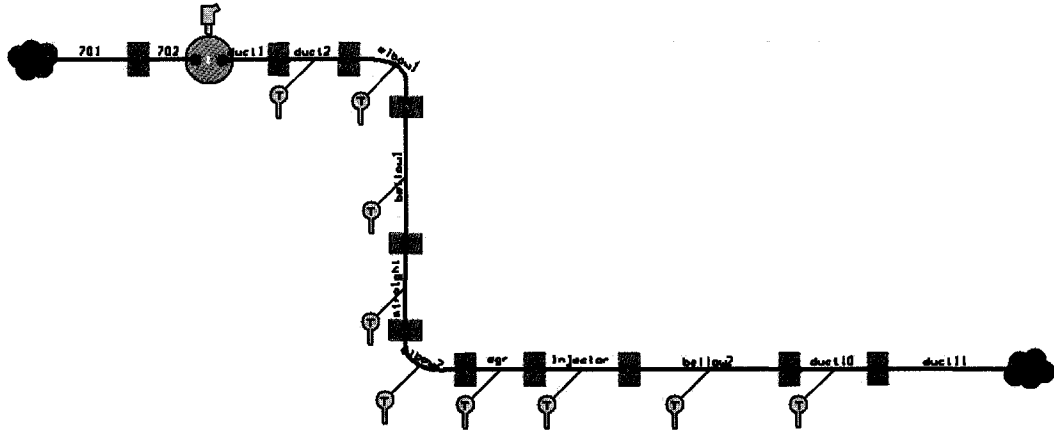
Figure 4.6: Exhaust System Model in WAVE

4.5. THERMOCOUPLE CALIBRATION

The thermocouples installed in the exhaust system were calibrated at $0^{\circ}C$ using an ice bath. The ice bath was maintained at a uniform temperature and the

58

thermocouple junction was immersed into it for 10 minutes. The immersed length of the thermocouple probe was kept long enough to ensure that the measuring junction temperature was not affected by a temperature gradient along the thermocouple wires. The details of the calibration are given in APPENDIX D.

4.6. MODEL CALIBRATION AND VALIDATION

Extensive experiments were performed to generate exhaust system temperature profiles that were then used for tuning and calibrating the heat transfer model. After the calibration was done, the model validation was carried out using different sets of experimental data that included both steady state and transient engine operations. The test matrix for the experiments is given in Table 4.2.

Table 4.2: Test Matrix for Exhaust System Thermal Response

Test #	Engine Speed (rpm)	Torque Range (Nm)	Time Duration (sec)	Engine operation	Purpose
1	~1400	43~50	1600	Steady State	Calibration
2	1360~2100	12~55	1700	Transient	Calibration
3	~1330	~50	1100	Steady State	Validation
4	1400~1500	10~50	2300	Steady State & Transient	Validation
5	700, 1400, 1800	3~6, ~53, ~10	2100	Transient (3 mode test)	Validation
6	1360~1480	10~50	1000	Transient	Validation
7*	1360~1420	20~40	600	Transient	Validation

* with EGR

The results for each of the tests are presented in the following sections:

59

4.6.1. Test # 1 (Calibration)

The engine operating conditions are shown in Figure 4.7. The engine was run at a high load at constant speed. The exhaust gas temperature was calculated from the pressure data recorded continuously during the test.
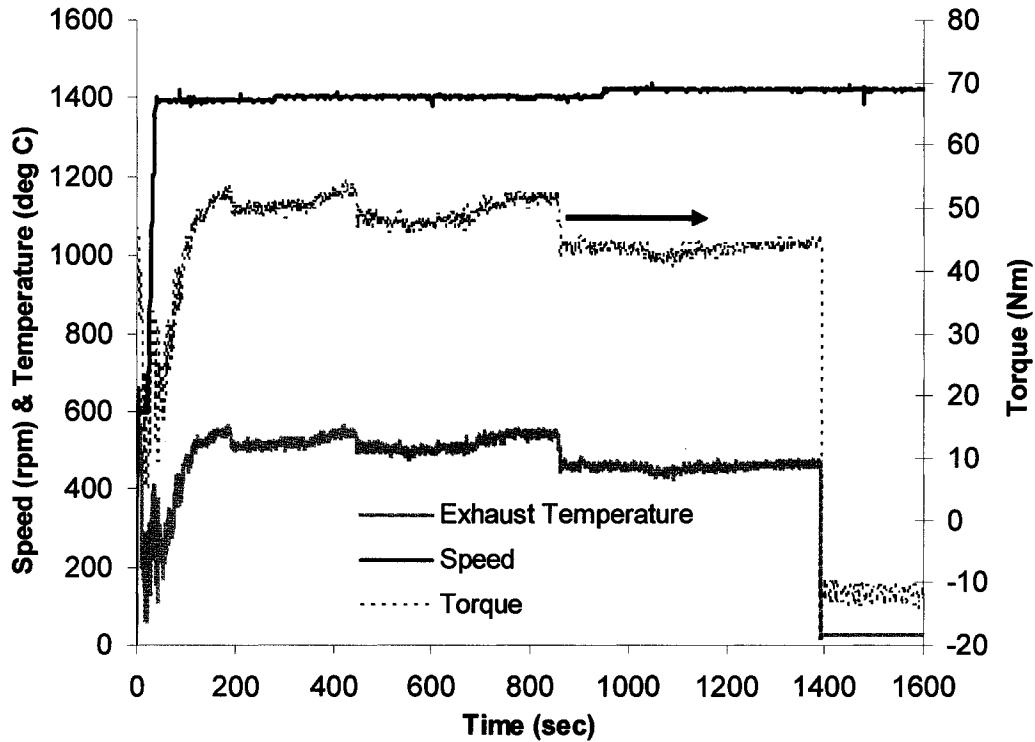
Figure 4.7: Engine Operating Conditions (Test # 1)

The exhaust gas temperatures recorded along the exhaust pipe and the gas temperatures predicted by the model for the same test conditions are shown in Figure 4.8. Although the point of interest is the temperature at the inlet of the aftertreatment device (given by T_g6), an effort was made to calibrate the model to accurately predict the temperatures at any location along the exhaust pipe. It can be seen that the predicted temperatures are in good agreement with the measured temperatures. Data for two thermocouples (# 1 and # 4) are not shown because of malfunction. These thermocouples were replaced with new ones from test # 3 onwards.

60
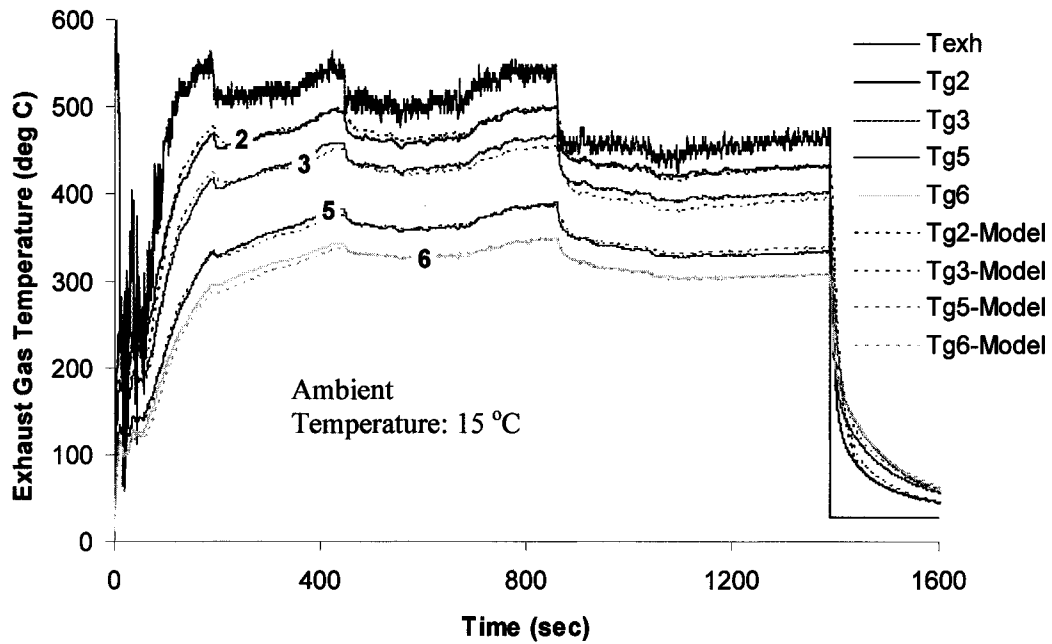
Figure 4.8: Gas Temperature Comparison (Test # 1)

The measured pipe-wall temperatures along with those predicted by the model are given in Figure 4.9. The results in this case are also in good agreement.

Figure 4.9: Pipe Wall Temperature Comparison (Test # 1)

The summary of the measured gas temperature and the calculated (model-based) gas temperature at the inlet of the aftertreatment device is given in Table 4.3:

Table 4.3: Summary of Results (Test # 1)

Time since Start (sec)	Engine-out Exhaust Gas Temperature (°C)	Measured Gas Temperature (T_g6) at Inlet of Aftertreatment Device (°C)	Calculated Gas Temperature at Inlet of Aftertreatment Device (°C)
1	95.7	14.5	14.1
50	234.4	126.2	119
100	470.2	201.7	185.6
180	538.3	288.3	278.8
500	507.6	329.7	329.3
800	548.6	345	345.6
1000	446	311.2	309.4
1330	471.7	306	305.4
1391	261.5	306.6	304.5
1400	28.4	206.6	232.2
1500	28.4	95.42	94.5
1600	28.4	60.3	62.4

The gas and wall temperatures predicted by the wave model for the same input conditions are given in Figure 4.10 and Figure 4.11 respectively.
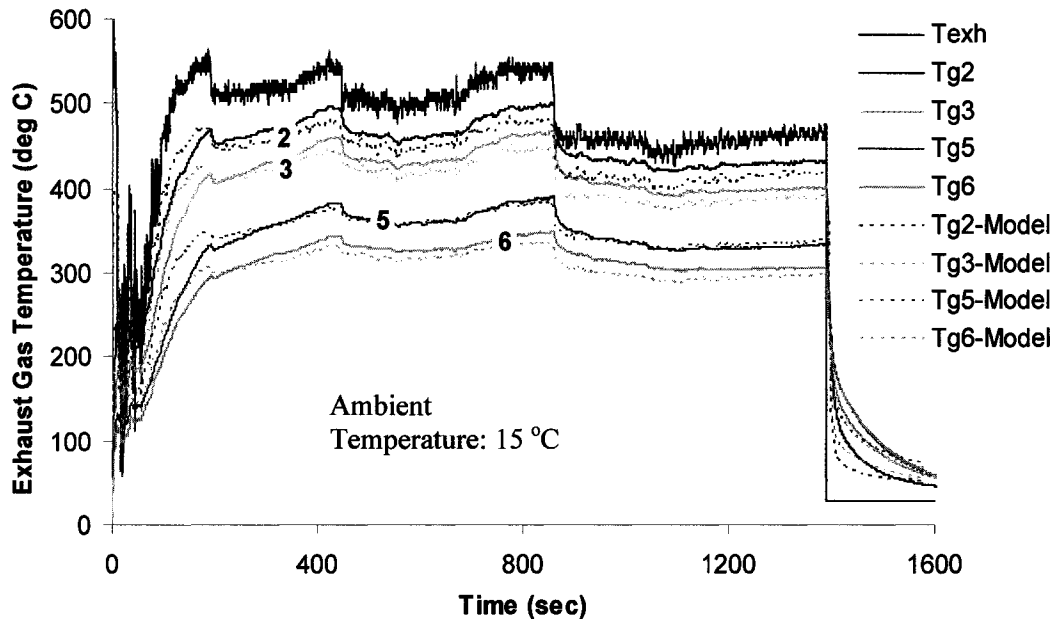
Figure 4.10: Gas Temperatures Predicted by WAVE (Test # 1)

62
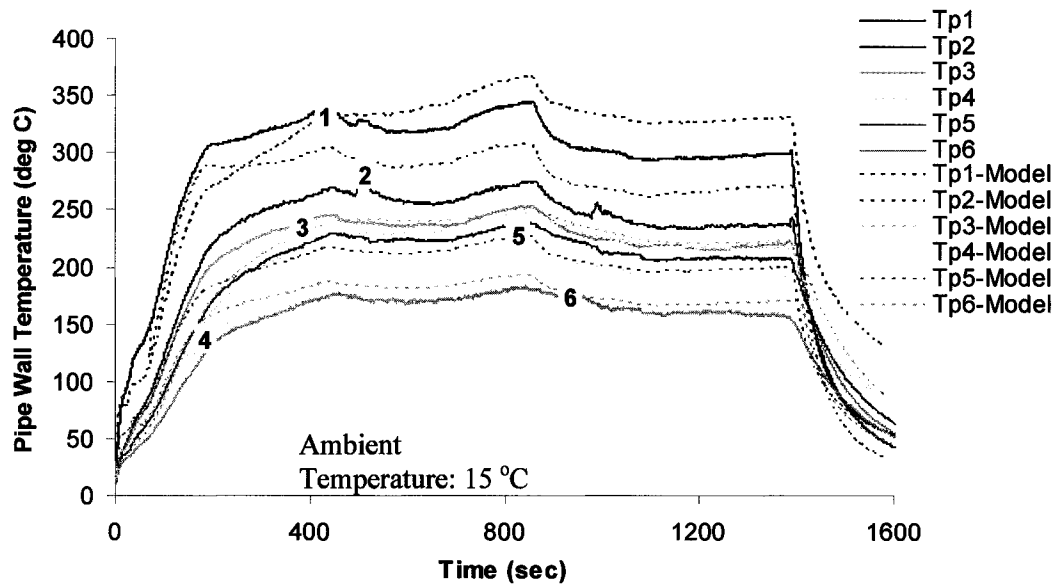
Figure 4.11: Pipe Wall Temperatures Predicted by WAVE (Test # 1)

The gas temperatures from the WAVE model are in general agreement with the measured temperatures. However, the model could not be tuned to accurately predict the wall temperatures. A major reason seems to be the use of a constant value for the external convection heat transfer coefficient in WAVE. To investigate this aspect, the external heat transfer coefficient calculated by the in-house model was plotted at 3 different locations in a pipe segment as indicated in Figure 4.12.
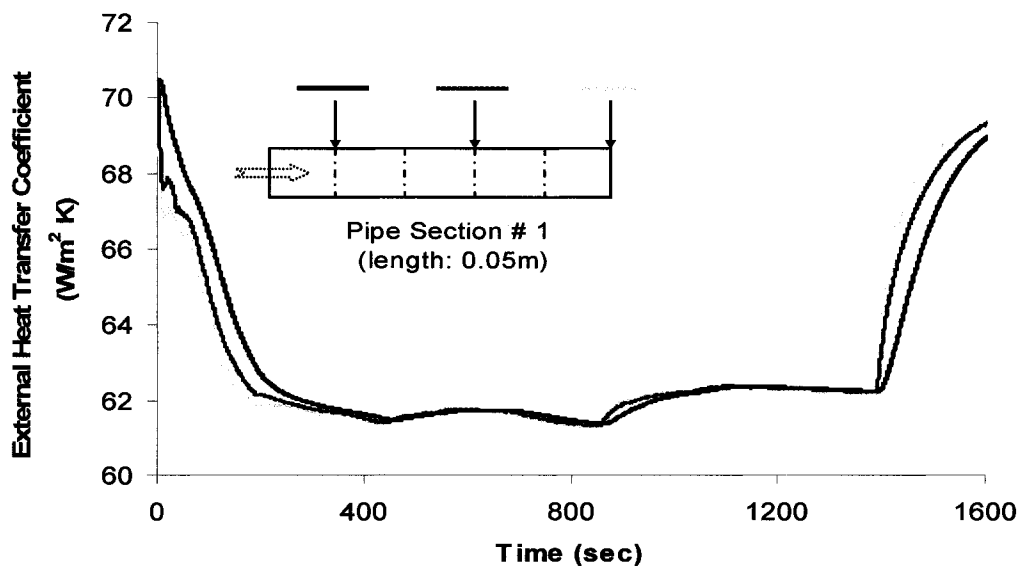
Figure 4.12: Variation of External Heat Transfer Coefficient with Time

It can be seen that the heat transfer coefficient is considerably affected by the pipe-wall temperature during warm-up and cooling phases. A small difference can also be also observed along the length of the pipe segment. Assuming a constant value will result in over-or-under predicting the wall temperature during transient conditions and will also affect the calculation of the exhaust gas temperature. In the following section, only a few results are therefore shown for the WAVE model.

4.6.2. Test # 2 (Calibration)

To check the model calibration under transient operating conditions and to refine it further, test # 2 was performed. After the initial engine warm-up phase, the engine load was alternately changed between high and low load states, with each state maintained for a time duration of 30 sec. the engine was stopped after approximately 10 minutes. This was followed by a short warm-up phase and load transients and then a constant torque operating mode in which the engine speed was varied from 1450 to 2100 rpm. The engine operating conditions for the first part are given in Figure 4.13.
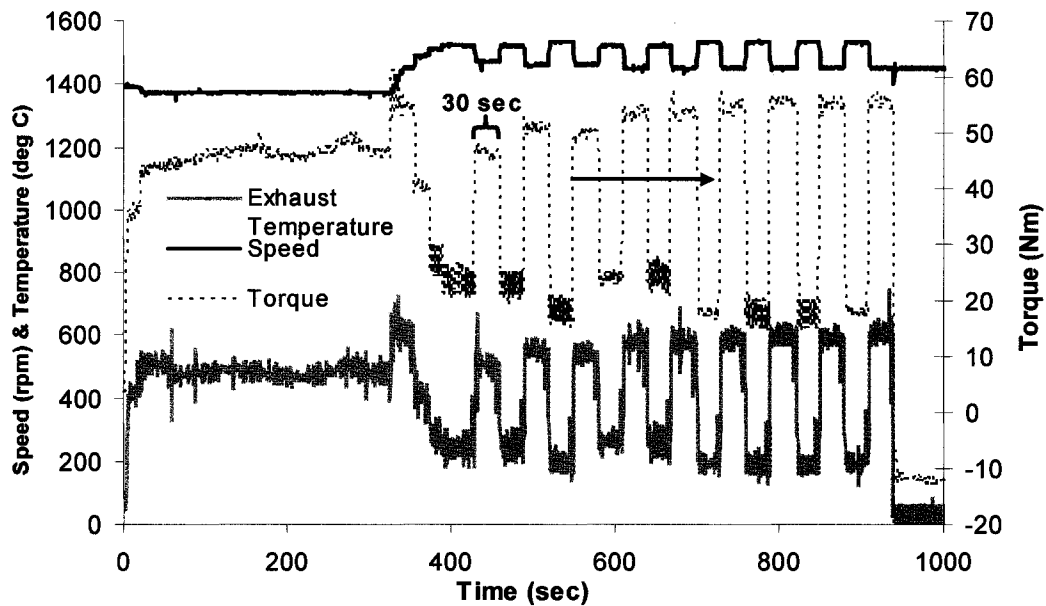
Figure 4.13: Engine Operating Conditions (Test # 2a)

The gas temperatures are shown in Figure 4.14 and an enlarged view of the transient portion is shown in Figure 4.15.
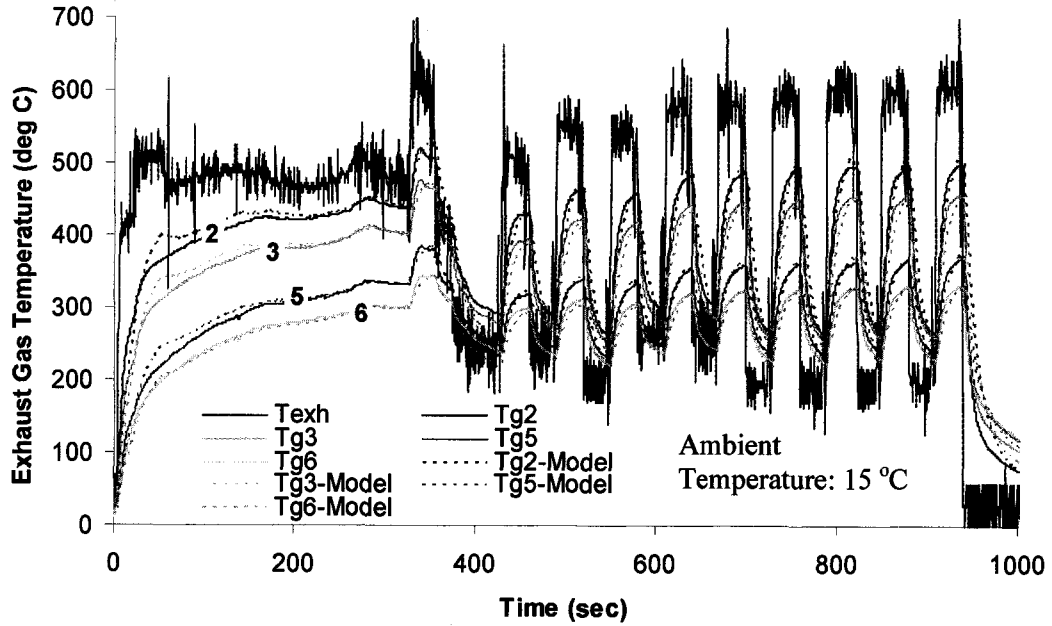
Figure 4.14: Gas Temperature Comparison (Test # 2a)
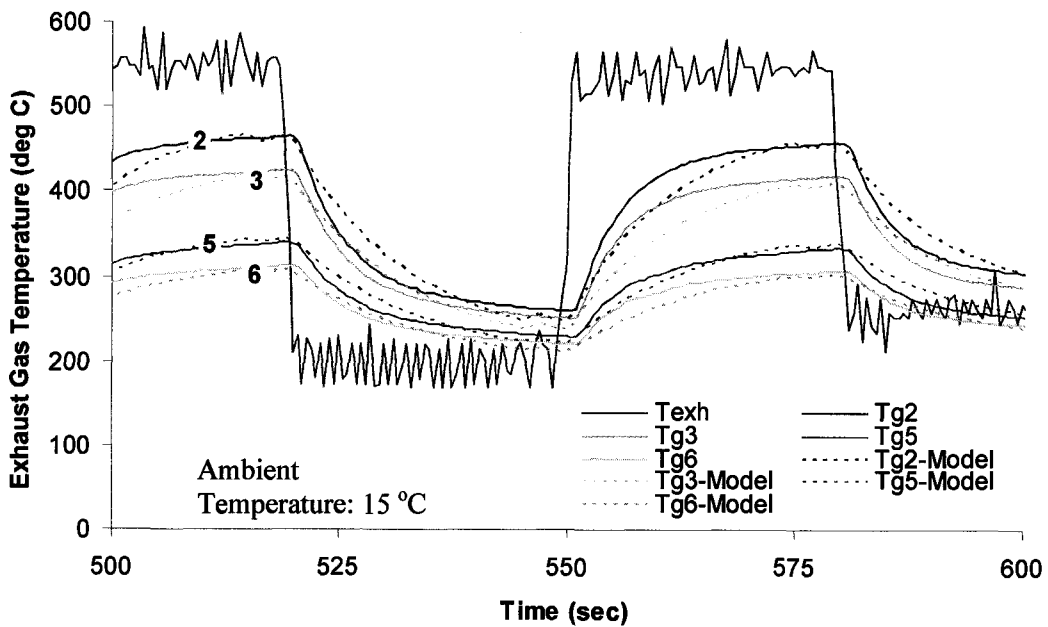
Figure 4.15: Zoomed View of the Gas Temperatures (Test # 2a)

65

The gas temperatures during the engine transients are in general agreement with the measured values. The same is true for the pipe-wall temperatures as shown in Figure 4.16.
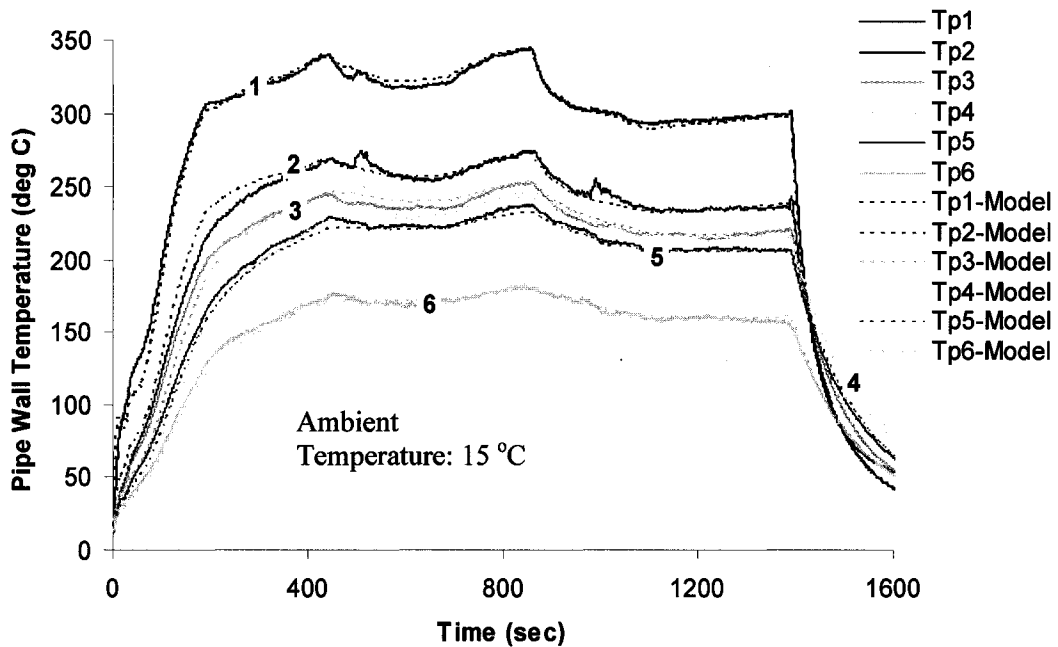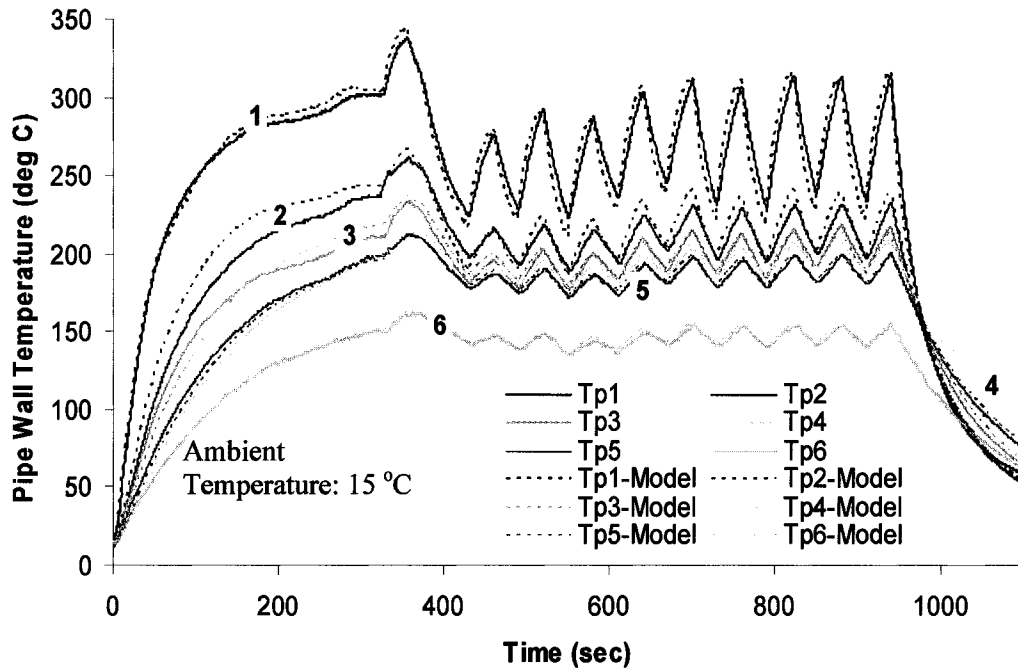

Figure 4.16: Pipe Wall Temperature Comparison (Test # 2a)

The comparison of the measured gas temperature (T_g6) and the calculated gas temperature (T_g6-Model) at the inlet of the aftertreatment device is given in Table 4.4 on the next page.

66

Table 4.4: Summary of Results (Test # 2a)

Time since Start (sec)	Engine-out Exhaust Gas Temperature (°C)	Measured Gas Temperature (T_g6) at Inlet of Aftertreatment Device (°C)	Calculated Gas Temperature at Inlet of Aftertreatment Device (°C)
5	280.8	33.2	22.3
50	505.4	193.6	198.3
100	487.1	238.1	233.8
300	483.1	301.6	299
400	229.2	256.7	239.8
431	462.7	238	220.5
460	511.5	299	291.4
461	239.5	298.4	287.3
490	268.9	235.2	227.4
491	545.4	235.7	232.7
520	548	312	306.5
521	297.7	306.7	297.8
550	276.7	221.3	212.2
939	579.3	330.8	329.1
940	28.4	329	321
1000	28.4	121.1	117.4
1100	28.4	68.7	70.8

The engine operating conditions for the constant torque test are shown in Figure 4.17.
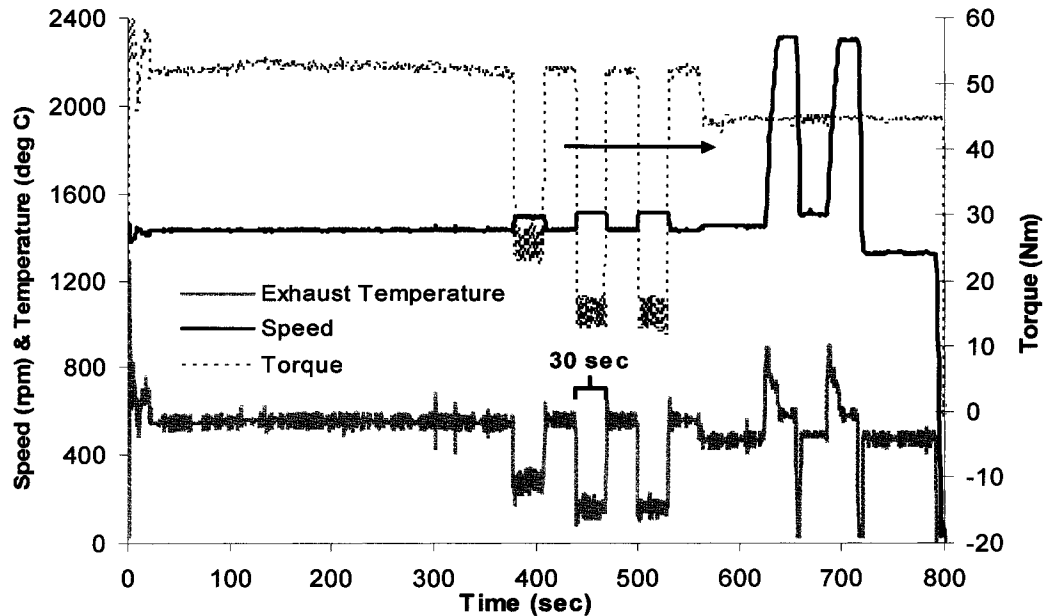
Figure 4.17: Engine Conditions for Constant Torque Operation (Test # 2b)

67

The heat transfer model was able to predict the gas temperatures with reasonable accuracy as shown in Figure 4.18.
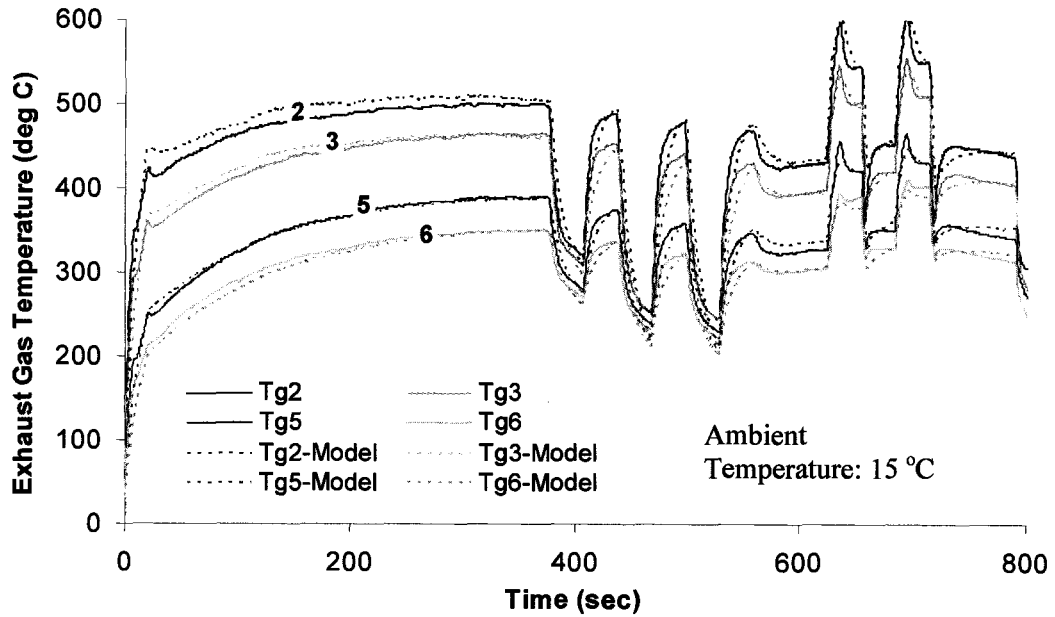
Figure 4.18: Gas Temperatures for Test # 2b

The wall temperatures generally followed the measured values but some deviation was observed during the constant torque mode as shown in Figure 4.19.
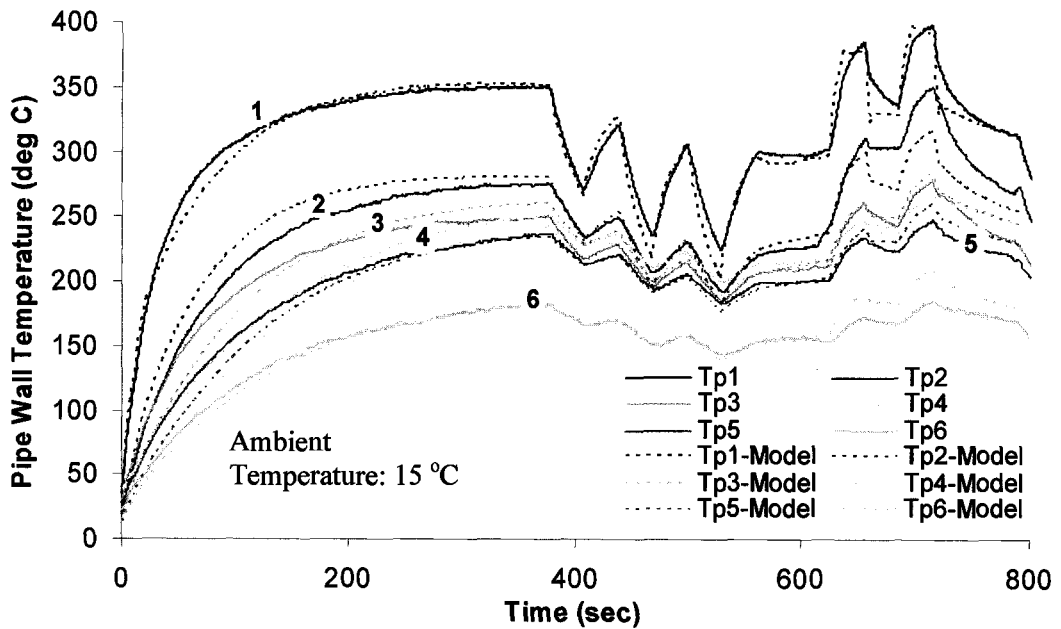
Figure 4.19: Pipe Wall Temperatures for Test # 2b

68

The summary of the results for the temperature at the inlet of the aftertreatment device is given in Table 4.5.

Table 4.5: Summary of Results (Test # 2b)

Time since Start (sec)	Engine-out Exhaust Gas Temperature (°C)	Measured Gas Temperature (T_g6) at Inlet of Aftertreatment Device (°C)	Calculated Gas Temperature at Inlet of Aftertreatment Device (°C)
5	645	151	132.9
50	524.4	247.9	236.6
200	553.7	329.7	324.2
375	538.3	350.9	349.8
379	255.8	345.7	345.2
409	245.6	280.5	269.5
410	321.9	291.2	276.5
439	553.8	332.9	332.5
440	461.8	320	321.4
469	146.3	239.9	219.4
470	406.6	253.7	230.1
499	564.3	324.2	321.2
625	471.7	305.5	308.7
628	791.9	347.6	342.9
657	610.8	335.5	335.6
665	488.8	329.1	313.7
685	483.4	332	327.9
695	714.3	409.3	393.2
715	584.9	403.5	382.7
725	471.7	329.2	320
790	466.6	313.3	321.9

For the heat transfer model, the maximum difference between the measured and the calculated values for the exhaust gas temperature was 24°C for thermocouple # 6 or about 7.1% of the measured value. Similarly, a maximum difference of 36°C was observed for the wall temperature (thermocouple # 2) which amounted to approximately 10.3% of the measured value.

In case of the WAVE model, the deviation from the measured temperature was larger, especially during the transient phase, the possible reasons for which have been stated in Section 4.6.1. Consequently, a maximum difference of 48°C for the gas temperature (thermocouple # 6) and 67°C for the wall

69

temperature (thermocouple # 2) was observed which corresponded to 19.4% and 23.9% of the measured values respectively.

The values given above are the maximum differences observed. During the calibration, an attempt was made to minimize the difference for thermocouple # 6 (at the inlet of the aftertreatment). The same was checked during the validation of the models.

It is quite difficult to outline a single cause for the difference between the measured and the calculated temperatures. Besides the inaccuracy in model calibration and the assumptions on which the heat transfer models are based, there can be other factors which may result in this difference. In the actual engine, the temperature of the gases exiting the engine cylinder is affected by the temperatures of the engine coolant and the engine lubricating oil. During the warm-up period and also during load transients, the oil and coolant temperatures may vary significantly as shown in Figure 4.20 for tests # 1 and # 2. This can have a strong influence on the heat transfer between the exhaust gas and the exhaust manifold, resulting in variation in the exhaust gas temperature entering the exhaust pipe.
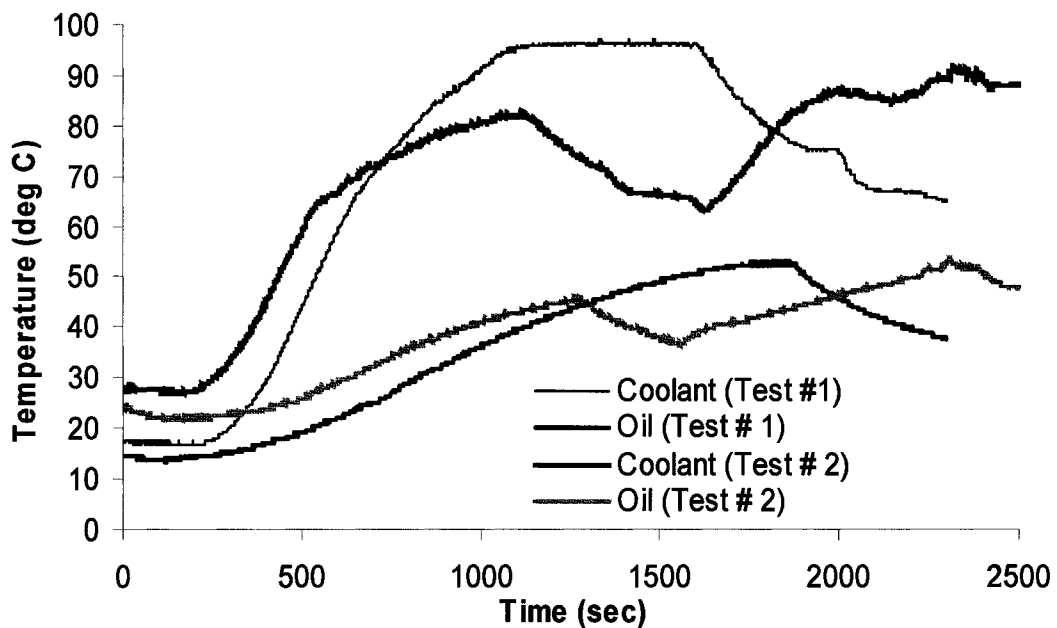
Figure 4.20: Variation in Engine Coolant & Oil Temperatures (Tests #1 & 2)

The heat transfer models described for the exhaust system do not account for the variations in the engine coolant and oil temperatures and their effect on the heat transfer inside the exhaust manifold. Therefore, this can also be a reason for the difference observed between the simulation results and the measured temperatures

4.6.3. Test # 3 (Validation)

The first validation was performed at steady engine operating conditions as shown in Figure 4.21.
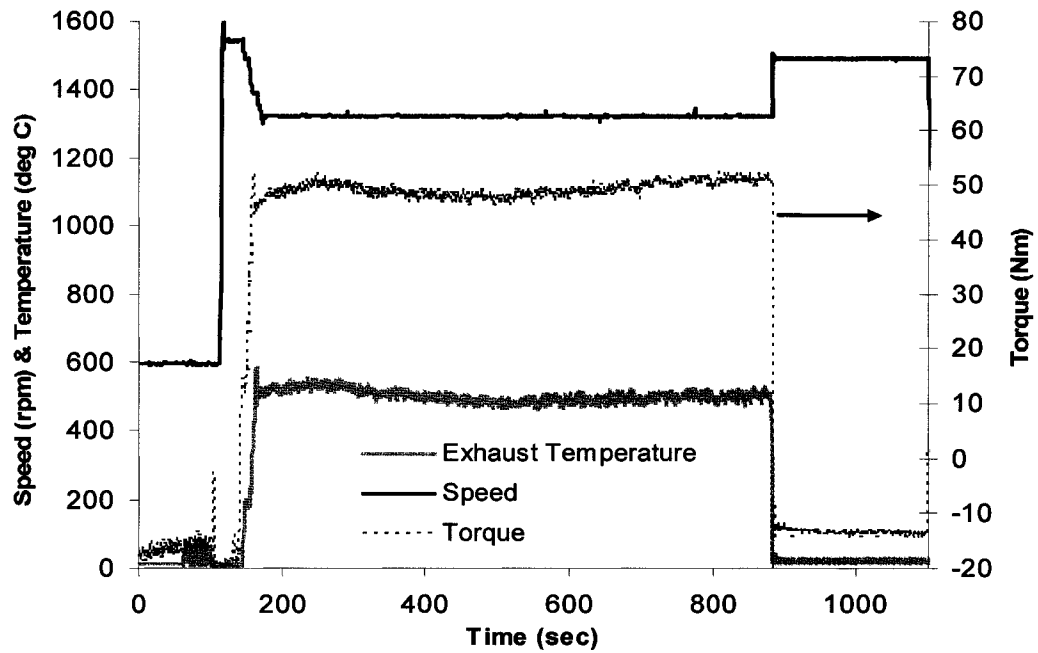
Figure 4.21: Engine Operating Conditions (Test # 3)

The calculated gas temperatures in Figure 4.22 on the next page show a good agreement with the measured temperatures, particularly for the thermocouples closer to the aftertreatment device.

71
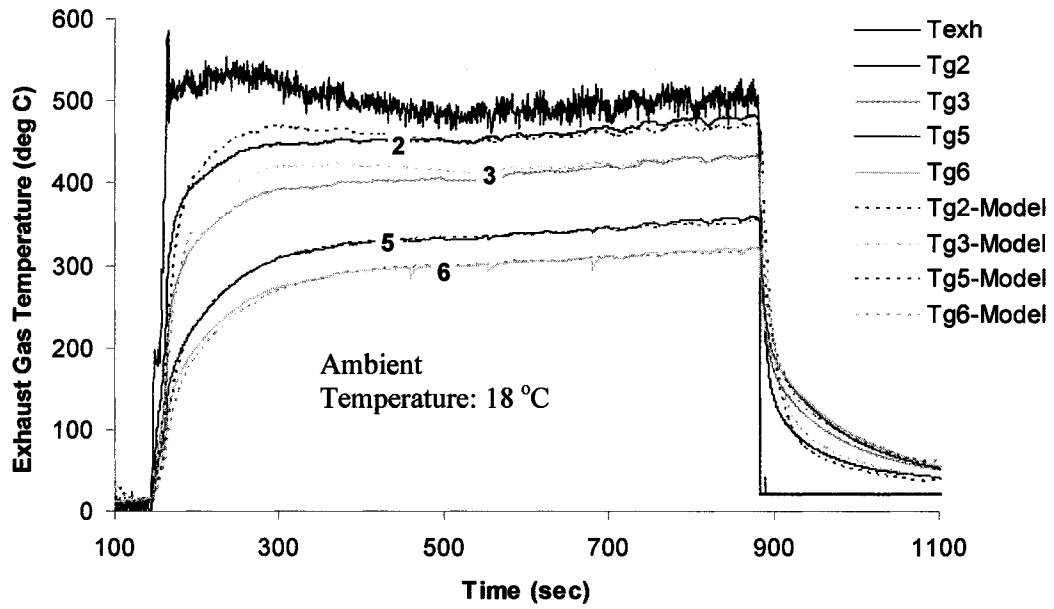
Figure 4.22: Gas Temperature Comparison (Test # 3)

A similar trend was observed for the pipe-wall temperatures as shown in Figure 4.23.
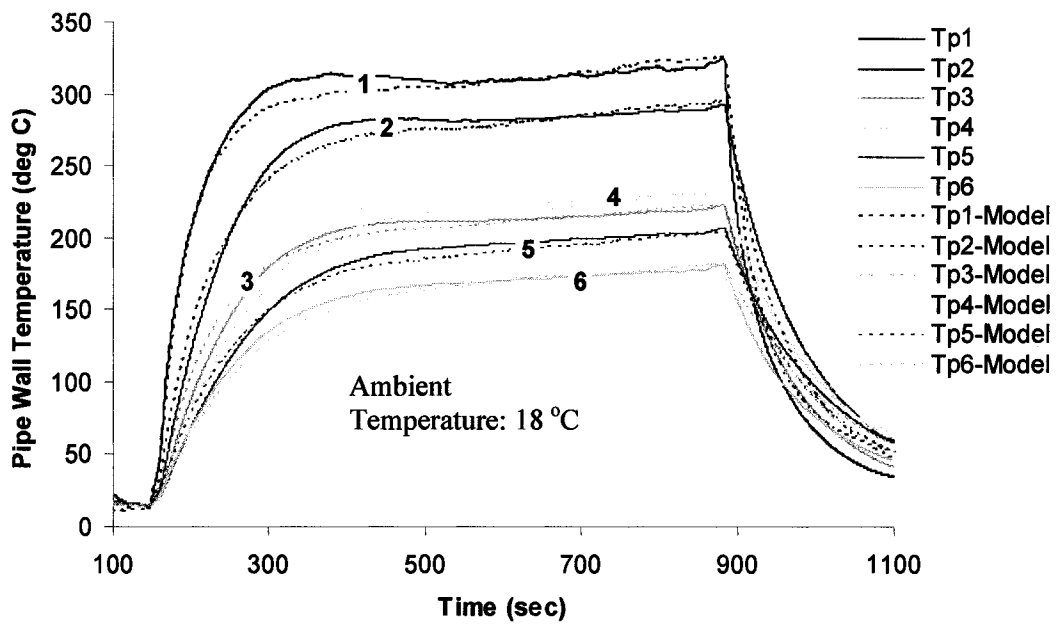
Figure 4.23: Pipe Wall Temperature Comparison (Test # 3)

The gas temperature comparison for the WAVE model (Figure 4.24) seemed to confirm the drawback of specifying a constant external heat transfer

72

coefficient. The wall temperatures shown in Figure 4.25 also indicate the necessity of using temperature resolved heat transfer parameters.
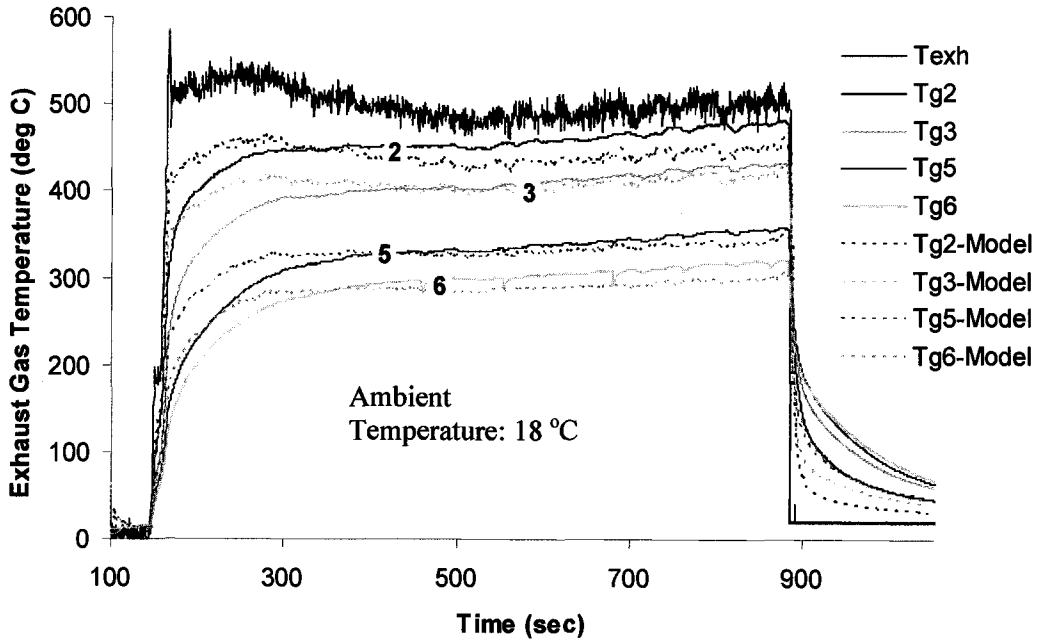
Figure 4.24: Gas Temperatures with WAVE (Test # 3)
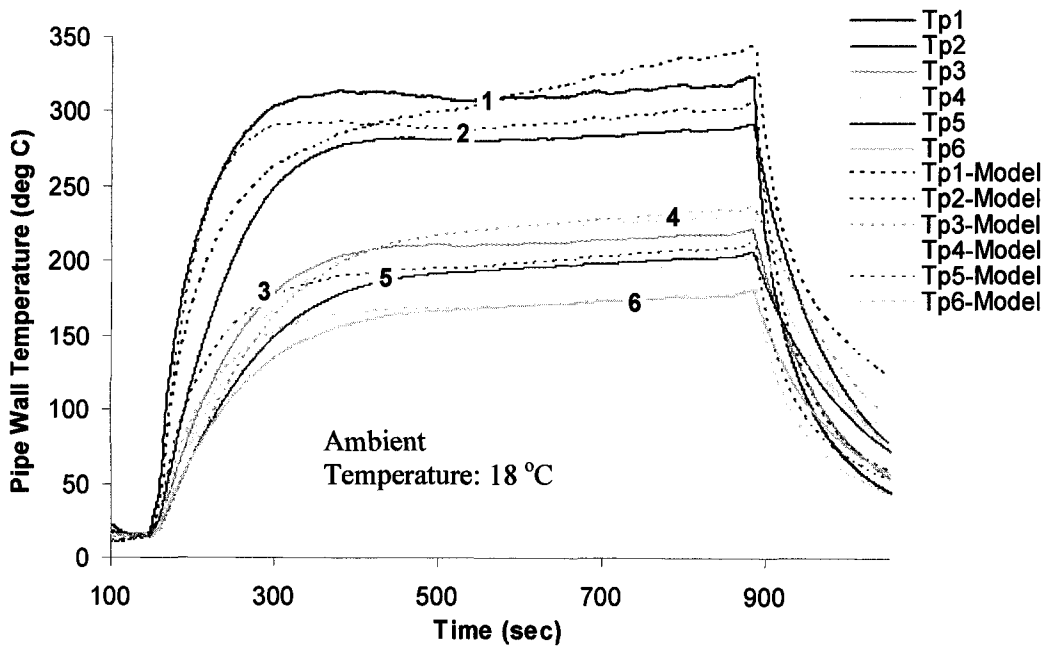
Figure 4.25: Wall Temperatures with WAVE (Test # 3)

73

The temperature comparison between the measured and the model predicted exhaust gas temperature at the inlet of the aftertreatment device is shown in Table 4.6.

Table 4.6: Summary of Results (Test # 3)

Time since Start (sec)	Engine-out Exhaust Gas Temperature ($^{\circ}$C)	Measured Gas Temperature (T_g6) at Inlet of Aftertreatment Device ($^{\circ}$C)	Calculated Gas Temperature at Inlet of Aftertreatment Device ($^{\circ}$C)
150	179.3	36.7	21.5
170	511.1	142.8	113.3
200	516	200.1	190.5
300	511.9	273.8	269.5
400	496.3	296.3	291.8
500	484.2	298.7	299.2
600	493.1	303.5	304
700	499.8	310.6	309.1
800	498.6	317.1	315
880	492.8	320	320.9
900	20.8	188.8	203.2
950	20.2	126.3	120.8
1000	22.3	91.35	90.1
1050	21.2	69.6	70
1080	20.4	60.2	61.5

For analyzing the exhaust system thermal response, the main interest lies in the exhaust gas temperature along the exhaust pipe in general and at the inlet of the aftertreatment device in particular. Therefore, only the comparisons of the exhaust gas temperatures along the length of the exhaust system are shown for the rest of the validation tests.

4.6.4. Test # 4 (Validation)

This validation test consisted of an initial engine warm-up period of about 12 minutes followed by transient load changes of different durations as indicated in Figure 4.26 on the next page. The duration of the transients was about 4~5 times longer than the duration during the calibration tests # 2. This was done to ensure that the validation was not limited to the engine operating conditions set during model calibration.

74
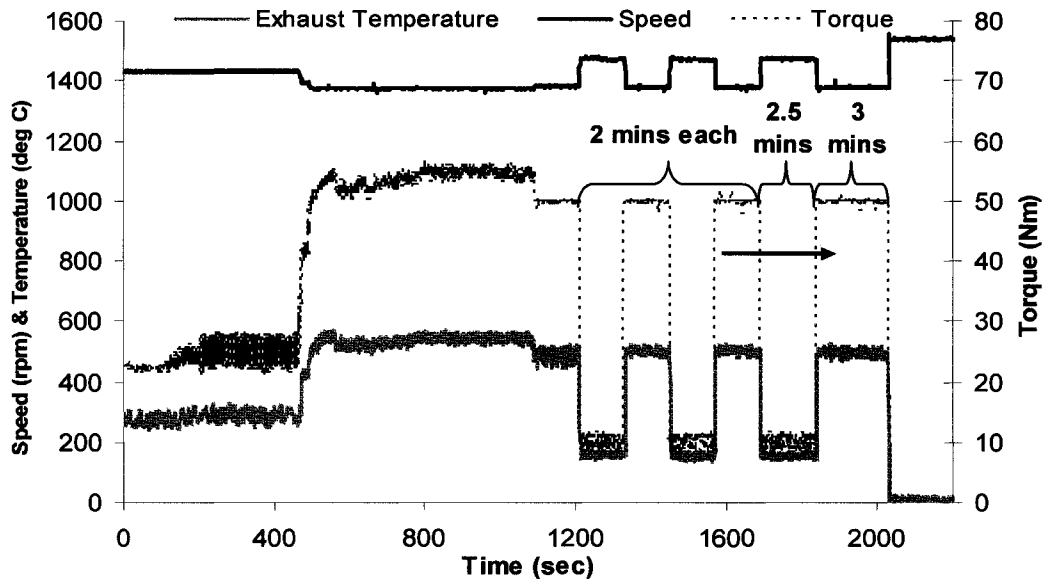
Figure 4.26: Engine Operating Conditions (Test # 4)

The gas temperatures are shown in Figure 4.27. The inset shows the temperature comparison during the transients.
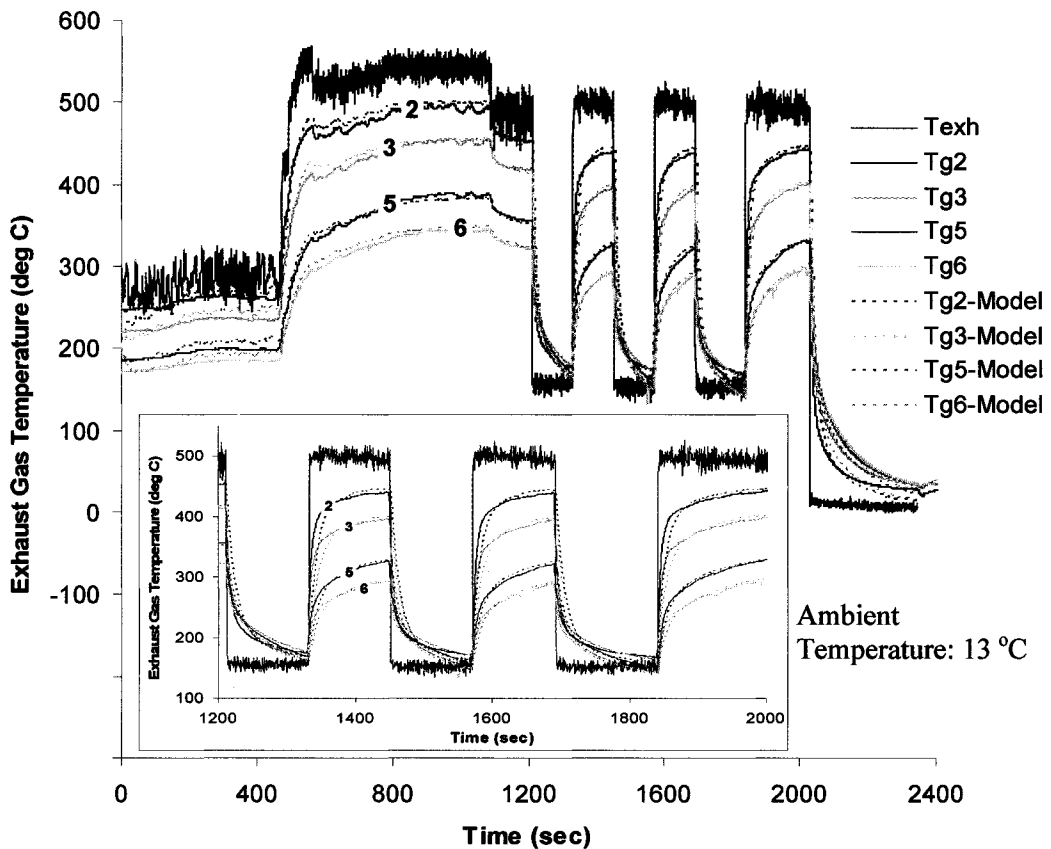
Figure 4.27: Gas Temperature Comparison (Test # 4)

75

It can be seen that the model was able to simulate the different engine operating conditions and the calculated temperatures show good agreement with the measured gas temperatures as shown in Table 4.7.

Table 4.7: Summary of Results (Test # 4)

Time since Start (sec)	Engine-out Exhaust Gas Temperature (°C)	Measured Gas Temperature (T_g6) at Inlet of Aftertreatment Device (°C)	Calculated Gas Temperature at Inlet of Aftertreatment Device (°C)
1	294	171.3	198
200	281.5	180.4	186.2
400	295.6	184.8	190.6
469	295.2	187.9	192.5
475	390.5	205.6	197.8
500	490	244.4	243.4
600	517	299.8	308.5
800	540.8	335.5	339.8
1000	524.8	341.9	346.8
1211	492.4	322.1	322.9
1213	174.9	299.8	312
1332	155.9	176.3	158.5
1334	504.2	199.5	167.2
1451	509.2	287.9	296.6
1453	160.3	265.4	288.5
1571	155	151.8	147.6
1573	495.1	162.1	157.1
1691	491	289	292.3
1693	209.6	267.7	288.5
1841	141.4	143.3	138.3
1843	479.1	145.7	151
2030	494.3	296.7	301.6
2032	19.1	276	282.4
2100	12.8	110.9	100.6

4.6.5. Test # 5 (Validation)

The emission tests for diesel engines commonly include a number of modes or specific engine conditions on which the vehicle must be tested. To see if the models were able to predict the thermal response during such a test, a 3-mode test was conducted. The specifications of the mode test are given in Table 4.8.

Table 4.8: Specifications of the 3-Mode Test

Mode #	1	2	3
Speed	700 rpm	1400 rpm	1800 rpm
Torque	3~6 Nm	~53 Nm	~10 Nm
Duration	~3 min	~3 min	~3 min

The engine conditions during the test are shown in Figure 4.28. The Yanmar engine has a mechanical fuel injection control system which resulted in difficulties in setting the desired condition as is evident from the figure.
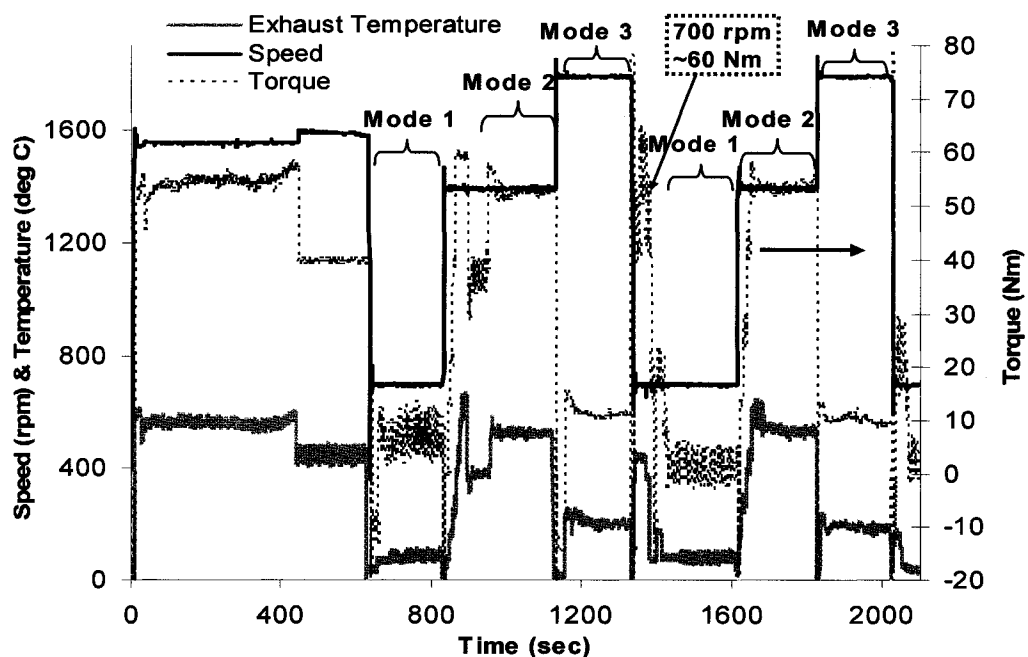
Figure 4.28: Engine Operating Conditions (Test # 5)

77

The comparison of the gas temperatures is shown in Figure 4.29. The model was able to predict the gas temperatures with reasonable accuracy.
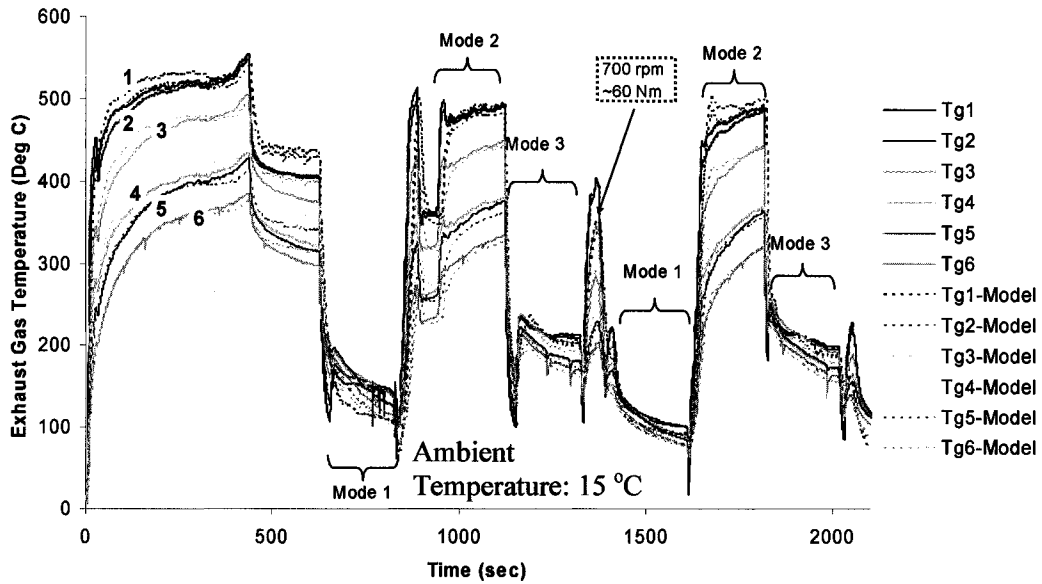
Figure 4.29: Gas Temperature Comparison (Test # 5)

The mode test was repeated twice to check for consistency and to ensure that the calculated results were repeatable. It can be seen from Figure 4.30 that the calculated results were able to meet that requirement.
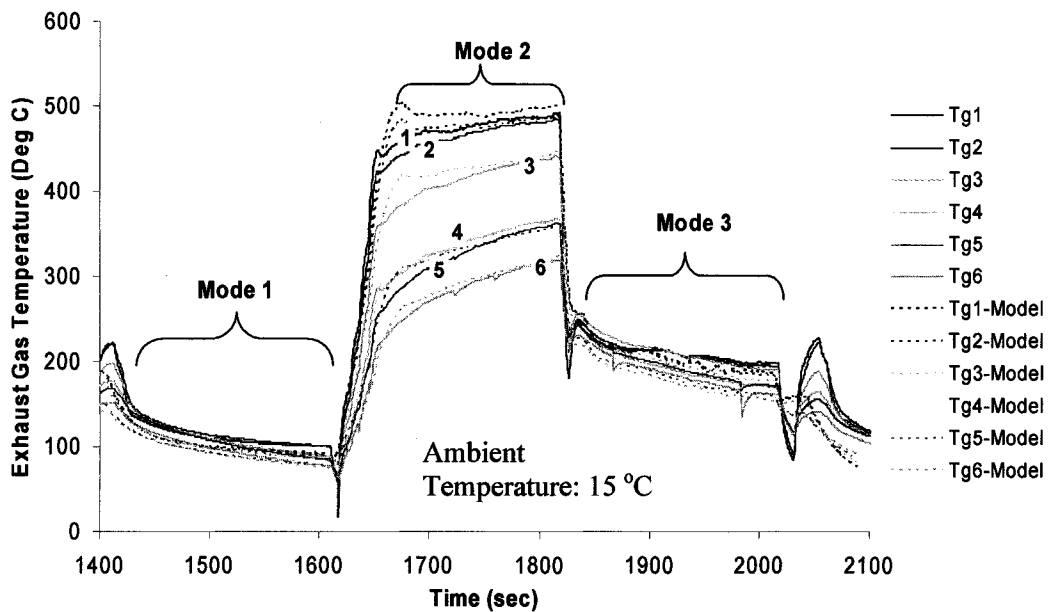
Figure 4.30: Gas Temperatures during 2nd Set of 3-Mode Test (Test # 5)

78

A summary of the measured and calculated gas temperatures at the inlet of the aftertreatment device is given in Table 4.9.

Table 4.9: Summary of Results (Test # 5)

Time since Start (sec)	Engine-out Exhaust Gas Temperature (°C)	Measured Gas Temperature (T_g6) at Inlet of Aftertreatment Device (°C)	Calculated Gas Temperature at Inlet of Aftertreatment Device (°C)
1	58.7	14.3	13.2
10	585.4	55	35.3
50	568.5	234.2	232.8
200	568.5	343.8	340.5
440	585.3	384.5	375.7
450	453.2	346.1	350.7
625	438.3	297.4	313.7
630	50.3	260.6	285.7
700	87.4	162.2	152.6
830	86.8	101.5	101.2
900	335	228.7	251.8
950	373.3	261.8	229.3
1000	526	303.2	292.2
1123	526.8	333.1	325.9
1130	27.7	245.5	252.1
1170	232.7	212.8	187.5
1330	191.4	145.7	160.9
1350	445.6	182.8	173
1370	445.7	202.4	196.7
1400	161.3	148.7	144
1420	73.5	142.6	130.4
1600	92.8	78.9	76.4
1630	289	106.1	94.4
1670	574.8	241.8	241.5
1750	533.8	297.1	297.3
1815	532.2	318.8	319.1
1900	204.9	191.8	185.5
2020	176.7	148.5	153.4

79

The gas temperatures calculated by the WAVE model are shown in Figure 4.31. The calculated temperatures were able to predict the trend but the actual values were generally under-predicted.
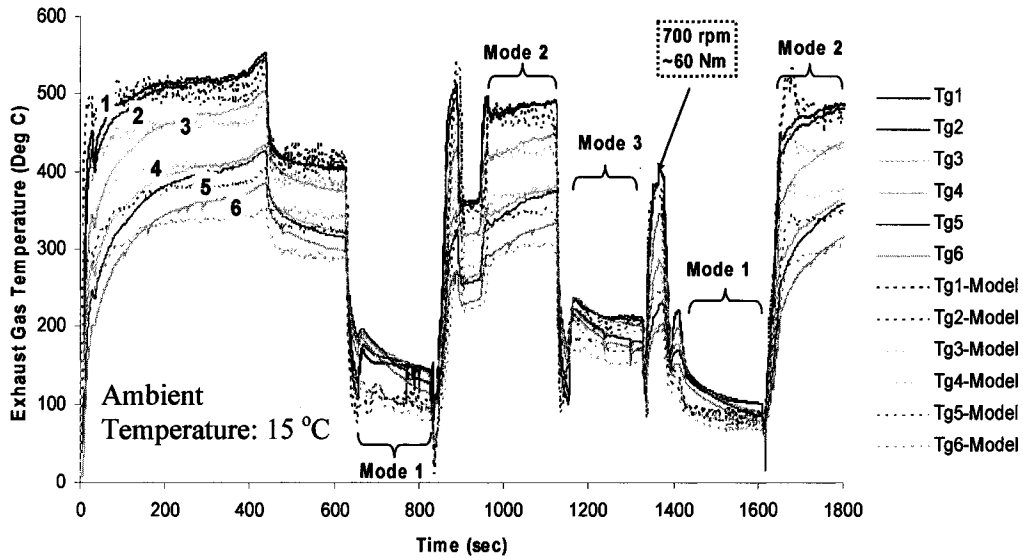
Figure 4.31: Gas Temperatures from WAVE (Test # 5)

4.6.6. Test # 6 (Validation)

In this test, two sets of transients were performed to generate different temperature spans as shown in Figure 4.32.
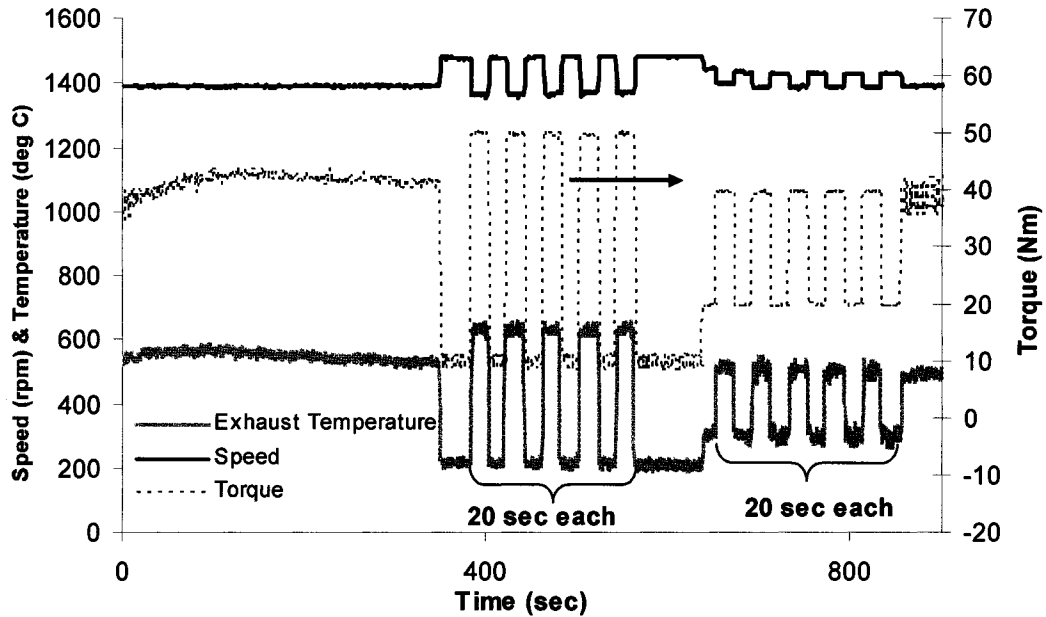
Figure 4.32: Engine Operating Conditions (Test # 6)

80

The resulting gas temperatures for the first set of transient operation are shown in Figure 4.33 and for the 2nd set of transient operation are shown in Figure 4.34. For the short duration of the transients, the model was able to predict the gas temperature at the inlet of the aftertreatment with reasonable accuracy.
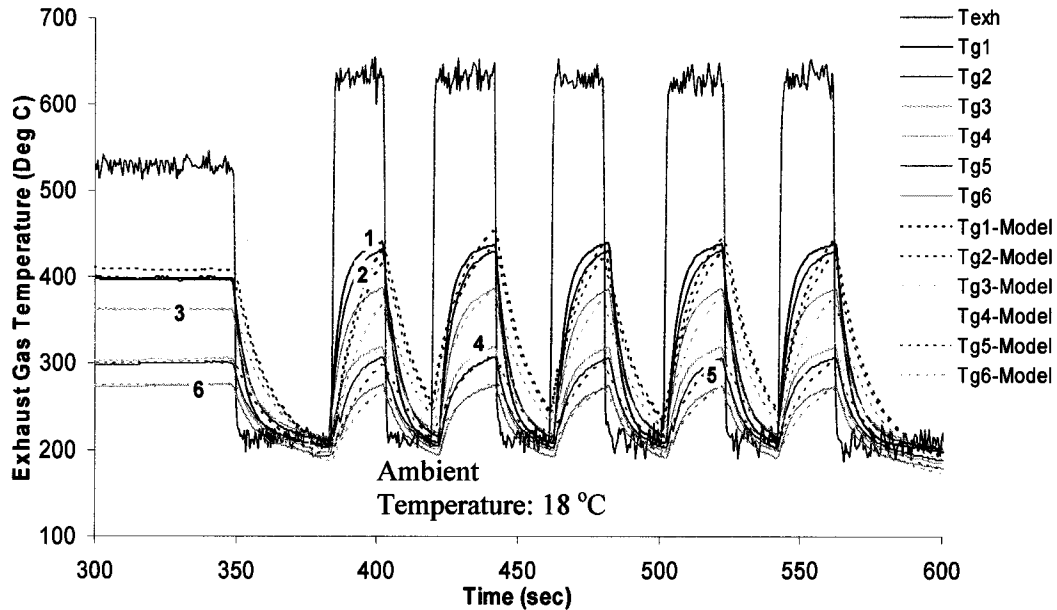
Figure 4.33: Gas Temperatures for 1st Set of Transients (Test # 6)
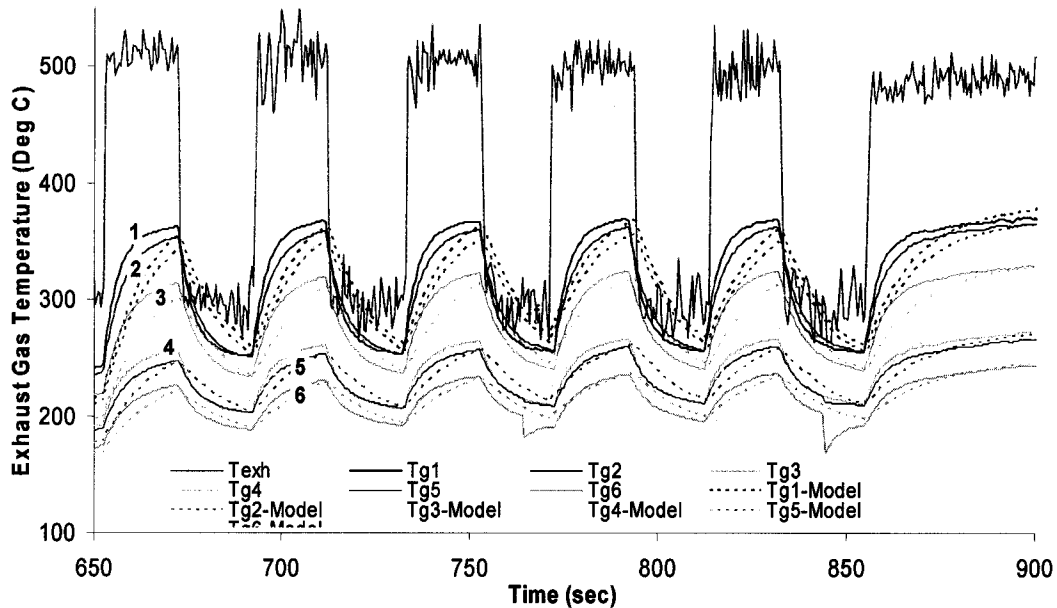
Figure 4.34: Gas Temperatures for 2nd Set of Transients (Test # 6)

81

The measured and calculated gas temperatures at the inlet of the aftertreatment device at different points during the test are given in Table 4.10.

Table 4.10: Summary of Results (Test # 6)

Time since Start (sec)	Engine-out Exhaust Gas Temperature (°C)	Measured Gas Temperature (T_g6) at Inlet of Aftertreatment Device (°C)	Calculated Gas Temperature at Inlet of Aftertreatment Device (°C)
50	558	192.3	183.8
200	540	263.2	262.2
348	526	275.1	274.9
351	224.5	254.8	265
384	218.3	200.9	186.3
386	631	216.1	199.6
402	631.8	274.5	266.7
404	226.5	258.4	261.9
419	205.5	197.8	203.5
425	619.4	224	232.3
441	640.4	273.3	276.6
445	207.1	242.8	256.9
461	204.6	194.2	200.6
465	620.9	213.1	218.9
480	629.4	270.9	269.8
485	204.6	245.8	243.8
500	206.6	193.6	196.5
505	630.6	206.4	214.3
522	635.1	272.7	270.1
565	200.3	247.7	250.1
635	195.2	166.2	154.1
654	502.9	186.3	175.7
672	517.9	226.6	221.6
675	293.6	212.6	215.5
692	309.2	188.2	189.7
695	511	202.8	196.2
712	502.3	230.8	228.5
715	287.7	213.2	220.7
732	304.3	191.8	193.7

4.6.7. Test # 7 (Validation)

The last test consisted of engine transients with 30 sec duration. However, the main difference from the previous tests was the use of EGR during part of the test as indicated in Figure 4.35.
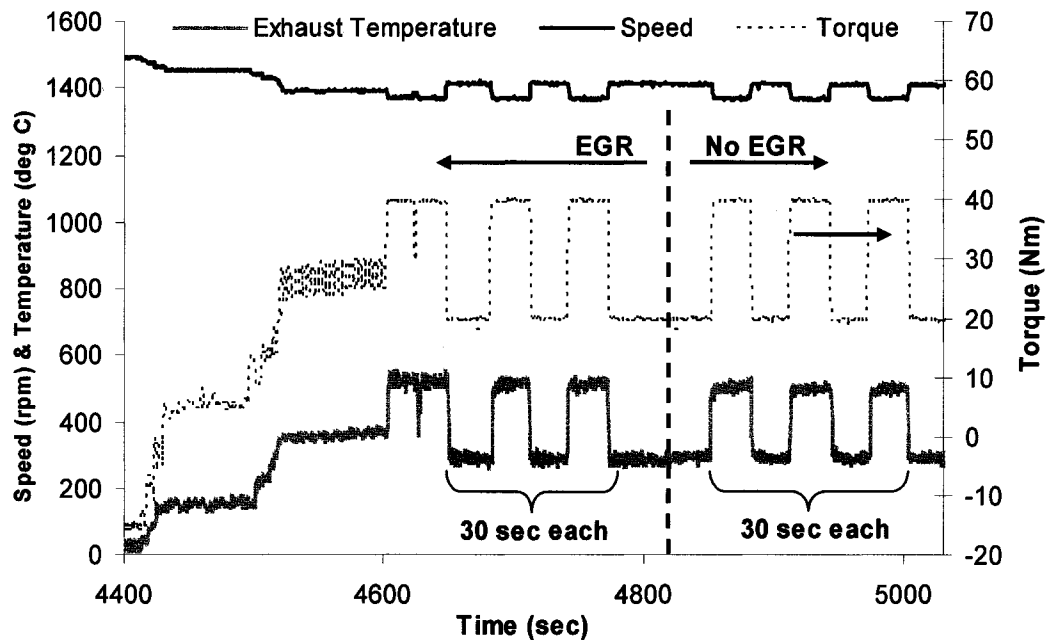
Figure 4.35: Engine Operating Conditions (Test # 7)

EGR can have two main effects on the exhaust gas exiting the engine cylinder. First, the higher CO_2 contents of the exhaust gas will change the heat capacity of the exhaust gas which can affect the heat transfer in the exhaust pipe to varying extent, depending upon the quantity of EGR used. Secondly, the flowrate in those sections of the exhaust pipe which are downstream of the EGR loop is less than the exhaust flow rate out of the engine. Due to these effects, modelling of the diesel exhaust as air is not suitable when using EGR Without accounting for these effects in the heat transfer model, the prediction of the exhaust gas temperature may deviate from the measured temperatures along the exhaust pipe.

83

To check the response of the heat transfer model to the engine conditions shown in Figure 4.35, the simulation was run and the resulting gas temperatures are shown in Figure 4.36.
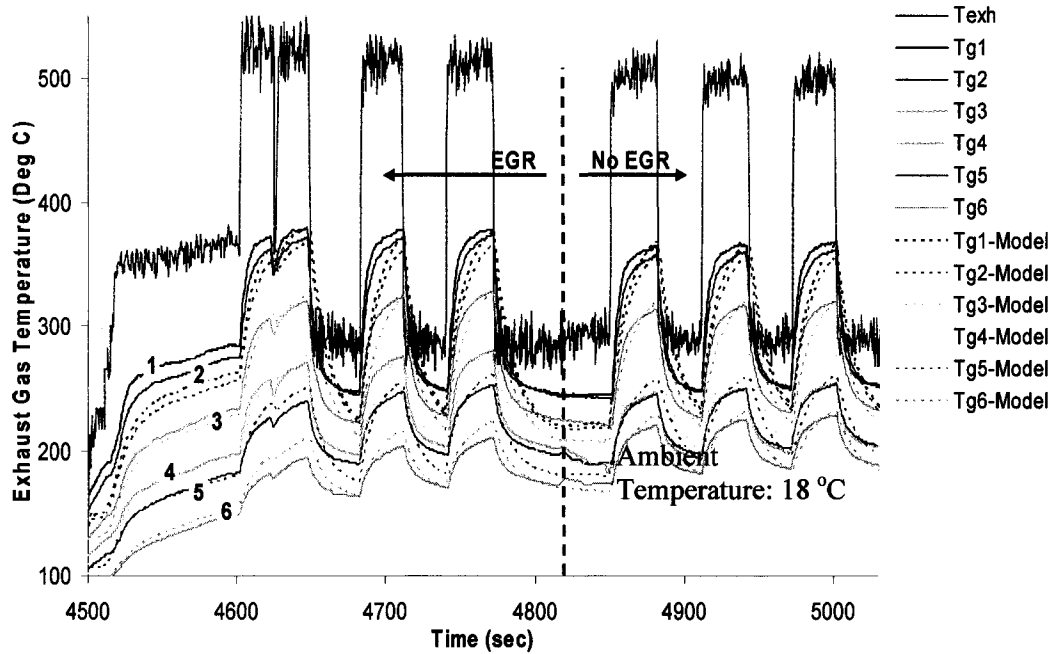
Figure 4.36: Gas Temperature Comparison (Test # 7)

The EGR loop was installed in section # 6 of the exhaust pipe (Figure 4.5) corresponding to thermocouple # 4. Up to the time when EGR was applied, the calculated gas temperature at the inlet of the aftertreatment $(T_g6$ Model) followed the general trend of the measured temperature (T_g6) but showed greater deviation during the transients. Once EGR was turned off, the difference between the two temperatures started to reduce.

The measured exhaust gas temperature at the inlet of the aftertreatment device during the test is shown along with the calculated exhaust gas temperature in Table 4.11 on the next page.

84

Table 4.11: Summary of Results (Test # 7)

Time since Start (sec)	Engine-out Exhaust Gas Temperature (°C)	Measured Gas Temperature (T_g6) at Inlet of Aftertreatment Device (°C)	Calculated Gas Temperature at Inlet of Aftertreatment Device (°C)
4425	129.6	62	50.4
4500	138.7	90.2	87.9
4502	201.8	92	90.7
4520	348.9	104.4	106
4600	366.7	149.3	154.4
4605	535.7	160.9	164.9
4648	534.6	194.5	210.8
4650	289.7	185.9	205.3
4682	285.4	163.9	163.6
4686	512.7	178.6	176.7
4700	520.5	198.1	206.6
4710	522.8	203	215.7
4714	269	196.3	205
4740	287	171.8	170.7
4744	527.1	179.8	185.3
4771	527.5	210.3	222.8
4776	287.4	195.7	207.5
4850*	287	174.3	166.7
4854	497.1	184.7	180.8
4880	519.7	220.7	228.4
4884	301.5	210.3	223.8
4910	289.3	182.8	182.4
4914	490	193.9	189.9
4943	495.1	221.9	231.8
4950	304.2	198.7	213.6
4973	298.3	189.6	184.2
4980	509.6	214.6	204.7
5001	507.2	228	231.9
5004	287.8	219.5	224.3
5030	289.7	189.6	185.3

* EGR turned off at this time

85

The effect of EGR on the engine-out emissions is shown in Figure 4.37. The primary effect of EGR is to reduce the NOx emissions as the higher CO_2 content increases the heat capacity of the cylinder charge, thereby reducing the combustion temperature. However, the CO emissions increase, particularly at high loads when the higher CO_2 concentration reduces the availability of oxygen to the burning fuel, resulting in incomplete combustion of fuel. When EGR is turned off, the NOx emissions increase sharply with a simultaneous decrease in the CO emission as is the case in conventional diesel combustion.
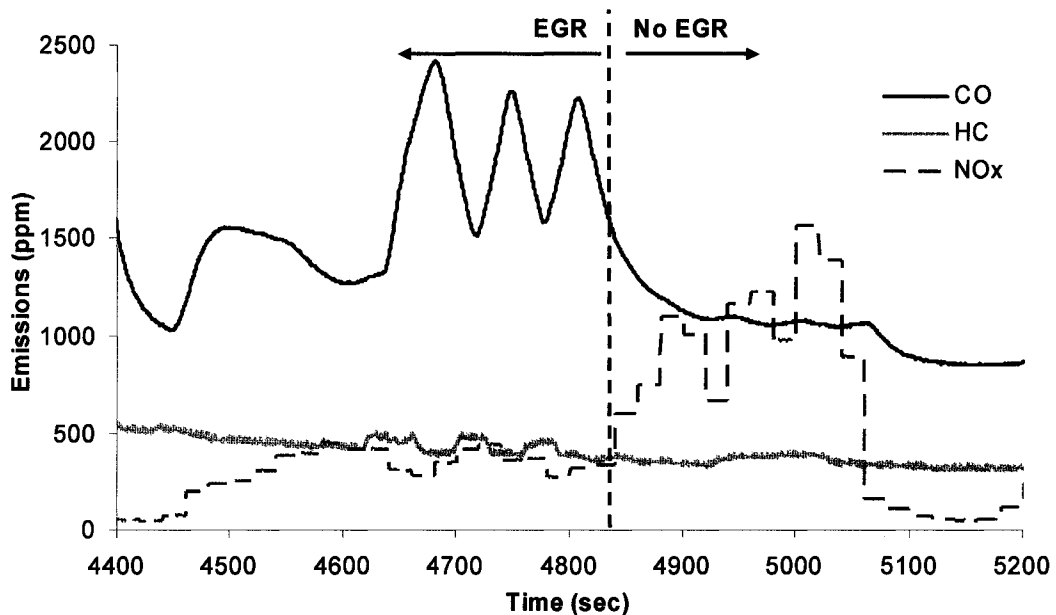
Figure 4.37: Engine–out Emissions (Test # 7)

4.7. EFFECT OF DOUBLE-WALL EXHAUST PIPE

The double-wall exhaust pipe may significantly reduce the heat loss from the exhaust pipe, thereby providing a higher exhaust gas temperature at the inlet of the aftertreatment device. To simulate the heat transfer characteristics of the double-wall pipe and appreciate the potential benefits, simulations were run using both the in-house code and the WAVE model for some of the experiments carried out on the single-wall Yanmar exhaust system. It is pertinent to mention here that as a double-wall pipe was not available for actual engine tests, the simulation results outline the potential for improvement in the thermal response of the exhaust system. The results provided in the following section should be analyzed for

86

providing a possible trend rather than the actual values. To quantify the actual improvement, it is necessary to validate these results through conduct of verification experiments. The specifications of the double-wall pipe structure used in the simulations are given in Table 4.12.

Table 4.12: Double-Wall Pipe Specifications for Simulations

Type	Double –wall Pipe
Length (till inlet of aftertreatment)	~1.55 m
Total Mass	~ 8.3 kg
Pipe Material	Stainless Steel
Outer Pipe Outer Diameter	58.4 mm
Outer Pipe Wall Thickness	1.78 mm
Inner Pipe Outer Diameter	50.8 mm
Inner Pipe Thickness	1 mm
Air Gap Thickness	2 mm

The engine conditions from Test # 2a (Figure 4.13) were used as the input. The gas temperatures calculated for both the single-wall and the double–wall structures at two locations along the exhaust pipe are shown in Figure 4.38.
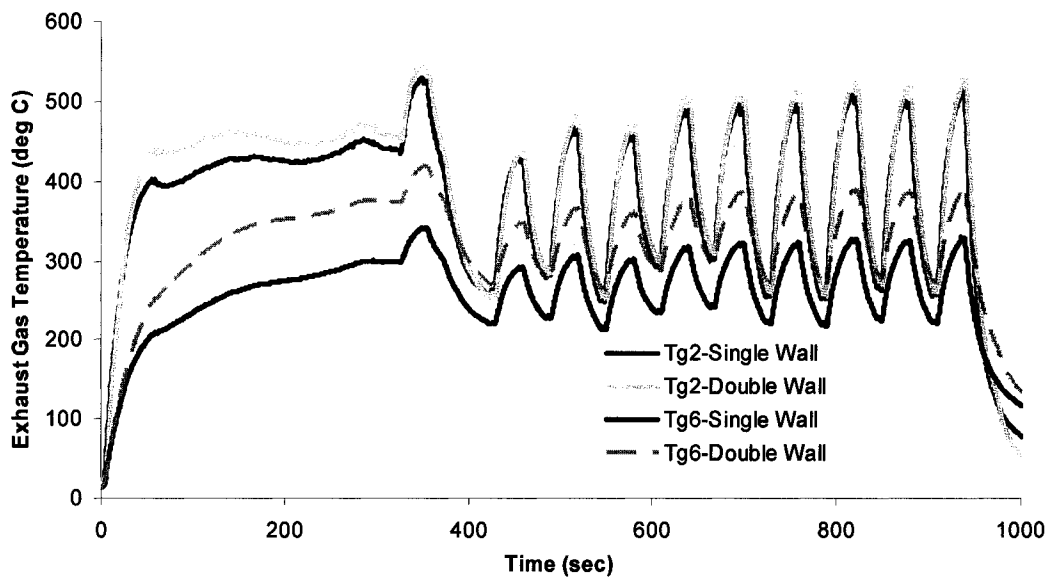
Figure 4.38: Effect of Double-Wall Pipe (Simulation)

The results indicate that the air gap between the two layers of the double-wall pipe may be effective in reducing the heat loss from the exhaust gas and

87

therefore, providing a higher temperature at the inlet of the aftertreatment device compared to the single-wall pipe. A maximum increase of around 74°C in the exhaust gas temperature at the inlet of the aftertreatment was predicted with the double-wall pipe.

To ascertain the difference in the thermal energy loss between the two pipe structures, an energy efficiency analysis was performed at conditions existing after 6 minutes of engine run (during the warm-up period). The results indicated that energy recovery up to 16% could be possible with the double-layer exhaust pipe as shown in Figure 4.39. The heat loss from the double-layer exhaust pipe was less with the result that the temperature at the inlet of the aftertreatment device and hence the energy available was higher in case of the double-layer pipe structure.
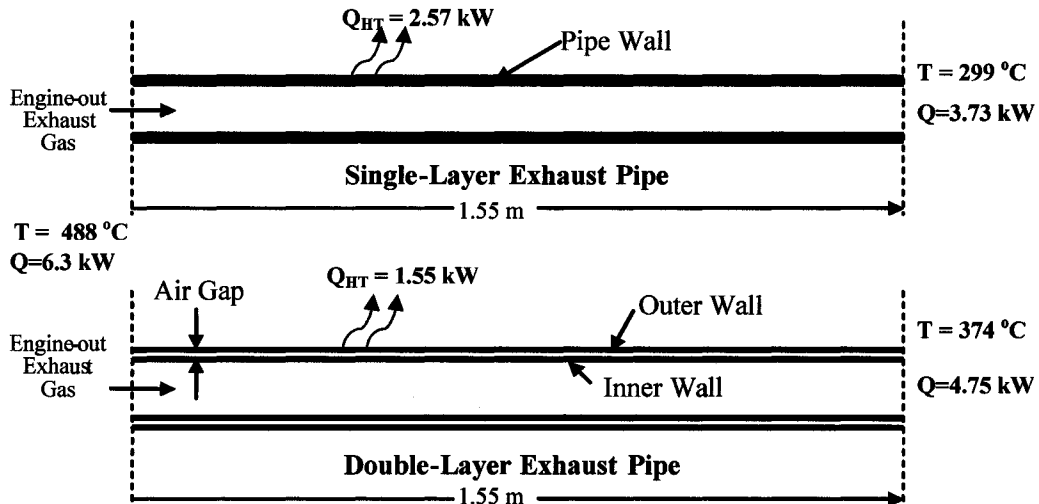
Figure 4.39: Energy Availability for Different Exhaust Pipe Structures

4.8. CONCLUDING REMARKS OF CHAPTER 4

The heat transfer in the exhaust system was estimated by developing a 1-D transient heat transfer model. The model is capable of simulating both the single-wall and the double-wall pipe structures and takes into account the effects of pipe bends, flanges etc on the heat transfer. A similar model was also setup using WAVE software. To calibrate and validate the models, the exhaust system of the Yanmar single cylinder diesel engine available in the Clean Diesel Engine Laboratory was prepared. Thermocouples were embedded in the exhaust system to

measure both the exhaust gas and the pipe-wall temperatures. Extensive tests were performed to cover a wide range of engine operating conditions including steady-state and transient operations. The model results showed good agreement with the experimental results. The heat transfer characteristics of a double-wall exhaust pipe were simulated and the potential benefits were highlighted through an energy efficiency analysis.

5.   THERMAL RESPONSE CHARACTERIZATION

The transient thermal response of the exhaust system depends on the configurations of the exhaust pipes that include the pipe structure, the wall thickness, and the exterior thermal management. Therefore, the exhaust gas temperature at the inlet of the aftertreatment responds slowly to sharp changes in the engine-out exhaust temperature. Also, the thermal energy loss to the environment along the exhaust pipe results in a considerably lower exhaust temperature at the inlet of the aftertreatment device.

Based on the calibration and validation results described in Chapter 4, an effort was made to characterize the thermal response of the exhaust system by quantifying two effects:

(1)   the 'delaying' effect which can provide an estimate of the time window required to enable aftertreatment operations, and

(2)   the 'heat loss' effect which can approximate the temperature drop due to heat loss in the exhaust system and therefore, allow the required in-cylinder operations to be adapted accordingly.

Knowledge of the temperature-time history at the inlet of the aftertreatment device is necessary for efficient aftertreatment operation. If the 'heat loss and delay' effects caused by the exhaust system are known, the in-cylinder events can be synchronized to deliver the desired energy spike at the required time.

The 'heat loss and delay' effects of the Yanmar exhaust system were first investigated by analyzing the results presented in Chapter 3. The results observed were also corroborated with additional simulation results by simulating sharp spikes in the engine-out exhaust gas temperature and analyzing their effect at the inlet of the aftertreatment device.

90

5.1. THERMAL RESPONSE – EXPERIMENTAL RESULTS

The engine-out exhaust gas temperature along with the measured and the calculated gas temperatures at the inlet of the aftertreatment device for Test # 3 are shown in Figure 5.1. At the start of the test, the exhaust system was at ambient temperature. It can be seen that during the warm up process, while the engine-out exhaust gas temperature is quite high (sharp rise), the gas temperature at the inlet of the aftertreatment device increases at a much slower rate (delaying effect). Moreover, the heat loss from the exhaust flow results in a much lower steady state temperature (T_g6).
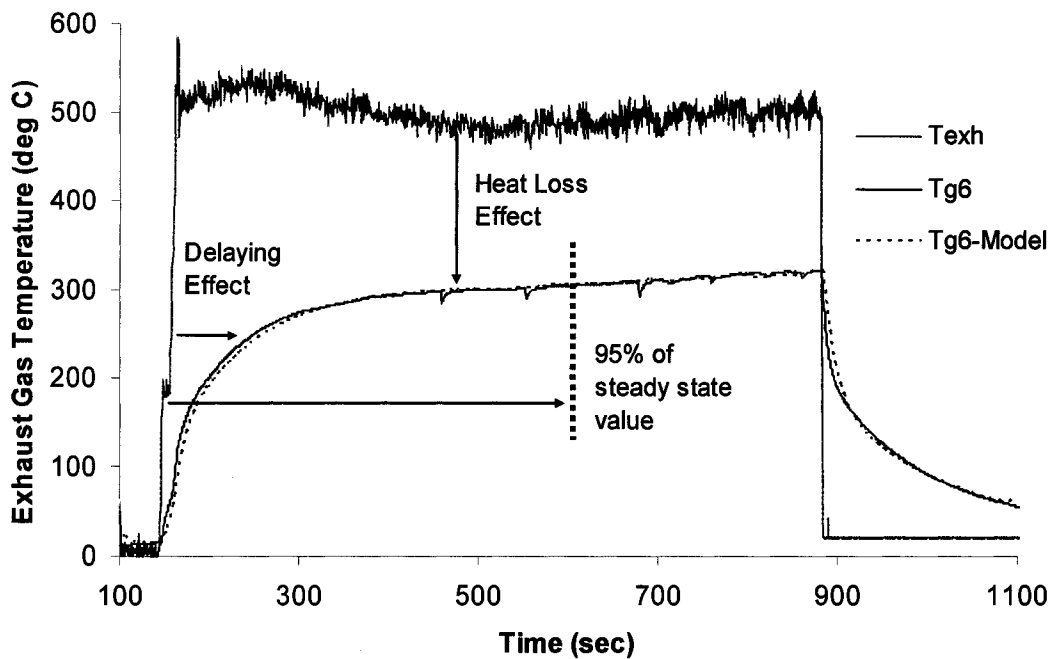
Figure 5.1: Thermal Response at Inlet of Aftertreatment (Test # 3)

To quantify the delay, the definition of the time constant used in resistor-capacitor (RC) circuits was adapted. For an RC circuit, the time required to charge a capacitor to 63.2% of the applied voltage or to discharge it to 36.8% of its initial voltage is known as the time constant (τ) of the circuit. A total of 5 time constants are required for the circuit to approach 99.3% of the step change value. The concept is shown in Figure 5.2 on the next page.

91
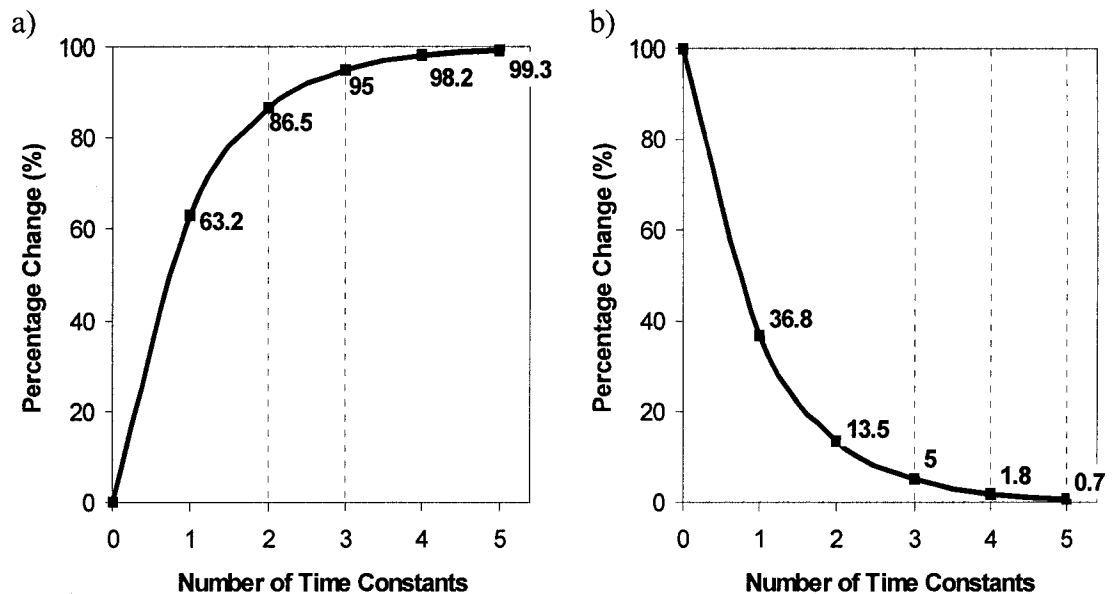
Figure 5.2: The Concept of Time Constant for (a) Heating and (b) Cooling

A similar approach was used for characterizing the delay effect. A time constant of the exhaust system (τ_{exh}) was defined as the time required to reach 63.2% of the final steady-state temperature attained at the inlet of the aftertreatment device after a step-change in the engine-out exhaust gas temperature. It is important to highlight here that the τ_{exh} differs from the electrical time constant in two respects:

(1)   The electrical time constant is defined in terms of the step change in the applied voltage. This corresponds to the step-change in the engine-out exhaust gas temperature. However, the τ_{exh} has been defined in terms of the step change that occurs at the inlet of the aftertreatment due to a larger step change in the engine-out exhaust gas temperature.

(2)   It takes 5 time constants for the circuit to reach 99.3% of the step change value. However, as will be shown later, this statement was not valid in case of τ_{exh}.

The time constant analogy was applied to the results shown in Figure 5.1 for both the heating and cooling processes and the outcome is shown in Figure 5.3.
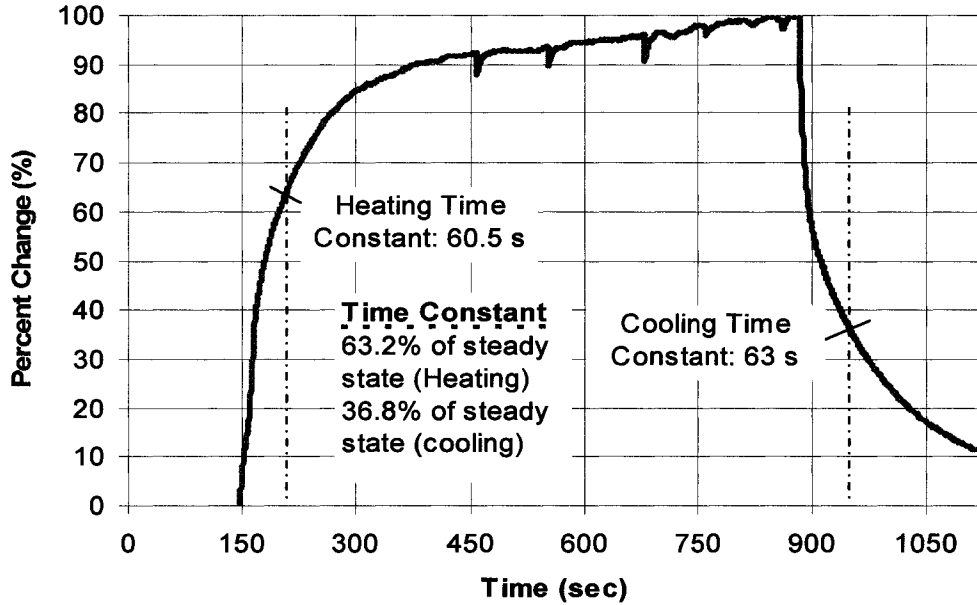
Figure 5.3: Application of τ_{exh} to Test # 3 Results

During the heating (warm-up) process, the τ_{exh} was about 60 sec while during the cooling process, the τ_{exh} came to about 63 sec. The same process for repeated for the results from Test # 4 shown in Figure 5.4.
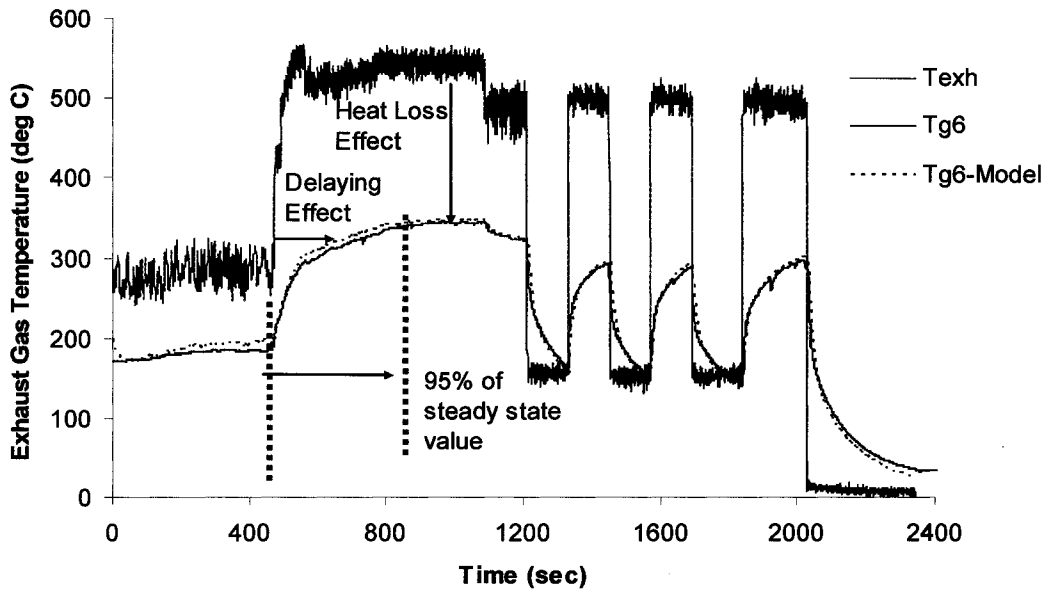
Figure 5.4: Thermal Response at Inlet of Aftertreatment (Test # 4)

The percentage change in the temperature at the inlet of the aftertreatment device and the resulting time constants τ_{exh} for the initial heating and final cooling phases are shown in Figure 5.5.
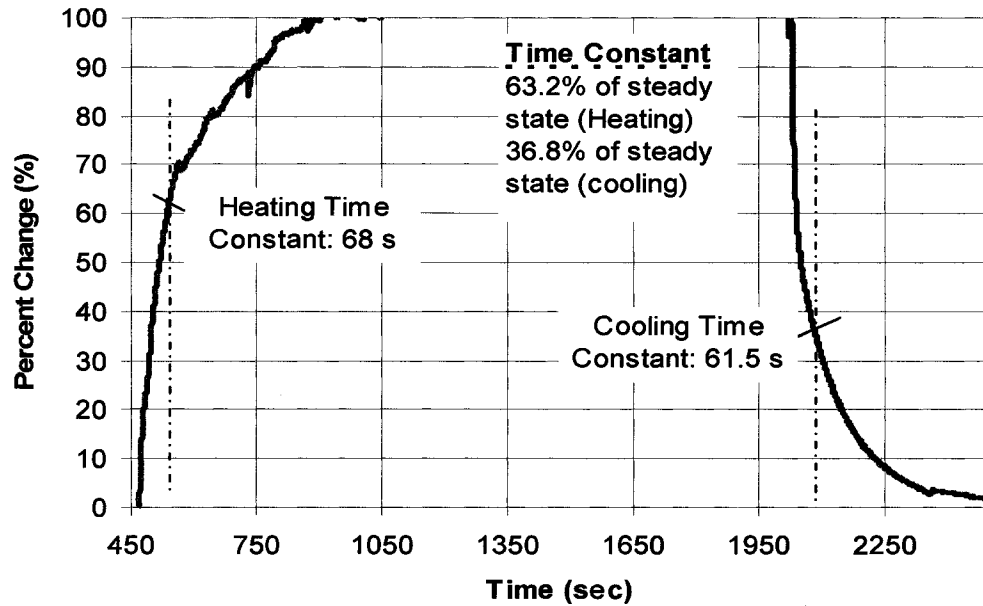
Figure 5.5: Application of τ_{exh} to Test # 4 Results

To verify if the τ_{exh} concept was applicable over a wider range of engine operation and the values of τ_{exh} infact were representative of the Yanmar exhaust system, the result from test # 5 shown in Figure 5.6 was analyzed.
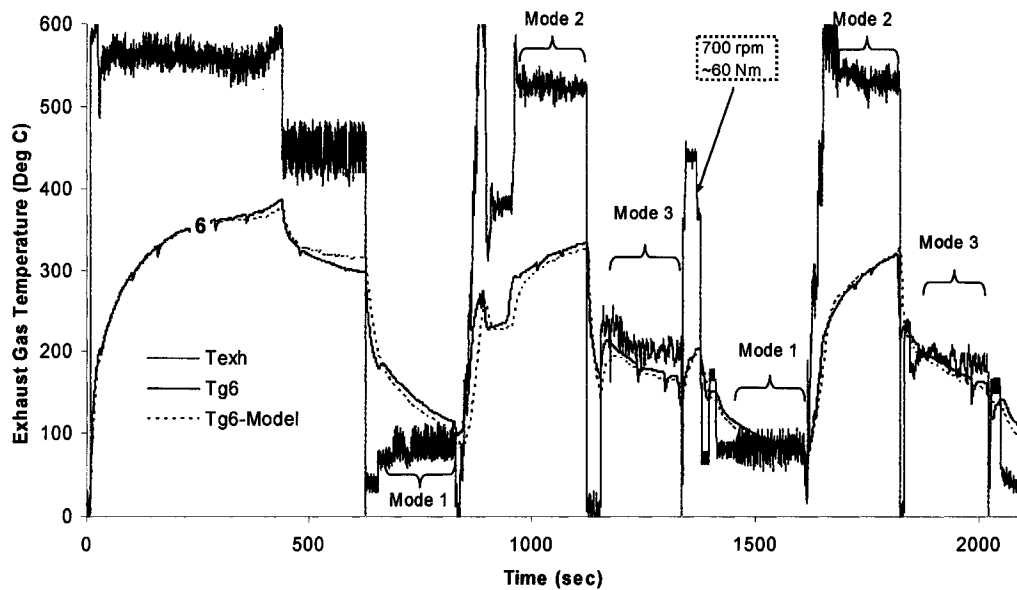
Figure 5.6: Thermal Response at Inlet of Aftertreatment (Test # 5)

94

The value of the time constant τ_{exh} for the initial heating phase of the test is shown in Figure 5.7.
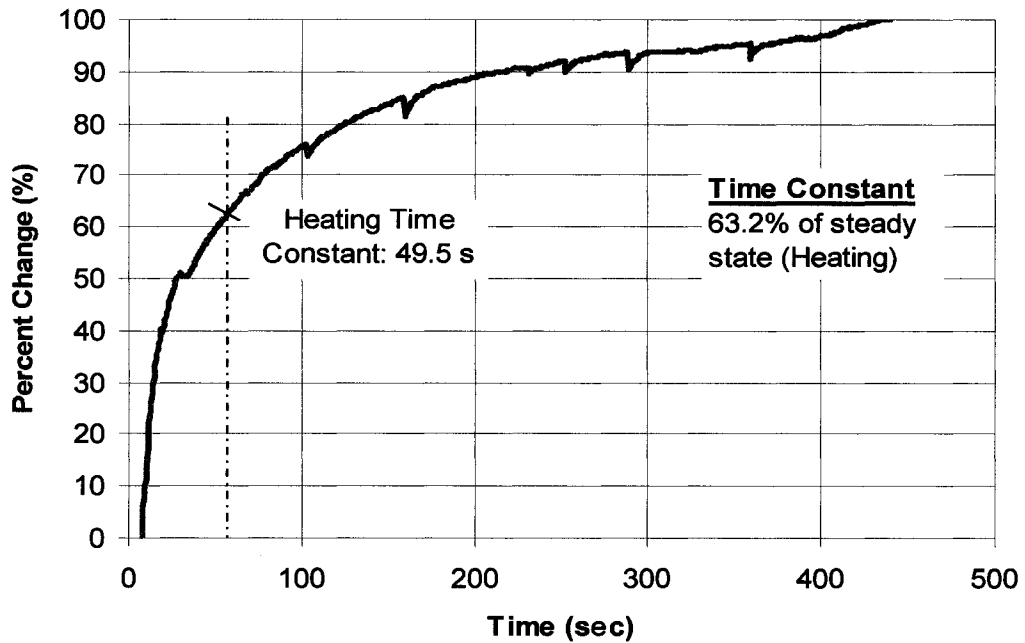
Figure 5.7: Application of τ_{exh} to Test # 5 Results

The τ_{exh} concept was not applied to the transient processes since the final steady state temperature was not known. The time constant for the transient phases was calculated once the final steady state temperatures were estimated by quantifying the heat loss as explained later on.

5.2. SIMULATIONS & RESULTS

A number of simulations were run by varying the exhaust flowrate and the ΔT_{exh} to simulate different engine operating conditions. The time duration of each state was fixed to allow the exhaust system to approach steady-state values. The engine-out exhaust temperature was then changed sharply and the system was again allowed to reach steady-state values. The response of the system to both cooling and heating processes was analyzed. The results for a few of these simulations are presented case-wise.

5.2.1. Warm-up and Cooling Processes (Case # 1)

The simulated engine conditions for the cooling process are shown in Figure 5.8 and the results are shown in Figure 5.9.
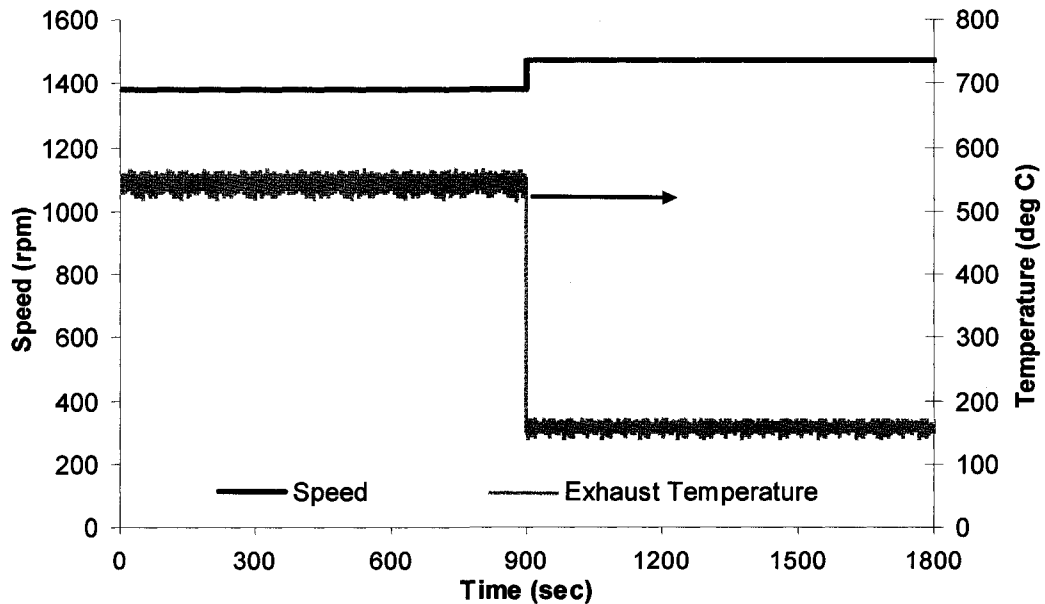
Figure 5.8: Simulated Engine Conditions (Case # 1)

In all the results, only the exhaust gas temperature and the temperature at the inlet of the aftertreatment device (T_g6) have been shown.
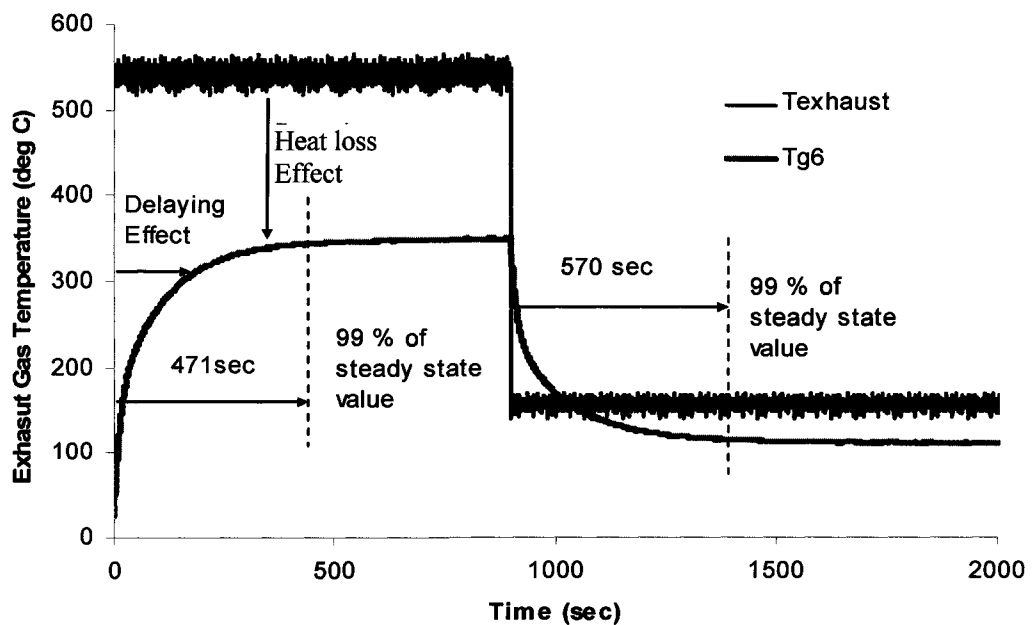
Figure 5.9: Thermal Response at Inlet of Aftertreatment (Case # 1)

96

The first part simulated the warm-up process where the exhaust system was initially at ambient temperature. As indicated in Figure 5.9, the thermal response of the exhaust system results in a significant delay and loss of thermal energy from the exhaust flow which is evident by the much lower steady state temperature (T_g6). During the cooling process, the exhaust helps to maintain a higher temperature at the aftertreatment inlet by heating up the exhaust gas as it flows down the exhaust plenum.

The time constant analogy was applied to the results of Figure 5.9 and the outcome is shown in Figure 5.10.
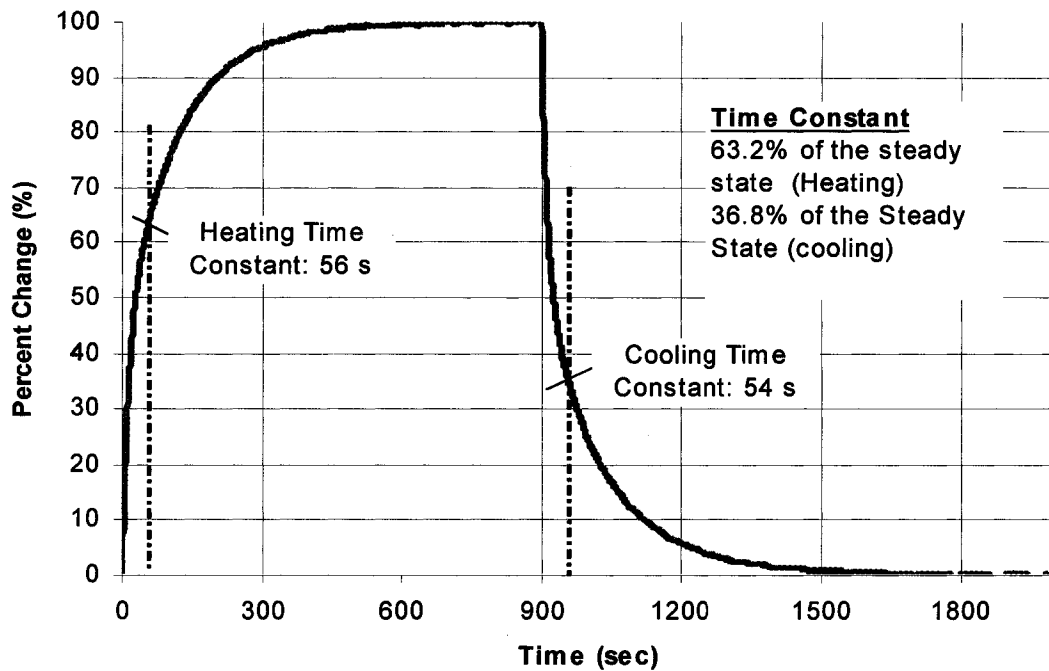
Figure 5.10: Application of τ_{exh} to Case # 1

During the heating (warm-up) process, the τ_{exh} was about 56 sec while during the cooling process, the τ_{exh} came to about 54 sec. Moreover, it was observed that about 8~9 time constants were required to attain about 98% of the steady state temperature at the inlet of the aftertreatment device due to the step change in the engine-out exhaust gas temperature.

97

5.2.2. Heating and Cooling Processes (Case # 2)

The system was brought to a steady-state condition and then an alternate high and low temperature spikes were produced as shown in Figure 5.11.
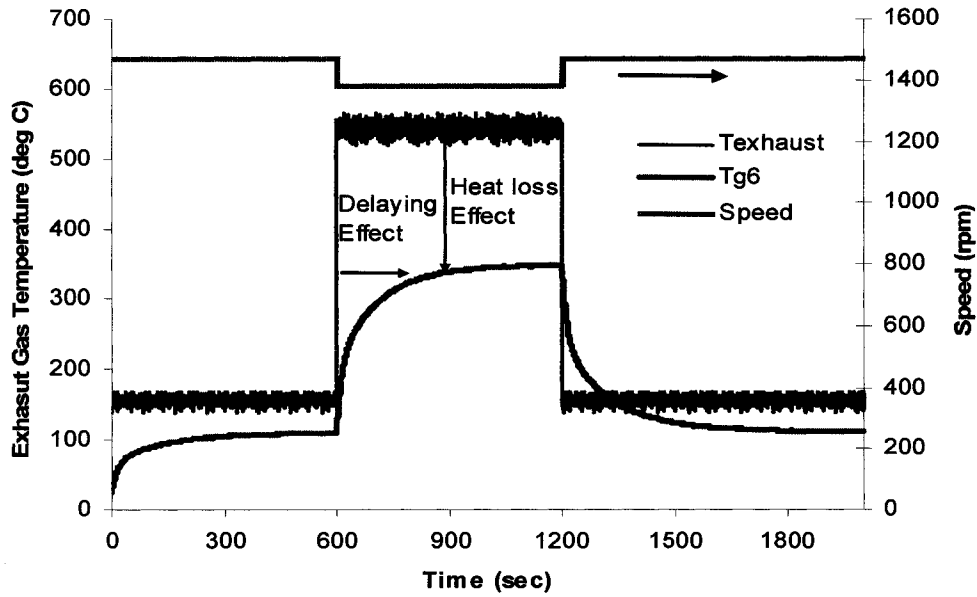
Figure 5.11: Simulation Conditions (Case # 2)

The percentage change in the temperature at the inlet of the aftertreatment device and the resulting time constants τ_{exh} for the 3 phases are shown in Figure 5.12.
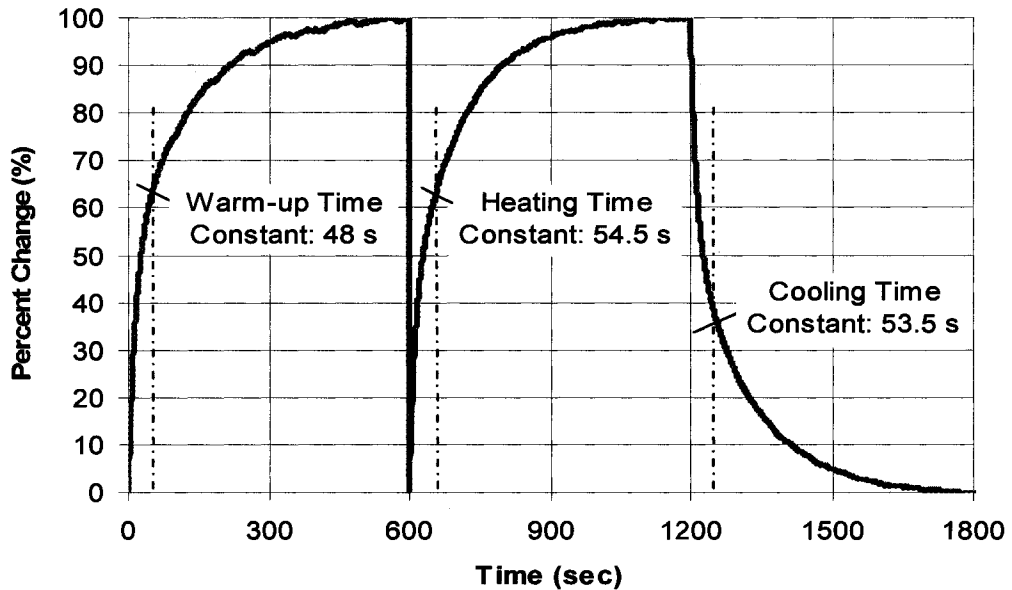
Figure 5.12: Calculated τ_{exh} (Case # 2)

98

The simulations results appeared to be in general agreement with the values of the time constant obtained from the experimental test results. Another parameter of interest in this analysis was the engine speed. At higher engine speeds, the exhaust flowrate is higher and the value of the τ_{exh} may be significantly affected by the increased exhaust gas flowrate. Consequently, it was thought that the value of τ_{exh} may decrease as the exhaust flowrate increased.

5.2.3. Warm-up, Cooling & Heating (Case # 3)

To analyze the warm up phase and further verify the validity of the τ_{exh} concept, Case # 3 was run with an initial warm-up phase, followed by a cooling and then a heating phase. A wider range of engine speeds was selected to assess the impact of increased exhaust flowrate on the validity of the time constant for the exhaust system. The simulation conditions are shown in Figure 5.13.
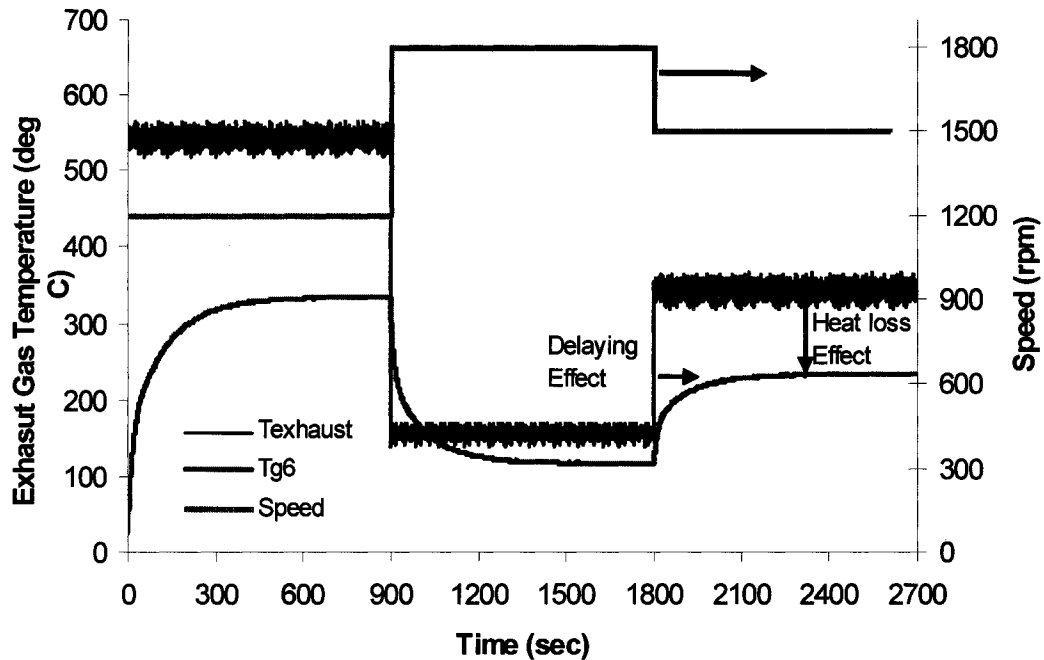
Figure 5.13: Simulation Conditions (Case # 3)

The relative change in the temperature at the inlet of the aftertreatment device for the 3 phases is shown in Figure 5.14. It was observed that τ_{exh} varied with a change in the exhaust flowrate. Other simulations were run to

99

cover the entire range of the Yanmar engine (800~2400 rpm) and the τ_{exh} for both heating cooling processes was plotted versus the engine speed as shown in Figure 5.15. It can be seen that τ_{exh} decreased as the engine speed was increased and generally followed this trend.
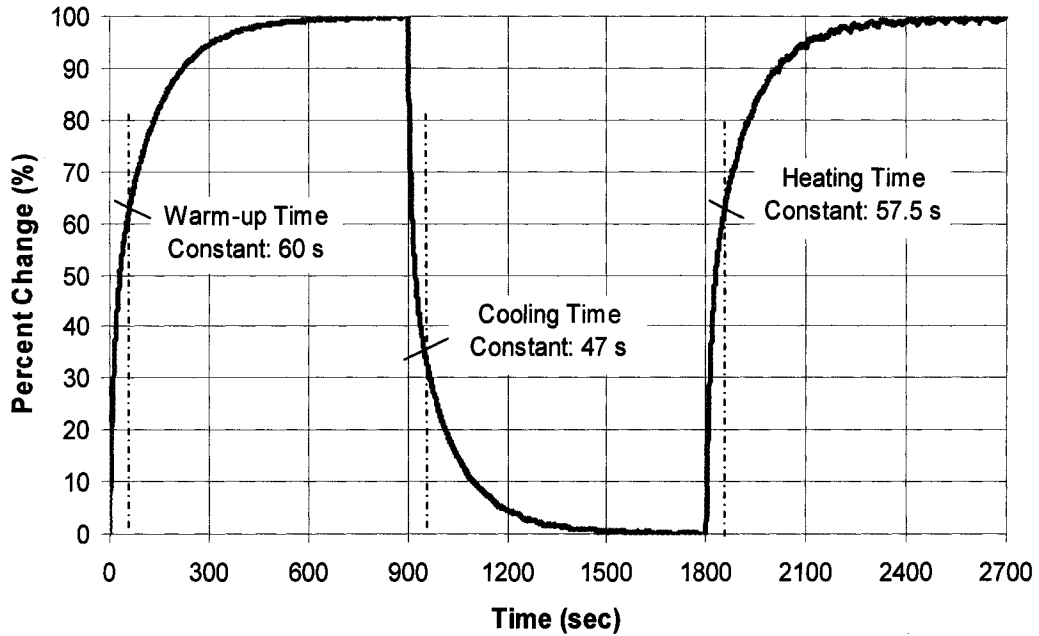
Figure 5.14: Calculated τ_{exh} (Case # 3)
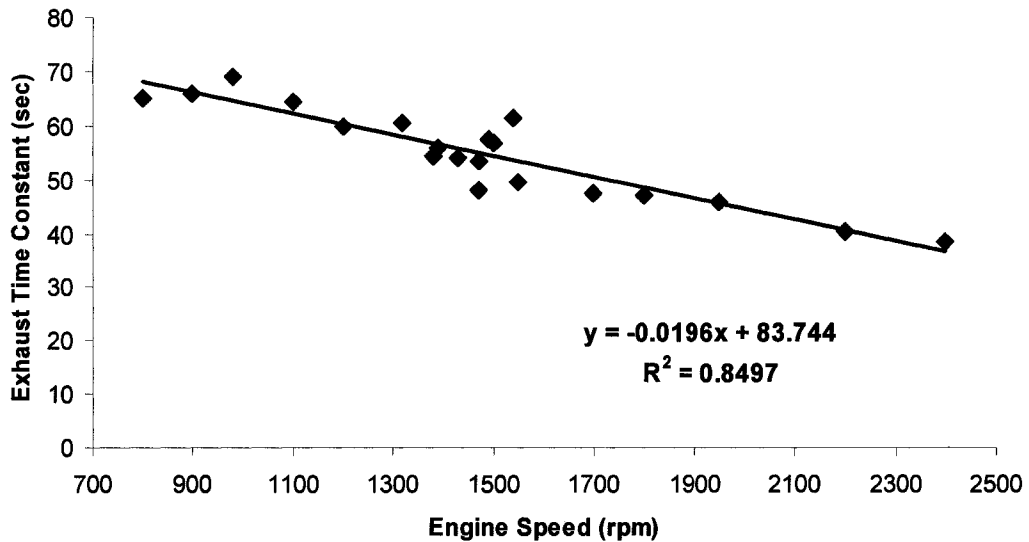
Figure 5.15: Effect of Engine Speed on τ_{exh}

100

Based on the experimental and simulation results presented above, the delaying effect can be quantified by using the concept of a time constant for the exhaust system. Moreover, the results also indicated that about 8~10 time constants were needed to reach 98% of the steady-state temperature value.

The 'heat loss' effect results in a lower temperature at the inlet of the aftertreatment device. To quantify the 'heat loss' effect of the exhaust system, the fraction of the exhaust energy lost in the exhaust system was calculated as given in Table 5.1.

Table 5.1: Data for Quantifying the Heat-loss Effect

Engine Speed (rpm)	Engine-out Exhaust Gas Temperature (^{o}C)	Temperature at Inlet of Aftertreatment (^{o}C)	Fraction of Exhaust Energy Lost
800	344	192	0.442
1200	540	334	0.381
1380	545	349	0.36
1380	540	347	0.357
1470	165	111	0.327
1470	164	113	0.311
1500	339	235	0.306
1800	162	117	0.278
2400	152	123	0.191
900	620	339	0.453
980	351	206	0.413
1700	620	416	0.329
1950	340	250	0.265
1320	506	320	0.368
1370	541	344	0.364
1550	554	371	0.33

The fraction of energy lost was used to define a 'heat loss coefficient' (Q_{Lexh}) for the exhaust system. The heat loss coefficient is the fraction by which the temperature or energy spike in the engine will be reduced once it reaches the inlet of the aftertreatment device. To observe the dependence of the heat loss coefficient on the engine speed and in turn, the exhaust mass flowrate, the heat loss coefficient was plotted against the engine speed as shown in Figure 5.16. It can be seen that the heat loss coefficient follows a nearly linear relationship with the engine speed for the given set of data.
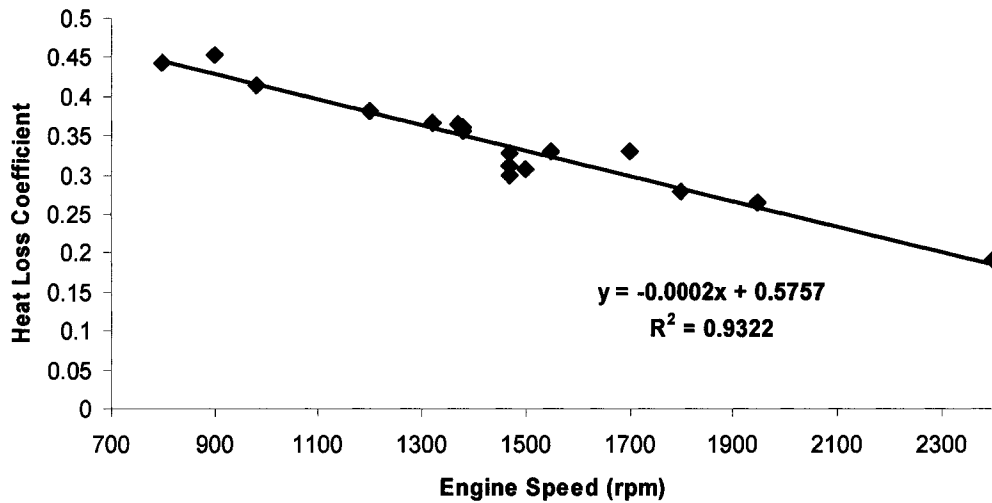
Figure 5.16: Plot of Q_{Lexh} against Engine Speed

5.3. OVERALL THERMAL RESPONSE

The overall thermal response of the Yanmar exhaust system can be characterized in term of the time constant τ_{exh} and the heat loss coefficient (Q_{Lexh}). For example, if at time t_i, the initial engine-out exhaust gas temperature is $T_{exh,i}$, the temperature at the inlet of the aftertreatment device is $T_{inlet,i}$, and a temperature spike equal to ΔT_{exh} is generated inside the engine, then the final steady state temperature at the inlet of the aftertreatment device $T_{inlet,f}$ at time t_f can be calculated from the following expressions:

$$T_{inlet,f} = \left(1 - Q_{Lexh}\right) T_{exh,f} \tag{47}$$

$$T_{exh,f} = T_{exh,i} + \Delta T_{exh} \tag{48}$$

102

$$T_{inlet,f} = T_{inlet,i} + \Delta T_{inlet} \qquad (49)$$

where

ΔT_{exh}	=	Increase in engine-out exhaust temperature
ΔT_{inlet}	=	Increase in the temperature at inlet of aftertreatment
Q_{Lexh}	=	heat loss coefficient based on the engine speed.

If this spike is required at time t at the aftertreatment device, then the time duration by which the spike must be advanced inside the engine to achieve 63.2% of the required increase is equal to the time constant τ_{exh} of the exhaust system.

To illustrate the application of the thermal response characterization, the results from Test # 4 shown in Figure 5.17, were used to calculate the heat loss coefficient, the exhaust time constant and the exhaust gas temperature at the inlet of the aftertreatment device after a step change in engine-out exhaust gas temperature.
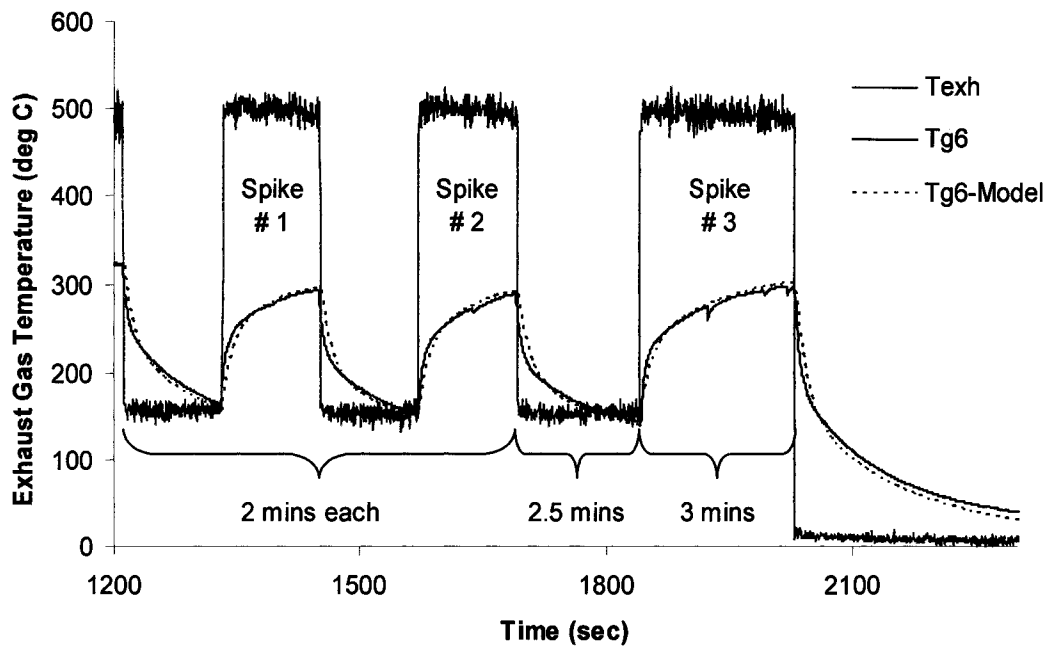
Figure 5.17: Thermal Response Analysis (Test # 4)

103

From the moment of the temperature spike inside the engine, the estimated temperature after 1 time constant based on the above procedure was calculated and compared with the measured temperatures after the same time period as shown in Table 5.2. It can be seen that the thermal response characterization method was able to predict the temperatures at the inlet of the aftertreatment device with reasonable accuracy.

Table 5.2: Thermal Response Characterization

Spike #	1	2	3
Engine Speed (rpm)	1380	1382	1376
Initial Engine-out Exhaust Gas Temperature (^{o}C)	164.6	169.1	156.6
Final Engine-out Exhaust Gas Temperature (^{o}C)	502	495.4	492.3
ΔT_{exh} (^{o}C)	337.4	326.3	335.7
Heat Loss Coefficient	0.299	0.299	0.3
Initial Temperature at Inlet of Aftertreatment (^{o}C)	163.2	151.2	142.7
Estimated Final Steady State Temperature at Inlet of Aftertreatment (^{o}C)	351.9	347.3	344.6
ΔT_{inlet} (^{o}C)	188.7	196.1	201.9
Time Constant (sec)	56.7	56.7	56.8
Estimated Temperature after One Time Constant (^{o}C)	282.4	275.1	270.3
Measured Temperature after One Time Constant (^{o}C)	274.9	268.3	262.3

104

5.4. CONCLUDING REMARKS OF CHAPTER 5

The thermal response from in-cylinder combustion to exhaust aftertreatment for the Yanmar diesel engine was characterized in terms of a heat loss coefficient and a time constant. The time constant for both cooling and heating processes were analyzed. Moreover, the effect of mass flowrate on both these factors was also highlighted. The procedure for quantifying the thermal response was illustrated by applying the characterization procedure to actual experimental results. The values given for the heat loss coefficient and the time constant are only applicable to the exhaust system of the Yanmar engine and applicable within the limits of the experimental and simulation results.

105

6. CONCLUSION

A thermal response analysis was carried out from in-cylinder combustion to exhaust aftertreatment. A single cylinder Yanmar diesel engine was modified to enable in-cylinder measurements. The exhaust system of the engine was setup to measure both the gas and wall temperatures at several locations along the exhaust pipe. Experimental investigation of the exhaust system thermal response was carried out at both steady-state and transient conditions. The thermal response of the complete system was also investigated theoretically with a 1-D transient heat transfer model.

6.1. IN-CYLINDER

The effect of post-injection on the exhaust gas temperature was simulated using WAVE. The results indicated that as the post fuel injection is progressively delayed, there is a trade off between the energy recovery and the exhaust temperature rise. The mid post injection, especially the late-mid post, has the strongest effect to raise the engine exhaust temperature, while its power production capability is compromised by the reduced effective cylinder expansion ratio of the post flame. The late-post injection has little power production capability because of the minimum effective expansion ratio. The same was verified through experimental investigations on a single cylinder diesel engine. To analyze the diesel combustion, an online heat release analysis program was written in LabVIEW. Moreover, a temperature reconstruction technique for estimating the instantaneous temperature using two thermocouples was also implemented. The measurement of in-cylinder temperature could not be accomplished because of the limitation of the thermocouple signal conditioning system. A few attempts with direct measurement using oscilloscope and other thermocouple conditioning modules did not also prove successful.

106

6.2.   EXHAUST SYSTEM

The heat transfer in the exhaust system was estimated by developing a 1-D transient heat transfer model. A similar model was also setup using WAVE software. To calibrate and validate the model, the exhaust system of the Yanmar diesel engine was setup. Thermocouples were embedded in the single-wall exhaust pipes to measure both the exhaust gas and the pipe-wall temperatures. A complex external convective flowfield around the exhaust system was setup. Extensive tests were performed on the Yanmar diesel engine to cover a wide range of engine operating conditions including steady-state and transient operations. The model results showed good agreement with the experimental results. The model was able to consistently predict the exhaust gas temperature at the inlet of the aftertreatment with less than 8% error. The heat transfer characteristics of a double-wall exhaust pipe were simulated and the potential benefits were highlighted through an energy efficiency analysis.

6.3.   THERMAL RESPONSE CHARACTERIZATION

The thermal response from in-cylinder combustion to exhaust aftertreatment for the Yanmar diesel engine was characterized in terms of a heat loss coefficient and a time constant. The time constant for both cooling and heating processes were analyzed. Moreover, the effect of mass flowrate on both these factors was also highlighted. The procedure for quantifying the thermal response was illustrated by applying the characterization procedure to actual experimental results. The characterization method was able to estimate the exhaust gas temperatures at the inlet of the aftertreatment device with reasonable accuracy. The values given for the heat loss coefficient and the time constant are only applicable to the exhaust system of the Yanmar engine and applicable within the limits of the experimental and simulation results.

6.4.   RECOMMENDATIONS FOR FURTHER WORK

The in-cylinder temperature measurements could not be accomplished due to problems with the data acquisition system. The same is being attempted by

107

developing differential amplifier and filter circuitry within the laboratory. If successful, it would help immensely in quantifying the characteristics of low-temperature combustion besides providing a better understanding of the post-injection strategy.

At present, the heat transfer model cannot account for the influence of EGR. The use of EGR will be mandatory along with aftertreatment systems and other advanced combustion modes in all future diesel engines. Therefore, the adaptation of the heat transfer model to account for EGR would be quite useful. Moreover, the use of external fuel injection close to the aftertreatment device is being actively researched. This would require the development and integration of a separate fuel injection model into the heat transfer model.

To accurately estimate the benefits associated with the use of a double-wall exhaust pipe with air-gap, it is necessary to experimentally measure its thermal response. This is currently being planned and once the facility is built, the theoretical results presented in this thesis can be confirmed.

The thermal response characterization using the concept of the exhaust time constant and the heat-loss coefficient provides a basis for improving the performance of aftertreatment systems. It is suggested that the concept be applied to actual aftertreatment systems to realize the validity and/or limitation of this approach.

REFERENCES

1. J. B. Heywood, 1988, *Internal Combustion Engine Fundamentals*, McGraw-Hill, ISBN 0-07-028637-X.

2. Diesel Technology Forum, March 2001, *Engineering Clean Air: The Continuous Improvement of Diesel Engine Emission Performance*. http://www.dieselforum.org/fileadmin/templates/whitepapers/DTF-ContinuousImprovement03-01.pdf – Accessed March 27, 2006.

3. M. Zheng, G. T. Reader, September 2004, *Energy Efficiency Analyses of Active Flow Aftertreatment Systems for Lean Burn Internal Combustion Engines*, Energy Conversion and Management, v 45, n 15-16, p 2473–2493.

4. S. Zidat and M. Parmentier, 2003, *Exhaust Manifold Design to Minimize Catalyst Light-off Time*, SAE Paper 2003-01-0940.

5. E. DeSousa, 1993, *Dual Wall Energy Conserving Pipes for Internal Combustion Engines*, SAE Paper 931095.

6. R. Bosch, 1996, *Automotive Handbook*, 4th Edition, Robert Bosch GmbH, ISBN 1-56091-918-3.

7. R. S. Benson, N. D. Whitehouse, 1979, *Internal Combustion Engines*, Pergamon Press, ISBN 0-08-022717-1.

8. U.S. Environmental Protection Agency – Office of Transportation and Air Quality, March 2004, *Highway Diesel Progress Review Report*, EPA420-R-04-004.

9. DieselNet, 2004, *Emission Standards– USA: Heavy-Duty Truck and Bus Engines*, www.dieselnet.com/standards/us/hd.html#y2007 – Accessed March 29, 2006.

10. Manufacturers of Emission Controls Association, 2004, *Clean Air Facts: Emission Controls for Diesel Engines*.

11. DieselNet, 2004, *Technology Guide: Paper Abstracts*, http://www.dieselnet.com/tginfo/abstracts.htm – Accessed March 29, 2006.

12. C. Havenith, R. P. Verbeek, J. P. Warren, N. Myers, 1997, *Transient Performance of a Urea DeNOx Catalyst System for Low Emissions Heavy-Duty Diesel Engines*, SAE Paper 970185.

13. Ph. Lefou, M. Guyon, C. Bert, 1998, *Impact of Sulphur on NOx Trap Catalyst Activity - Study of the Regeneration Conditions*, SAE Paper 982607.

14. M. F. J. Brunt, H. Rai,A. L. Emtage, 1998, *The Calculation of Heat Release Energy from Engine Cylinder Pressure Data*, SAE Paper 981052.

15. I. Choi, K. M. Chun, C-W Park, J. W. Hahn, 2000, *End-Gas Temperature Measurements in a DOHC Spark-Ignition Engine Using CARS*, SAE Paper 2000-01-0237.

16. R. S. Benson and G. W. Brundett, 1962, *Development of Resistance Wire Thermometer for Measuring Transient Temperatures in Exhaust Systems of Internal Combustion Engines,* Temperature – Its Measurement and Control in Science and Industry, **3**, Part 2, 631.

17. R. S. Benson, 1964, *Measurement of Transient Exhaust Temperatures in Internal Combustion Engines,* The Engineer, **217**, 377.

18. P. A. Konstantinidis, G. C. Koltsakis, A. M. Stamatelos, 1997, *Transient Heat Transfer Modelling in Automotive Exhaust Systems,* Proc. Instn Mech. Engrs, Part C, Journal of Mechanical Engineering Science, **211**, 1-15.

19. I. P. Kandylas, A. M. Stamatelos, 1999, *Engine Exhaust System Design based on Heat Transfer Computation,* Energy Conversion & Management, **40**, 1057-1072.

20. S. H. Chan, D. L. Hoang, P. L. Zhou, 2000, *Heat Transfer and Chemical Kinetics in the Exhaust System of a Cold-Start Engine fitted with a Three-way Catalytic Converter*, Proc. Instn Mech. Engrs, Part D, Journal of Mechanical Engineering Science, **214**, 765-777.

21. B. Mahr, 2002, *Future and Potential of Diesel Injection Systems*, THIESEL 2002 Conference on Thermo- and Fluid-Dynamic Processes in Diesel Engines.

22. H. Klein, S. Lopp, E. Lox, M. Kawanami, M. Horiuchi, 1999, *Hydrocarbon DeNOx Catalysis – System Development for Diesel Passenger Cars and Trucks,* SAE Paper 1999-01-0109.

23. Ricardo Software, 2005, *WAVE v7 Engine User Manual.*

24. M. Zheng, G. T. Reader, D. Wang, J. Zuo, R. Kumar, M. C. Mulenga, U. Asad, D. S-K Ting, and M. Wang, 2005, *A Thermal Response Analysis on the Transient Performance of Active Diesel Aftertreatment,* SAE Paper 2005-01-3885.

25. K. Kar, S. Roberts, R. Stone, M. Oldfield, B. French, 2004, *Instantaneous Exhaust Temperature Measurements using Thermocouple Compensation Techniques,* SAE Paper 2004-01-1418.

26. D. Bradley, K. J. Matthews, 1968, *Measurement of High Gas Temperatures with Fine Wire Thermocouples,* Journal Mechanical Engineering Science, **10**, n 4, 299-305.

27. M. Tagawa, Y. Ohta, 1997, *Two-Thermocouple Probe for Fluctuating Temperature Measurement in Combustion – Rational Estimation of Mean and Fluctuating Time Constants,* Combustion and Flame, **109**, 549-560.

28. M. Zheng, Y. Wu, G. Zhao, G. T. Reader, 2005, *Transient Temperature Estimation for Active-Flow Aftertreatment Control,* ICES 2005-1083, ASME.

29. Y. Moriyoshi, S-H. Choi, S. Kobayashi, T. Tsunekawa, 2006, *Measurement of the Local Gas Temperature at Autoignition Conditions inside the Combustion Chamber using a Two-Wire Thermocouple,* SAE Paper 2006-01-1344.

30. K. Kar, A. Swain, R. Raine, S. Roberts, R. Stone, 2006, *Cycle-by-Cycle Variations in Exhaust Temperatures using Thermocouple Compensation Techniques,* SAE Paper 2006-01-1197.

31. D. N. Assanis, Z. S. Filipi, S. B. Fiveland, M. Syrimis, 2000, *A Methodology for Cycle-By-Cycle Transient Heat Release Analysis in a Turbocharged Direct Injection Diesel Engine,* SAE Paper 2000-01-1185.

32. R. B. Krieger,G. L. Borman, 1966, *The Computation of Apparent Heat Release for the Internal Combustion Engines,* ASME Paper 66-WA/DGP-4.

33. T. J. Callahan, D. M. Yost, T. W. Ryan III, 1985, *Acquisition and Interpretation of Diesel Engine Heat Release Data,* SAE Paper 852068.

34. B. M. Grimm, R. T. Johnson, 1990, *Review of Simple Heat Release Computations,* SAE Paper 900445.

35. Y. A. Çengel, 1977, *Introduction to Thermodynamics and Heat Transfer,* McGraw-Hill, ISBN 0-07-011498-6.

36. C. Depcik, D. Assanis, 2002, *A Universal Heat Transfer Correlation for Intake and Exhaust Flows in a Spark-Ignition Internal Combustion Engine,* SAE Paper 2002-01-0372.

37. J. P. Holman, 1992, *Heat Transfer,* McGraw-Hill, ISBN 0-07-112644-9.

38. V. Gnielinski, 1976, *New Equations for Heat and Mass Transfer in Turbulent Pipes and Channel Flow,* International Chemical. Engineering, **16**, 359-368.

39. M. A. Hessami, A. Pollard,R. D. Rowe,D. W. Ruth, 1985, *A Study of Free Convective Heat Transfer in a Horizontal Annulus with a Large Radii Ratio,* Journal of Heat Transfer, **107**, 603-610.

40. A. Bejan, A. D. Kraus, 2003, *Heat Transfer Handbook,* John Wiley & Sons, ISBN 0-471-39015-1.

41. F. P. Incropera, D. P. Dewitt, 1996, *Fundamentals of Heat and Mass Transfer,* John Wiley & Sons, ISBN 0-471-30460-3.

42. EPA Emission Test Centre, 1994, *Thermocouple Calibration Procedure – Alternative Method 2,* http://www.epa.gov/ttn/emc/approalt/alt-011.pdf - Accessed April 24, 2006.

APPENDIX A

TEMPERATURE PREDICTION USING TWO-THERMOCOUPLE TECHNIQUE

To check the response of the two-thermocouple technique, thermocouples of different sizes as indicated in Table A.1 were installed radially in section # 4 of the exhaust pipe (Figure 4.5).

Table A.1: Thermocouples Sizes for Two-Thermocouple Technique

Thermocouple #	Size
1	1/8" shielded/grounded
2	1/16" shielded/grounded
3	0.005" bare wire

The engine operating conditions are shown in Figure A.1. Two sets of transients were done to generate fluctuations in the exhaust gas temperature.
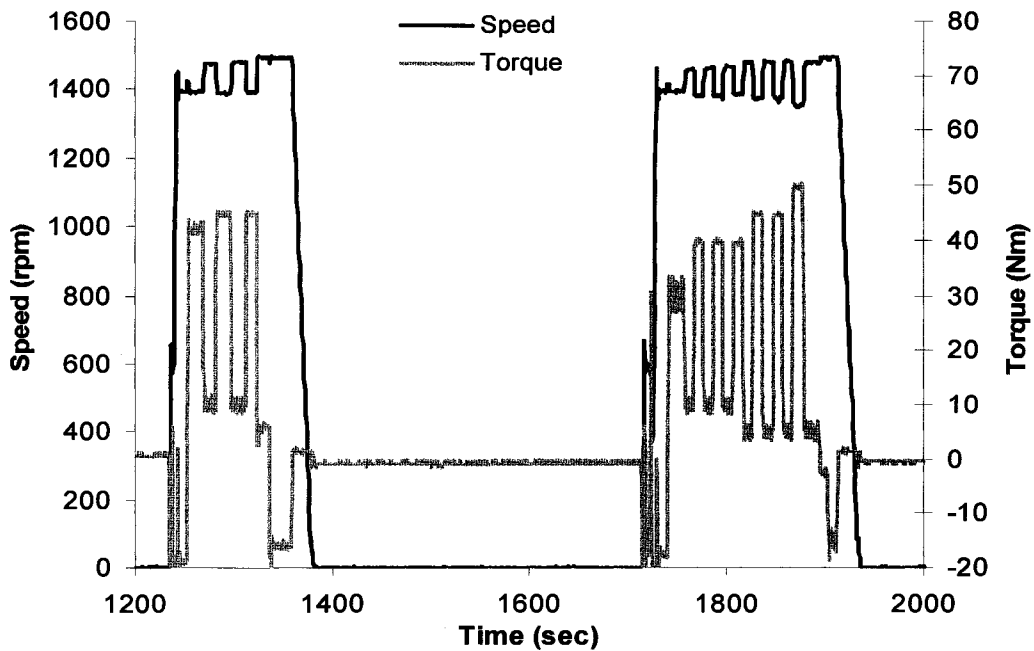
Figure A.1: Engine Operating Conditions (Two-Thermocouple Technique)

113

The predicted temperatures for the two thermocouples along with the measured temperatures are shown in Figure A.2. The predicted temperatures are able to capture the sharp change in temperature but the absolute values are generally over-predicted. By calibrating the model response, the reconstructed temperatures can give a good estimate of the actual gas temperature.
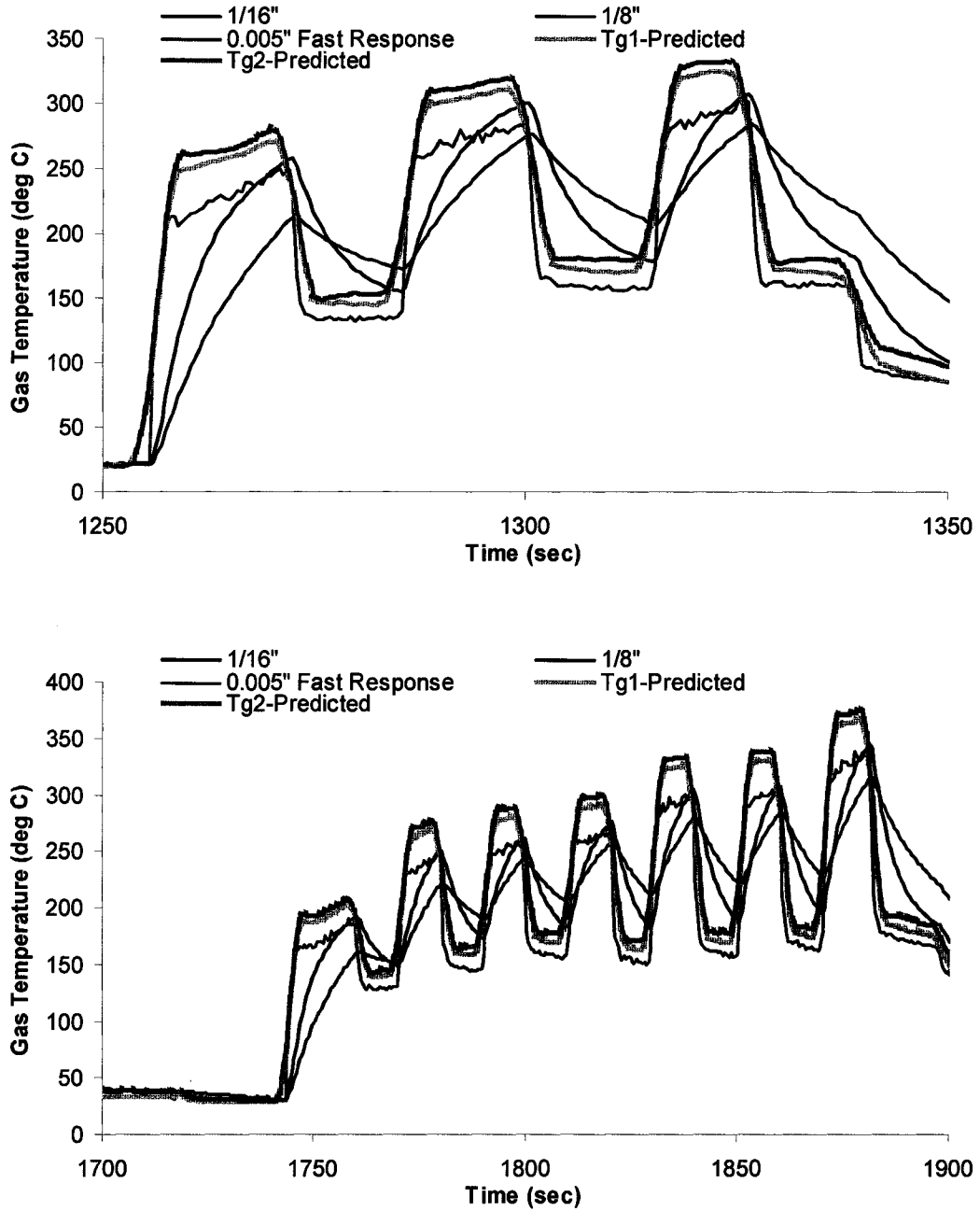
Figure A.2: Constructed Temperatures using Two-Thermocouple Technique-
Upper: 1st Transient Set, Lower: 2nd Transient Set

114

REAL-TIME HEAT RELEASE ANALYSIS TOWARDS ON-FLY COMBUSTION CONTROL FOR DIESEL ENGINES

Usman Asad, Ming Zheng, David S-K. Ting, Raj Kumar, Siddhartha Banerjee, Graham T. Reader
Mechanical, Automotive and Materials Engineering, University of Windsor, Ontario, Canada
Jimi Tjong
Ford Motor Company, Canada

ABSTRACT

The increasing complexities of the diesel combustion process and the active aftertreatment schemes have necessitated real-time analysis of the cylinder pressure data in diesel combustion research. In this paper, a PC-based fast heat release analysis program for diesel combustion is presented based on the first law of thermodynamics. The program computes the net heat-release rate in real-time from the cylinder pressure data acquired for the complete diesel cycle. Combustion parameters like the magnitude and the crank angle of the peak pressure, the rate of pressure rise, the magnitude and the crank angle of the maximum rate of pressure rise, logarithm of the pressure versus cylinder volume, indicated mean effective pressure and their cycle-to-cycle variation analyses are also computed in real-time. The implemented heat release model is described and the effect of specific heat ratio on the shape of the computed heat-release rates is analyzed. A preliminary analysis of the applicability of the heat release model to different engine operating conditions is also shown. Moreover, the effect of two data-acquisition methods on the accuracy of the computed heat release rate is also discussed.

INTRODUCTION

Measured cylinder pressure traces can provide an insight into the combustion process in a diesel engine. The thermodynamic analysis of this pressure data over the compression and expansion strokes can be effectively used to quantify the combustion parameters that include the indicated mean effective pressure (IMEP), the rate of heat-release, maximum rate of pressure rise etc. For diesel engine combustion studies, one common approach is the calculation of the rate of heat release with the units of joules/degree. The rate of heat release is a very important parameter since this may have a very significant influence on combustion noise, pressure rise rate and NOx emissions [1, 2].

When complicated commercial indicating equipment for combustion is not available, heat release analysis is usually performed offline from the cylinder

115

pressure data recorded during experiments. With multi-pulse fuel injection systems in which the injection pressure, injection scheduling and quantity are varying dynamically from cycle-to-cycle, there is a need to perform the heat release analysis in real-time, that is, the heat release rate is calculated and displayed immediately after each combustion cycle. This will not only provide instantaneous feedback after each cycle, it can also allow us to study the transient changes due to exhaust gas recirculation (EGR), intake boost etc. The cycle-by-cycle heat release analysis is only the precursor for the on-fly combustion control, which requires point-by-point crank angle-resolved calculation of the heat release rate and near-instantaneous feedback to the combustion controller.

One of the main requirements for the real-time programs is a short computational time in order to produce prompt outputs that can be used as feedback for combustion control purposes. Several technical challenges complicate this task. First, the time available for computing the heat release rate and other combustion parameters after the completion of the data acquisition, is only within a few micro-seconds. Second, the computational resources of the PC are shared with the operating system and other background processes. Furthermore, the noise in the pressure signal is amplified through the charge amplifier which can lead to significant errors in the computed results.

In the following sections, a phenomenological heat release model is presented together with a discussion on its applicability to different engine operating conditions. The procedure for carrying out the fast heat-release analysis using this model is given. Some issues related with the data acquisition are discussed and the solution presented.

THE HEAT RELEASE MODEL

The phenomenological "engine heat release" model is based on the First Law of Thermodynamics and encompasses the following assumptions [3, 4]:

- Uniform thermodynamic properties and gas composition throughout the combustion chamber; Heterogeneity of the charge is neglected (fuel vapor and products are treated as a mixture of ideal gases)
- The apparent heat release process is based on the averaged properties in a single zone.
- Equilibrium thermo-chemistry is assumed (chemical dissociation is ignored).
- The sensible enthalpy from the fuel injection is neglected.

Based upon these assumptions, the first law for the in-cylinder charge during the period from intake valve closure (IVC) to exhaust valve closure (EVC) for the crank angle interval $d\theta$, can be written as:

$$\frac{dQ_n}{d\theta} = \frac{dQ_{gr}}{d\theta} - \frac{dQ_{ht}}{d\theta} = \frac{dU}{d\theta} - p\frac{dV}{d\theta} \qquad (1)$$

116

where

dU	=	change in sensible internal energy
dQ_{gr}	=	gross heat release from fuel combustion
dQ_n	=	net heat release
dQ_{ht}	=	heat transfer to cylinder wall
dV	=	change in cylinder volume
p	=	cylinder pressure

Assuming the working fluid as an ideal gas, further equations can be derived as follows:

$$\frac{dU}{d\theta} = mc_v \frac{dT}{d\theta}, \quad p\frac{dV}{d\theta} + V\frac{dp}{d\theta} = mR\frac{dT}{d\theta}, \quad c_v = \frac{R}{\gamma - 1} \qquad (2, 3, 4)$$

where m is the trapped mass, R is the specific gas constant, c_v is the specific heat at constant volume, γ is the ratio of specific heats and T is the temperature.

Substituting equations (2) to (4) in equation (1) gives the apparent heat release rate equation:

$$\frac{dQ_n}{dt} = \frac{1}{\gamma - 1}\left[\gamma\, p\frac{dV}{dt} + V\frac{dp}{dt}\right] \qquad (5)$$

Equation (5) omits the effect of crevice volumes and assumes the charge to be at the same temperature. The cylinder pressure is assumed to be uniform throughout the combustion chamber which is valid for the direct injection diesel engines. Previous researches [5~10] have shown that, with the exception of cylinder charge to wall heat transfer, these additional effects are usually small and can be neglected with minimal loss of accuracy. The charge to wall heat transfer is also often omitted for simplicity and the heat release thus determined is referred to as the "net" heat release. When heat transfer effects are included, the heat release energy calculated is described as the "gross" heat release. Net heat release values are typically 15% lower than those obtained on a gross heat release basis [1]. Net heat release values are very often used in preference to gross heat release values because this reduces the amount of computation and avoids the need for heat transfer parameters to be specified.

The heat release rate from Equation (5) can either be obtained with constant gas properties or with crank angle-resolved gas properties. The magnitude of the specific heat ratio reduces with the increasing temperature since the latter normally increases the magnitudes of the specific heat. In direct-injection engines, the specific heat ratio changes significantly during the compression and expansion processes and, also from cycle-to-cycle, especially during transients. The common approach is to vary γ throughout the cycle as a function of temperature and several correlations can be found in the literature [4, 8, 11].

117

To observe the effect of temperature dependent γ, the cylinder pressure data recorded from actual experiments was used to calculate the heat release rate using Equation (5) and compared with the constant γ case as shown in Figure 1. The general shape of the heat release rate with temperature dependent γ remains the same before the start of combustion but the two curves have different magnitudes after that. Similar observations have been reported [1, 3, 8] that the general shape of the heat release curve remains the same while the magnitudes of the burn rates would be incorrect.
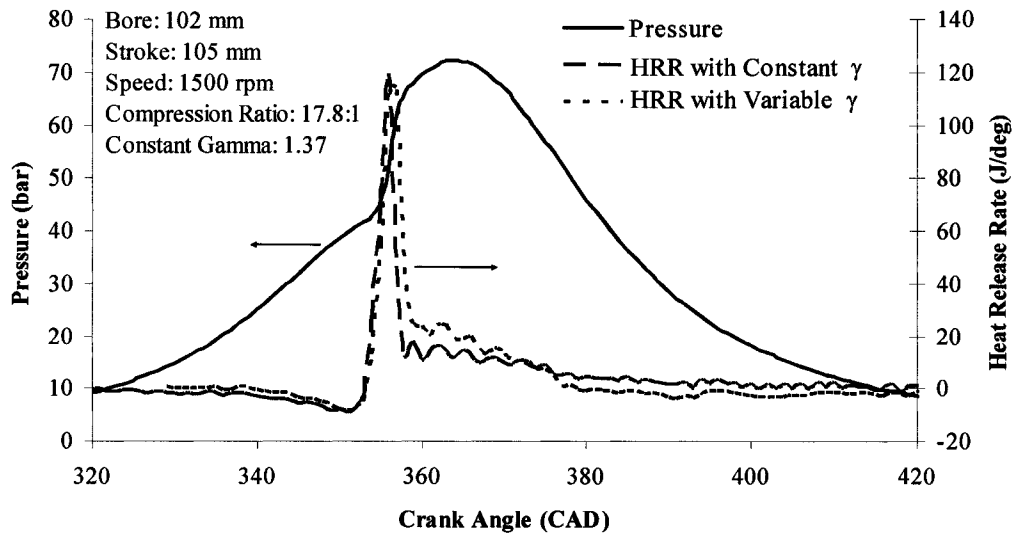
Figure 1: Comparison of Calculated Heat Release Rates with Constant & Variable γ

The heat release model presented is generally applicable to air breathing diesel engines, that is, the intake composition is assumed to be fresh air only. The modern diesel engines employ the heavy use of EGR for emission control purposes and as such, there are large variations in the composition of the intake mixtures. These large variations have a strong effect on the ignition delay period and the duration of the premixed combustion phase and hence, on the heat release rates. The heat release model given in Equation (5) therefore, may not be sufficient to accurately account for these effects on the heat release rates.

To investigate the magnitude of errors in the heat release rates with this simple model, experimental data using unconventional atmosphere conditions (20~40% CO_2, 20~40 % Ar) was used. The heat release rate was first computed with Equation (5) assuming constant gamma values. This was compared with the heat release rates computed with the Synthetic Atmosphere Engine Simulation (SAES^{TM}) software developed by Zheng and Reader [12, 13] which uses a comprehensive validated model for heat release calculation. The SAES model includes the effect of heat transfer, crevice volume, intake composition etc on the heat release rate.

118

Figure 2 shows the heat release curves obtained for two different cases. It can be seen that the heat release rate computed from Equation (5) is comparable in terms of the combustion phasing and varies in magnitude to some extent. While this might not be adequate for combustion control purposes, it should suffice for observing the transient effects of EGR. Moreover, investigations are being conducted at the authors' lab to further verify this comparison over a wide range of intake compositions and engine operating conditions. Hence, for the time being, it was decided to implement the simple heat release model for real-time calculations.
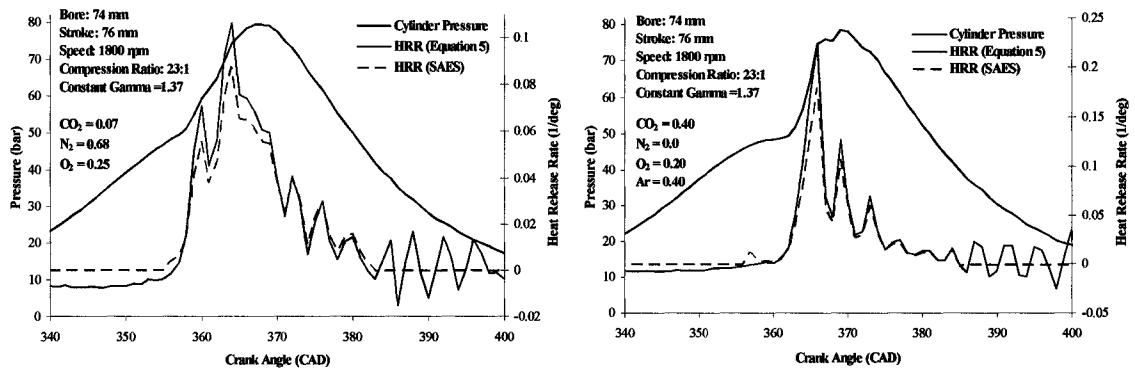
Figure 2: Comparison of Heat Release Rates for Different Intake Mixture Compositions

REAL-TIME HEAT RELEASE IMPLEMENTATION

The heat release model as presented earlier requires the following inputs.

TDC Position

For phasing the measured pressure data with the cylinder volume, it is necessary to accurately determine at what point in the engine's thermodynamic cycle, the data acquisition started [14]. The acquisition was programmed to begin when the crank is at TDC. Since the acquisition of the data may begin at either compression TDC or exhaust TDC, a simple check was used at the first acquisition by comparing data acquired at 0 and 360 degrees.

Crankshaft Position

To accurately align the cylinder pressure data with the corresponding cylinder volume, an external clock was used. This provided a Phase Locked Loop (PLL) signal that indicates when a certain amount of engine rotation has occurred [14]. The encoder used with the engine gives 3600 pulses per revolution (0.1 degree resolution).

Cylinder Pressure

The cylinder pressure was measured using a Kistler 6043A60 transducer which was mounted directly on the cylinder head.

The hardware and the software of the real-time heat release analysis are shown in Figure 3. The transient heat release analysis was programmed with LabVIEW software. The cylinder pressure data acquisition is externally triggered

119

and externally clocked, based on the encoder signal; the TDC signal acts as the external trigger and the timing index at every 0.1 degree crank angle acts as the external clock. The data-acquisition system gives the pressure data as an array of 7200 points for a complete thermodynamic cycle (2 revolutions of the crankshaft). The heat release rate is calculated online for each cycle along with combustion parameters like the peak pressure and the position of peak pressure, the maximum rate of pressure rise and position, IMEP etc.
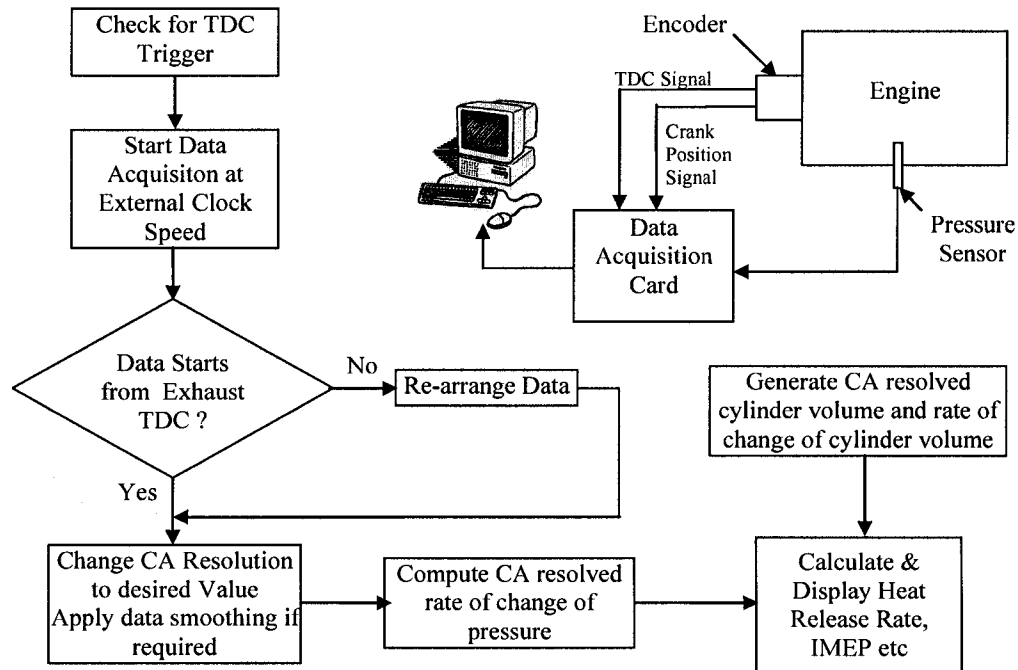
Figure 3: The Hardware and Software of the University of Windsor Real-time Heat Release Analysis System

RESULTS AND DISCUSSION

Data Acquisition Modes

There are many challenges in the actual implementation of the real-time heat release analysis. For instance, during the initial testing of the program, a drift of 2~8° in the cylinder pressure data was observed over a period of time. This incorrect crank angle phasing resulted in significant errors in the heat release rate. This problem was temporarily corrected if the program was re-initialized, indicating that the problem was probably software related.

The program initially worked in the continuous data acquisition mode in which once the trigger is detected the first time, the data is then continuously acquired for every consecutive cycle (7200 points) without checking for the trigger signal in between. This approach is correct as long as a few hundred cycles are acquired intermittently. However, for continuous operation, the problem with this approach is that any noise in the signals (causing false clock signals), conflict of

120

resources on the PC or some mechanical hardware limitations may cause an error in the crank angle phasing. To counter this problem, the program was modified to use the finite acquisition mode. This means that after each cycle (7200 points), the program waits for the TDC trigger signal and only then starts the next acquisition of the 7200 pressure data points. This ensures that the slightest error, if any in the crank angle phasing over a single cycle is not carried over to the next cycle. This mode is resource intensive and can only work if the PC resource limitation is not an issue. The program was tested in this configuration with no problem observed in the crank angle phasing over a range of engine loads and speed. Figure 4 shows the schematic diagram of the two data acquisition modes.
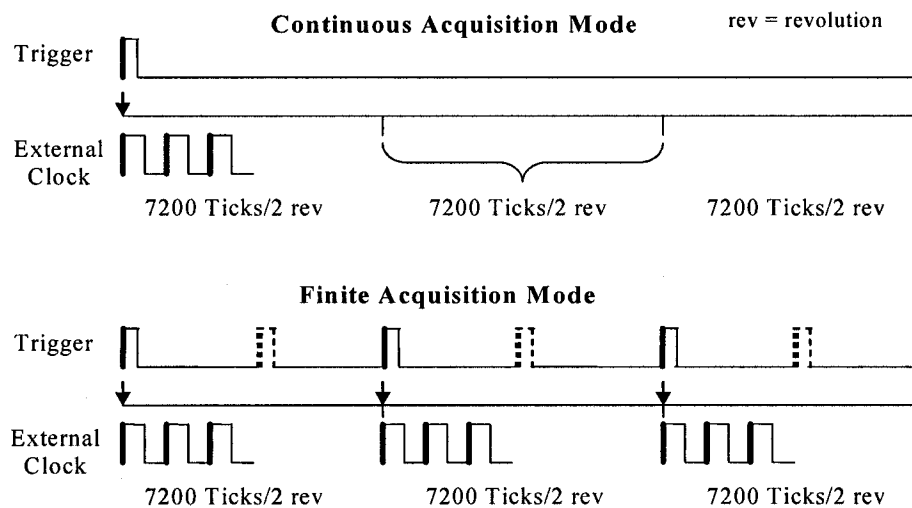
Figure 4: Schematic Diagram of the Data Acquisition Modes

Cycle-to-Cycle Variation Analysis

The analysis of the cylinder pressure traces is an effective tool to evaluate the cycle-to-cycle and cylinder-to-cylinder variations. The cycle-by-cycle combustion parameters can be evaluated in terms of their mean and standard deviation as well as the coefficient of variance (CoV) values. This can give the essential feedback on the stability of the combustion process and the influence of EGR. Although the common approach is to characterize the cycle-to-cycle variations in terms of CoV of the maximum cylinder pressure, the program calculates the CoV, mean and standard deviation values for the maximum cylinder pressure and the angle of its occurrence; the maximum rate of pressure rise and the angle of its occurrence and the IMEP. This is performed over a data window of 200 cycles and every new cycle replaces the first cycle in the data window.

The program has been used continuously in the authors' engine lab during numerous experiments including the transient effects of EGR, fuel injection quantity and scheduling etc. Figure 5a shows the transiently changing heat release rates with increasing CO_2 addition in the intake and Figure 5b shows the pressure traces and the heat release rates for cycles # 1, 4, 7, 10, 13 during a transient load change (starting at cycle # 2) for generating an exhaust temperature pulse.

121
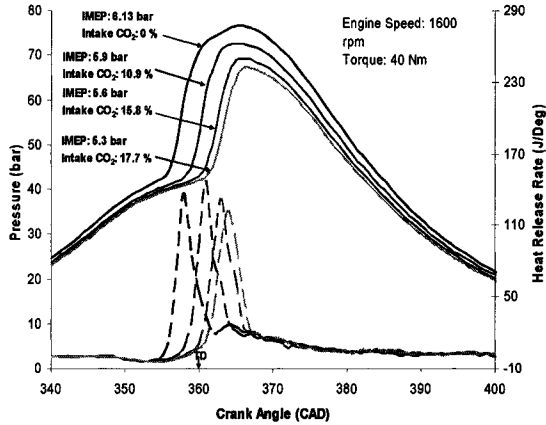
Figure 5a: Effect of Increasing Intake CO₂ Concentration on the Heat Release Rate
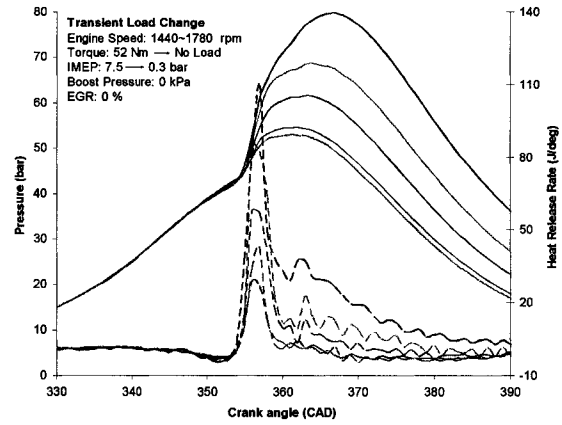
Figure 5b: Heat Release Rates during Transient Load Change for Afterteatment Research

Figure 6 shows the pressure and heat release rate profiles for all the 13 cycles of Figure 5b. As the load is reduced from 52 Nm to 'no load' condition, the change in the pressure traces result in a significant change in the heat release rates which can be observed in real-time.
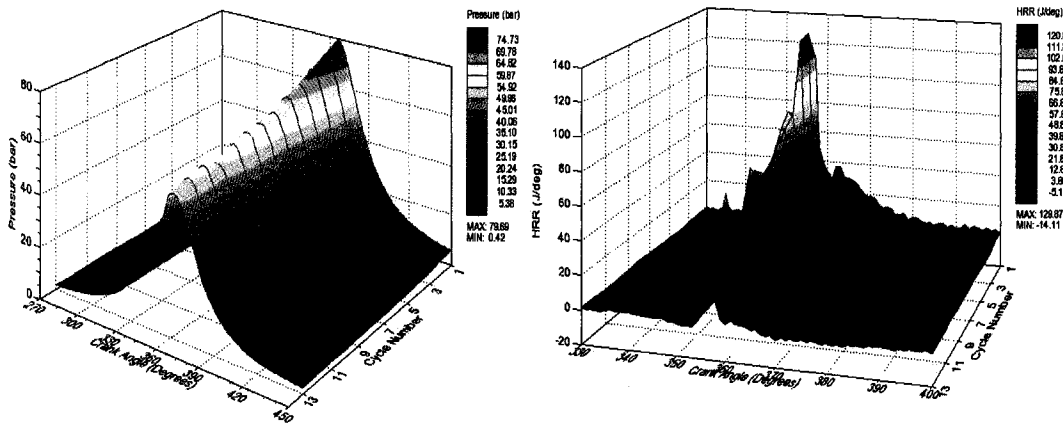
Figure 6: Surface plots of Cylinder Pressure Profiles and Heat Release Rates during the Load Transient (13 cycles)

CONCLUDING REMARKS

The real-time heat release analysis program serves as an effective tool for the combustion related research at the authors' lab and is a part of the on-going developments for the on-fly combustion control. These research activities includes high boost and high EGR dilution combustion, HCCI, multi-pulse common rail injection etc. The real-time heat release analysis provides fast feedback on the combustion process at the end of each successive cycle and is useful for observing

122

the transient effects of varying injection timing, EGR and other critical parameters. It is one-step further towards the on-fly combustion control setup. For on-fly combustion control, it is desired to have a point-by-point computation of the heat release rate so that the combustion process can be modified dynamically at any crank angle, based upon the previous crank angle history.

The fast heat release program has been implemented on a PC using a simplified heat release model. The heat release model results have been compared with those of complex validated models. A comparison of the computed heat release rates with constant and temperature-dependent specific heat ratios indicated that the general shape of the heat release remains the same but the magnitudes are different. As the absolute heat release values may be less essential for the real-time analysis, a constant γ value has been used in the current heat release program.

The two data acquisition modes commonly used for acquiring cylinder pressure data, externally triggered and externally clocked have been discussed. The finite data acquisition mode is suitable for acquiring data for longer periods of time while the continuous data acquisition mode gives satisfactory results over a few hundred cycles of data.

ACKNOWLEDGEMENTS

REFERENCES

1. Heywood, J. B., 1988, "Internal Combustion Engine Fundamentals", McGraw-Hill, ISBN 007028637X.
2. Brunt, M. F. J., Rai, H., Emtage, A. L., 1998, "The Calculation of Heat Release Energy from Engine Cylinder Pressure Data", SAE 981052.
3. Assanis, D. N., Filipi, Z. S., Fiveland, S. B., Syrimis, M., 2000, "A Methodology for Cycle-By-Cycle Transient Heat Release Analysis in a Turbocharged Direct Injection Diesel Engine", SAE 2000-01-1185.
4. Rocco, V., 1993, "D.I. Diesel Engine In-Cylinder Pressure Data Analysis under T.D.C. Setting Error", SAE 930595.
5. Krieger, R.B. and Borman, G.L., 1966, "The Computation of Apparent Heat Release for the Internal Combustion Engines," ASME Paper 66-WA/DGP-4.
6. Amman, C.A., 1985, "Cylinder-Pressure Measurements and Its Use in Engine Research" SAE Paper 852067, 1985.
7. Grimm, B.M., and Johnson, R.T., 1990, "Review of Simple Heat Release Computations", SAE Paper 900445.
8. Gatowski, J.A., Balles, E.N., Chun, K.M., Nelson, F.E., Ekchian J.A. and Heywood, J.B., 1984, "Heat Release Analysis of Engine Pressure Data," SAE Paper 841359.

9. Callahan, T.J., Yost, D.M., and Ryan III, T.W., 1985, "Acquisition and Interpretation of Diesel Engine Heat Release Data," SAE Paper 852068.

10. Foster, D.E., 1985, "An Overview of Zero- Dimensional Thermodynamic Models for IC Engine Data Analysis," SAE Paper 852070.

11. Brunt, M. F. J., Platts, K. C., 1999, "Calculation of Heat Release in Direct Injection Diesel Engines", SAE 1999-01-0187.

12. Zheng, M., 1993, "Thermodynamic Modeling and Experimental Investigation of a Synthetic Atmosphere Diesel Engine System", PhD thesis, University of Calgary, Calgary, Alberta.

13. Zheng, M. & Reader, G. T., 1996, "Synthetic Atmosphere Engine Simulations (SAES^{TM})", Version 2.01, University of Calgary, Calgary, Alberta.

14. Brown, B. R., 2001, "Combustion Data Acquisition and Analysis", M.Eng. Project Report, Loughborough University, Leicestershire, UK.

CONTINUOUS PRESSURE DATA – RECORDING AND PROCESSING

LabVIEW PROGRAM FOR RECORDING PRESSURE

The LabVIEW program acquires the cylinder pressure data at 0.1 degree crank angle interval, based on the encoder signal. Since the acquisition can start from either compression or exhaust TDC, the program automatically adjusts the data to start from the intake process. The data-acquisition system gives the pressure data as an array of 7200 points for each combustion cycle. The crank angle resolution is changed to 1 degree using a 10-point arithmetic-mean sample compression technique, resulting in a 720 points array of pressure data. The pressure data is recorded into binary files with 32-bit hexadecimal precision. The program saves 2000 cycles in one file. The file numbering is done sequentially and automatically.

C CODE FOR PROCESSING THE PRESSURE DATA

```
/*     This code calculates the average engine-out exhaust gas temperature
by processing the cycle-by-cycle recorded pressure data into time-resolved
temperature data*/

#include <stdio.h>
#include <math.h>
#include <stdlib.h>

void main()
{
        FILE *fp,*ft,*fu;
        int b,c,i,j,k,m,n; // counter for various loops
        int d;          // number of values in the engine speed input file
        int num=1;      // number of pressure data files to read
        int cc;         // check for valid menu input
        int a[4];       // array to store values during 32-bit hexadecimal
                        conversion
        int sof;        // start of file - check if pressure data recorded
                        from compression TDC
        int ncyc[20000];     // array to store the number of recorded
                        pressure cycles
        float offset;   // value to correct the baseline pressure
        float bore;     // engine bore
        float stroke;   // engine stroke
        float L;        // length of connecting rod
        float CR;       // compression ratio
        float Vc;       // clearance volume
        float R;        // ratio of connecting rod length to crank
                        radius
        static float V[720];// array to store the crank-angle resolved
                        cylinder volume
        static float pr[20000][720];    // array to store cycle-by-cycle
                                pressure values
```

125

```
                static float avg[20000][720];      // array to store time-resolved
                                                   pressure values
                static float mrate[20000];         // array to calculate mass flow
                                                   rate at each time step
                static float T[20000][720];        // array to store calculated
                                                   values of crank-angle resolved
                                                   mean cylinder temperature
                float speed[20000]; // array to store the engine speed data read
                                    from the input file
                float Texh[20000];  // array to store the calculated exhasut gas
                                    temperature at exhaust valve opening

                const float GC=287.15;      // specific gas constant
                const float PI = 3.14159;

                char filename[16];          // name of the input files
                char*x;                     // character pointer to swap the 32 bit
                                            hexadecimal values
                char q;                     // value entered at the menu

                struct binary               // structure to read 32 bit binary values
                {
                        float b;
                };
                struct binary e;

        //      Default engine parameters

                bore=0.102;
                stroke=0.105;
                L=0.176;
                CR=17.8;


        //      Input number of pressure data files

                printf("\n\nEnter No of Files: ");
                scanf("%d",&num);
                fflush(stdin);


                d=0;
                ft=fopen("speed.txt","r");

                if (ft==NULL)
                {
                        puts("\nERROR! Cannot find file\n");
                        exit(0);
                }

                while (!feof(ft))
                {
                        fscanf(ft,"%f",&speed[d]);
                        ncyc[d]= speed[d]/(120*2)-1;
                        d++;
                }
                d--;
                fclose(ft);


Menu:
        //      system ("cls");

                printf("\n(1)Change Skew Value? (Default:1.5)");
                printf("\n(2)Change Engine Configuration? (Default: YANMAR)");
                printf("\n(3)Exit Program?");
                printf("\n(0)Run Program!!");
                printf("\n\nEnter Choice: ");
                q=getche();

                if ((q=='1')||(q=='2')||(q=='3')||(q=='0'))
                        cc=1.5;
```

126

```c
        else
                goto Menu;

switch (q)
{
case '1':
                printf("\n\nDefault Skew Value at 270 CAD is 1.5");
                fflush(stdin);
                printf("\n\nAssign new skew value (y/n): n\b");
                c=getche();
                if (c=='y')
                {
                        printf("\n\nEnter New Skew Value: ");
                        scanf("%f",&cc);
                }
                goto Menu;

case '2':

                system ("cls");

                printf("\n\nDefault Engine Configuration is:\n\n");
                printf("\nCylinder Bore = 0.102 m\n");
                printf("\nPiston Stroke = 0.105 m\n");
                printf("\nConnecting Rod Length = 0.176 m\n");
                printf("\nCompression Ratio = 17.8 \n\n\n");
                printf("\n\nChange Engine Configuration (y/n): n\b");
                c=getche();
                if (c=='y')
                {
                        printf("\n\nCylinder Bore (0.102): ");
                        scanf("%f",&bore);
                        printf("\nPiston Stroke (0.105): ");
                        scanf("%f",&stroke);
                        printf("\nConnecting Rod Length (0.176): ");
                        scanf("%f",&L);
                        printf("\nCompression Ratio (17.8): ");
                        scanf("%f",&CR);
                }
                goto Menu;

case '3':
                goto quit;

default:;
}

system ("cls");
printf("\n\nPlease Wait....");

m=0;
k=0;
while (k!=num)
{
        printf("\n\nEnter Filename:  ");
        scanf("%s",&filename);

        fp=fopen(filename,"rb");

        if (fp==NULL)
        {
                puts("\nERROR! Cannot find file\n");
                getch();
                exit(0);
        }

        fseek(fp,28,SEEK_SET);      //skip header bytes

// conversion from 32 bit hexadecimal to decimal floating point
```

127

```
                        while (!feof (fp))
                        {
                                for(n=0;n<720;n++) // 720 points for (1 cycle)
                                {
                                        fread(&e,sizeof(e),1,fp);

                                        x=&e.b;

                                        for (i=0;i<4;i++)
                                        {
                                                a[i]=*x;
                                                x++;
                                        }
                                        x--;
                                        for (i=0;i<4;i++)
                                        {
                                                *x=a[i];
                                                x--;
                                        }

                                pr[m][n]=e.b;
                                }
                        m++;

                        }
                        fclose (fp);
                        k++;
                }


//      corrected data with reference to 270 CAD

        sof=179;
        for (i=0;i<m;i++)
        {
                offset=cc-pr[i][sof];// Difference of value at 270 CAD & 1.5

                for (j=0;j<720;j++)
                        pr[i][j]=pr[i][j]+offset;
                        //Write skewed values in the array avg[]
        }


//      average the cycle-by-cycle pressure data to time-based pressure
data

        b=0;
        for (i=0;i<d;i++)
        {
                for (j=0;j<ncyc[i];j++)
                {
                        for (k=0;k<720;k++)
                        {
                                avg[i][k]=avg[i][k]+pr[b][k];
                        }
                        b++;
                }

        }

        for (i=0;i<d;i++)
        {
                for(k=0;k<720;k++)
                {
                        avg[i][k]=avg[i][k]/(ncyc[i]);
                }
        }

        R=2*L/stroke;
        Vc=(PI*pow(bore,2)/4*stroke)/(CR-1);    // Calculate Clearance
Volume
```

128

```
        for (i=0;i<720;i++)                    // Calculate V-theta for 720 CAD
        {
                V[i]=Vc*(1+0.5*(CR-1)*(R+1-cos((i+1)*PI/180)-pow(pow(R,2)-
pow(sin((i+1)*PI/180),2),0.5)));
        }

//      calculate the mass flow rate

        for (i=0;i<d;i++)
        {
                mrate[i]=0.000857*0.9*1.28;
        }

//      calculate the mean  cylinder temperature

        for (i=0;i<d;i++)
        {
                for (k=0;k<720;k++)
                {
                        T[i][k]=avg[i][k]*1e5*V[k]/(mrate[i]*GC);

                }
        }

        for (i=0;i<d;i++)
        {
                Texh[i]=T[i][532];

        }

//      write the exhaust gas temperature data to a file

        fu=fopen("exh-temp.xls","w");
        for (i=0;i<d;i++)
                        fprintf(fu,"%f\n",Texh [i]);

        fclose (fu);

        printf("\n\n\n DONE!");

quit:
        getch();

}
```

129

APPENDIX D

CALIBRATION DETAILS FOR EXHAUST THERMOCOUPLES

The calibration was performed using a single-point calibration procedure. This procedure is recommended by the Emission Test Centre of the EPA. It states that

> *"A single-point calibration procedure that checks the operation of a thermocouple system within ±1.0 percent of the absolute measured temperature is all that is necessary to check the system for the presence of disconnected wire junctions, other loose connections, or a potential miscalibrated readout. A system that performs accurately at one temperature is expected to behave similarly at other temperatures."* [42].

This procedure was applied on the thermocouples using an ice bath maintained at 0°C and the results are shown in Table D-1.

Table D-1: Thermocouple Calibration Data

Thermocouple #	Size	Observed Temperature at 0°C
Tg1	1/16"	-0.504
Tg2	1/16"	-0.073
Tg3	1/16"	-0.38
Tg4	1/16"	-0.107
Tg5	1/16"	-0.063
Tg6	1/16"	-0.032
Tp1	1/32"	-0.136
Tp2	1/32"	-0.071
Tp3	1/32"	-0.009
Tp4	1/32"	-0.015
Tp5	1/32"	-0.028
Tp6	1/32"	-0.007

The stated accuracies for the various components in the data acquisition system are given in Table D-2. Since the highest temperatures encountered in a diesel exhaust system do not exceed 800°C, this value was used to estimate the maximum errors in the measured values.

Table D-2: Stated Accuracies for Data Acquisition Components

Component	Listed Accuracy	Maximum Error at 800°C
Thermocouples	2.2°C or 0.75% whichever is greater	±6°C
Thermocouple Wires	1.2°C at 200°C or 0.6%	±4.8°C
Thermocouple Conditioning Module	± 0.25°C at 250°C or 0.1%	±0.8°C

The accuracy of the system can then be broadly expressed as ~1.5% for temperature measurements upto 800°C and the maximum relative uncertainty in the temperature measurement comes to approximately ±11.6°C.

VITA AUCTORIS

NAME:	Usman Asad
PLACE OF BIRTH:	Rawalpindi, Pakistan
YEAR OF BIRTH:	1974
EDUCATION:	St. Mary's Academy, Rawalpindi, Pakistan
	1978-1989
	University of Engineering & Technology, Lahore, Pakistan
	1992-1995 B.Sc. Engineering